AD-A162 139 A MODEL FOR PREDICTING THERMOMECHANICAL RESPONSE OF LARGE SPACE STRUCTURE..(U) TEXAS A AND M UNIV COLLEGE STATION MECHANICS AND MATERIALS RE.. D H ALLEN ET AL. 1/3

UNCLASSIFIED JUN 85 MM-4875-85-11 AFOSR-TR-85-1016 F/G 22/2 NL

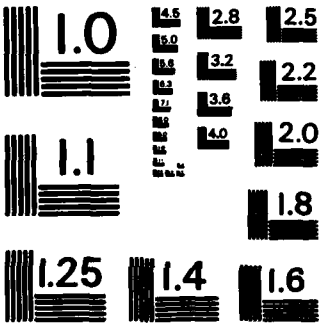

MICROCOPY RESOLUTION TEST CHART
NATIONAL BUREAU OF STANDARDS-1963-A

Mechanics and Materials Center
TEXAS A&M UNIVERSITY
College Station, Texas

A MODEL FOR PREDICTING THERMOMECHANICAL RESPONSE OF LARGE SPACE STRUCTURES

ANNUAL TECHNICAL REPORT

D.H. ALLEN
AND
W.E. HAISLER

AIR FORCE OFFICE OF SCIENTIFIC RESEARCH
OFFICE OF AEROSPACE RESEARCH
UNITED STATES AIR FORCE
CONTRACT NO. F49620-83-C-0067

MM 4875-85-11

JUNE 1985

REPORT DOCUMENTATION PAGE

1a. REPORT SECURITY CLASSIFICATION: Unclassified	1b. RESTRICTIVE MARKINGS:
2a. SECURITY CLASSIFICATION AUTHORITY:	3. DISTRIBUTION/AVAILABILITY OF REPORT: Unlimited — Approved for public release; distribution unlimited.
2b. DECLASSIFICATION/DOWNGRADING SCHEDULE:	
4. PERFORMING ORGANIZATION REPORT NUMBER(S): MM 4875-85-11	5. MONITORING ORGANIZATION REPORT NUMBER(S): **AFOSR-TR- 85-1016**
6a. NAME OF PERFORMING ORGANIZATION: Aerospace Engineering Dept. / 6b. OFFICE SYMBOL (If applicable):	7a. NAME OF MONITORING ORGANIZATION: Air Force Office of Scientific Research
6c. ADDRESS (City, State and ZIP Code): Texas A&M University, College Station, Texas 77843	7b. ADDRESS (City, State and ZIP Code): Bolling AFB, Washington, D.C. 20332
8a. NAME OF FUNDING/SPONSORING ORGANIZATION: Air Force Office of Scientific Res. / 8b. OFFICE SYMBOL (If applicable): AFOSR/NA	9. PROCUREMENT INSTRUMENT IDENTIFICATION NUMBER: F49620-83-C-0067
8c. ADDRESS (City, State and ZIP Code): Bolling AFB, Washington, D.C. 20332	10. SOURCE OF FUNDING NOS. — PROGRAM ELEMENT NO.: 61102F; PROJECT NO.: 2302; TASK NO.: B/1; WORK UNIT NO.:
11. TITLE (Include Security Classification): A Model for Predicting Thermomechanical Response of Large Space Structures	
12. PERSONAL AUTHOR(S): D.H. Allen and W.E. Haisler	
13a. TYPE OF REPORT: Annual / 13b. TIME COVERED: FROM May '84 TO April 85	14. DATE OF REPORT (Yr., Mo., Day): June, 1985 / 15. PAGE COUNT: 195
16. SUPPLEMENTARY NOTATION:	

17. COSATI CODES			18. SUBJECT TERMS (Continue on reverse if necessary and identify by block number)
FIELD	GROUP	SUB. GR.	large space structures; thermal loads; constitutive properties; finite element methods; environmental effects

19. ABSTRACT (Continue on reverse if necessary and identify by block number)

It is known that large space structures will be subjected to thermomechanical loadings and environmental conditions which are likely to degrade the constitutive properties of the structural materials, thus leading to possible failure of these vehicles. Therefore, it is desirable to develop new analytical models which are capable of accounting for these degraded properties so that design procedures can be improved. There are three important aspects of such an effort: selection and development of constitutive models for degrading materials which are applicable to large space structures, construction of analytic models for predicting the dynamic response of these structures, and experimentation to determine the precise nature of the material parameters to be utilized in the analytical model. These three components of the research must be tied together into a single concise effort in order to obtain a useful model.

(over)

20. DISTRIBUTION/AVAILABILITY OF ABSTRACT: UNCLASSIFIED/UNLIMITED ☒ SAME AS RPT ☐ DTIC USERS ☐	21. ABSTRACT SECURITY CLASSIFICATION:
22a. NAME OF RESPONSIBLE INDIVIDUAL: A. Amos	22b. TELEPHONE NUMBER (Include Area Code): (202) 767-4937 / 22c. OFFICE SYMBOL: AFOSR/NA

SECURITY CLASSIFICATION OF THIS PAGE

This research project is a three year effort to develop an analytical model capable of predicting the response of space structures with degrading material properties under quasi-static as well as dynamic cyclic thermomechanical loading conditions. This report details the research completed during the second year of AFOSR contract no. F49620-83-0067.

A MODEL FOR PREDICTING THERMOMECHANICAL RESPONSE OF LARGE SPACE STRUCTURES

Annual Technical Report

Submitted by

D. H. Allen

and

W. E. Haisler

AEROSPACE ENGINEERING DEPARTMENT

TEXAS A&M UNIVERSITY

to the

Air Force Office of Scientific Research
Office of Aerospace Research
United States Air Force

MM 4875-85-11

Contract No. F49620-83-C-0067
June 1985

TABLE OF CONTENTS

1. INTRODUCTION

1.1 Summary

It is known that large space structures will be subjected to thermomechanical loadings and environmental conditions which are likely to degrade the constitutive properties of the structural materials, thus leading to possible failure of these vehicles. Therefore, it is desirable to develop new analytical models which are capable of accounting for these degraded properties so that design procedures can be improved. There are three important aspects of such an effort: selection and development of constitutive models for degrading materials which are applicable to large space structures, construction of analytic models for predicting the dynamic response of these structures, and experimentation to determine the precise nature of the material parameters to be utilized in the analytical model. These three components of the research must be tied together into a single concise effort in order to obtain a useful model.

This research project is a three year effort to develop an analytic model capable of predicting the response of space structures with degrading material properties under quasi-static as well as dynamic cyclic thermomechanical loading conditions. This report details the research completed during the second year of AFOSR contract no. F49620-83-0067.

1.2 Statement of Work

A model is being developed for predicting the thermomechanical response of large space structures to cyclic transient temperature loading conditions. The research is being conducted in the following stages:

1) selection and specialization of thermomechanical constitutive equations to be utilized in the analysis of large space structures;
2) construction (where necessary) of coupled energy balance equations (modified Fourier heat conduction equations) applicable to the constitutive models selected in item 1);
3) casting (where necessary) the resulting field laws into coupled and uncoupled variational principles suitable for use with the finite element method;
4) finite element discretization of the variational principles for several element types;
5) experimentation to determine material properties to be utilized in the constitutive models; and
6) parametric studies of the quasi-static and dynamic response of large space structures undergoing thermomechanically and environmentally degraded material properties.

The experimental effort (discussed in 5) is being supported by DOD equipment grant no. 841542. The total research effort outlined above spans a three year period. The following section details results obtained during the second year.

2. RESEARCH DURING SECOND YEAR

2.1 Summary of Completed Research

The following tasks have been completed during the second year of research:

1) development of generalized constitutive equations for metal matrix composites with distributed damage;
2) experimentation to determine material parameters for the model developed in item 1);
3) completion of algorithmic development for space structures with damage induced and spacially variable stiffness loss;
4) completion of parametric studies for graphite/epoxy composite space structures using item 3);
5) completion of algorithmic development for viscoplastic space structures with thermomechanically induced heating;
6) completion of parametric studies for aluminum space structures using item 5); and
7) completion of development of bounding techniques for hysteretically induced temperature rise in thermoviscoplastic space structures.

In addition, the following tasks are well underway at the completion of the second year of research:

1) development of an analytic method for modeling beam-like structural components with damage induced stiffness loss;
2) development of a finite element model for beam-like space structures with spatially degrading material properties and subjected to solar flux heating and radiation boundary conditions; and
3) development of a model for predicting the structural response of space structures with load induced damage which causes changes in structural damping.

The items briefly outlined above will be detailed further in the following sections.

2.2 Development of Constitutive Equations

As stated in the original three year proposal [1], one objective of the research was to identify constitutive equations which account for material property degradation in polymeric composites, metal matrix composites, and high strength metal alloys. Constitutive equations for polymeric composites and high strength metal alloys were found to exist in the research literature, and candidate models were chosen and reported in the first annual report [2]. However, no appropriate models for metal matrix composites were found in the literature. Therefore, it was decided to develop a constitutive model for metal matrix composites which would be applicable to space structures[3]. The current state of this model development will be detailed in this section.

2.2.1. Generalized Model Development for Metal Matrix Composites

Because metal matrix composites are expected to be utilized commonly in space structural applications, it was felt that some constitutive model development was warranted for this class of materials. The distinguishing feature of metal matrix composites is the substantial inelastic (either elastic-plastic or viscoplastic) nonlinearity which occurs in the matrix. On the other hand, chopped fiber metal matrix composites do not exhibit the degree of layered anisotropy observed in laminated continuous fiber polymeric composites. Due to these differences, the internal state in metal matrix composites can be significantly different from polymeric composites. Accordingly, a generalized model was developed for this material. Although the model is an extension of previous research on polymeric composites [4], the mechanics of damage development are totally different. The details of this model are given in Appendix 6.1. A synopsis of the important results is given in this section.

The model utilizes the thermodynamics with internal state variables (ISV) [5] to develop the following stress-strain relations:

$$\sigma_{ij} = C_{ijkl}(\varepsilon_{kl} - \alpha_{1kl} - \alpha_{4kl} - \varepsilon^{T}_{kl}) \quad , \quad (1)$$

where σ_{ij} = stress tensor,

ε_{kl} = strain tensor,

C_{ijkl} = constant modulus tensor of the composite,

α_{1kl} = ISV representing plastic strain,

α_{4kl} = ISV representing damage, and

ε^{T}_{kl} = thermal strain tensor.

For the case without second phase material and no damage, the model reduces to classical plasticity equations [6].

Furthermore, for the uniaxial case, the model reduces to Kachanov's damage model [7] when plastic strain is negligible.

Many of the space structural applications of interest in this research involve uniaxial stress states, such as in the case of truss structures, and Euler-Bernoulii beam structures [8]. Therefore, the uniaxial equations have been studied in detail. These are, for the isothermal case:

$$\sigma_{xx} = E(\varepsilon_{xx} - \alpha_{1xx} - \alpha_{4xx} - \varepsilon^{T}_{xx}) \quad , \quad (2)$$

where E is Young's modulus. A graphical representation of this relation is shown in Fig. 1, where it is shown that the history dependent damage parameter α_{4xx} can be determined by observing the tangent modulus on unloading.

The following section details the experimental effort developed under the current contract to verify and characterize the model, as well to develop the internal state variable growth laws, for a typical chopped fiber metal matrix composite.

2.2.2. Experimental Research on Metal Matrix Composites

The primary objective of the experimental effort is to develop a technique for determining and evaluating damage in metal metrix composites. This technique must be capable of detecting cracks and voids (free surfaces) in the composite. These cracks are generally on the order of microns in characteristic dimension, so that scanning electron microscopy is required to measure the damage. Specimens have been loaded to different levels and the damage studied at each increment. Once the amount of damage is determined it can be input into the general constitutive model for metal matrix composites(See Section 2.2.1.).

The material used in this study was obtained from ARCO Metals Silag Operation in Greer, S.C. The composition of the material is 6061 Aluminum with a twenty percent volume fraction of F-9 silicon carbide whiskers. Plate is made from the materials by a powder metallurgy process and cast into billets. The billets are then rolled, extruded or machined to the desired shapes. The SiC whiskers average two microns in diameter and twenty microns long. The composite has a T-6 temper. Tensile test coupons have been machined in accordance with ASTM E-8 (Tension testing of metallic materials) to the dimensions shown in Fig. 2. For the initial portion of the study all specimens have been machined with the same orientation with respect to the plate for the purpose of uniformity (with respect to the SiC whisker orientation). A second phase of the testing involves the use of tensile test specimens oriented perpendicular to the initial specimens.

A mechanical test system was necessary to load specimens to different levels & measure responses so that the damage at various load levels could be determined. An Instron model 1125 screw-driven test system with 2" wedge action grips was used. Longitudinal displacement data were obtained by the use of an MTS model 632.11B-20 1" gage length extensometer. The displacement

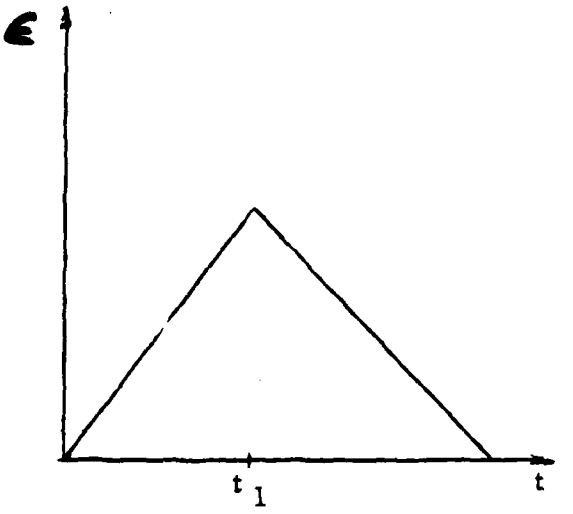

Figure 7

Input Strain Profile

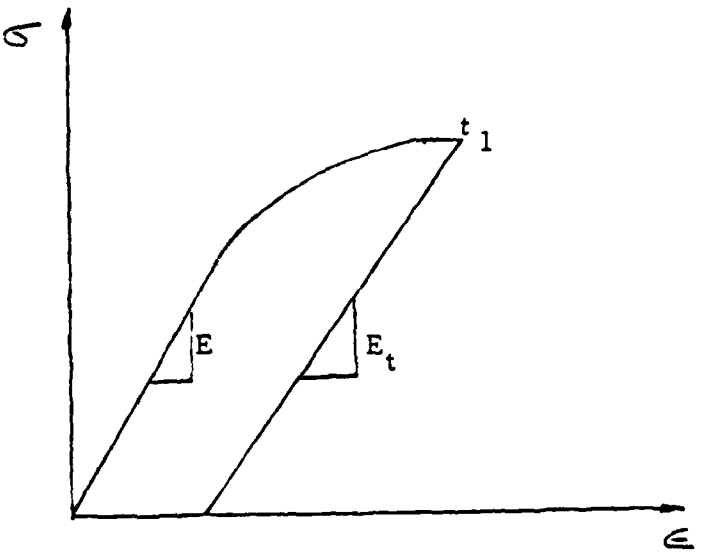

Figure 8

Stress-Strain Curve

Fig. 1. Hypothetical Stress-Strain Behavior of a Chopped-Fiber Metal Matrix Composite with Damage.

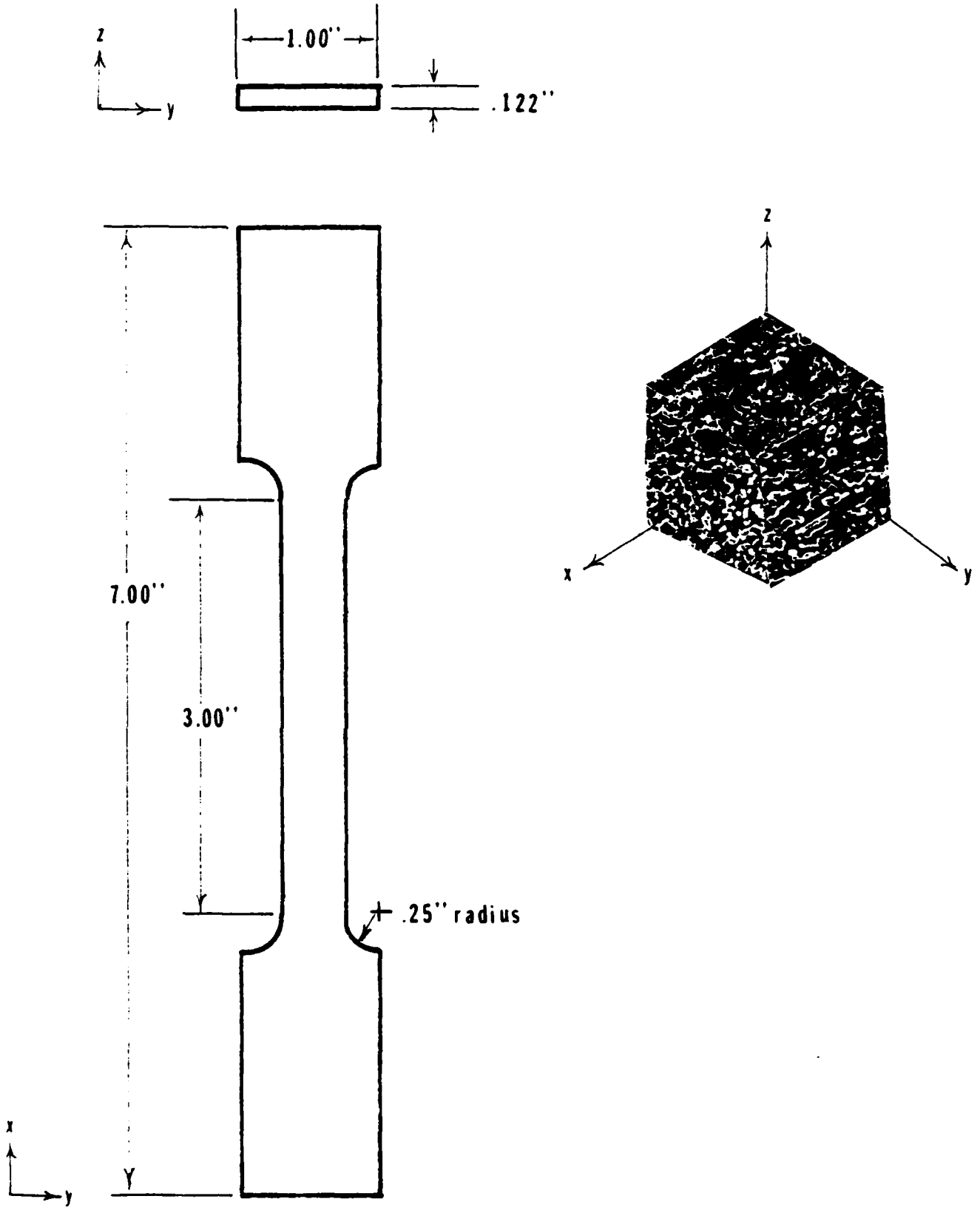

Fig. 2. Description of Metal-Matrix Coupons Used in the Experimental Program.

information was amplified by an in-house signal conditioner and load information was amplified by the Instron controller. Both load and displacement information were plotted by an analog X-Y recorder and input to a computer data acquisition system. This data acquisition system consisted of a DEC model PDP 11/23 Plus computer with an A to D converter manufactured by ADAC Corporation. With this system, load, time, and longitudinal displacement data could be stored and a real time plot of load versus displacement could be monitored during the actual tests.

The mechanical tests were performed by first loading the specimen in the Instron, calibrating and zeroing the extensometer using an extensometer displacement calibrator, calibrating the load cell and plotter, then securing the extensometer to the edge of the coupon with rubber bands.

All tests were monotonic with a cross-head speed of .05 in/min. Several specimens were tested to failure to obtain a data base about the ultimate strength of the material. After the mechanical response of the material was determined, specimens were loaded past yield at 500 pound increments so that the damage at each increment could be determined.

Once the metal matrix composite coupons were loaded, the next step in the process was to prepare them for examination with the scanning electron microscope. Tensile coupons must be sectioned into pieces that are about 1/2in X 1/2in. This was accomplished by using a Micro-Matic precision slicing and dicing machine using abrasive cutting wheels. Since there was a question about the degree of anisotropy caused by the fiber orientation in the plane of the plate, two sections were cut from each coupon so that the two orthogonal views of the coupon could be viewed under the microscope. The sectioned pieces were then mounted in a conductive mounting material (Konductomet I) manufactured by Buehler. Mounting was accomplished by the use of a Leco PR-22 Pneumatic Mounting Press with a core cycle of nine minutes at 4200 psi & 300F. The Konductomet I material is essentially a carbon filled phenolic that is designed for electron microscopy specimen use. After mounting, the specimens must be polished so that the structure can be seen in a plane. Polishing is very critical because if it is not done properly, detail can be lost or polishing induced artifacts will be created. The SiC/Al composite presents other problems. There is a vast difference between the hardness of SiC and aluminum. Unless great care is taken and an appropriate grade of abrasive compound is used, an uneven terrain is created by the removal of the softer aluminum matrix leaving exposed SiC whiskers. The mounted specimens were wet sanded in one direction on each of the following grits of sandpaper: 240, 320, 400, 600. After each grit, the specimen was washed in water to remove any residue, then sanded on the next finer grit in a different direction until all remaining evidence of the previous sanding direction was removed. The specimen was then cleaned ultrasonically in MEK. Diamond abrasive polishing compound was chosen for the fine polishing. Both the polishing compounds and cloths were obtained from Buehler. This was a necessity because of the hardness of the SiC particles. Rough polishing was accomplished by using a polishing wheel with Metadi seven micron polish on a nylon cloth.

Each specimen was polished until all visible scratches from the 600 grit sandpaper were removed. The specimens were then ultrasonically cleaned in MEK and hand polished with Metadi II three micron, then Metadi one micron heavy polishing compounds on TEXMET polishing cloths. After each change in polishing compound, it was imperative to thoroughly clean all residue of the previous compound. If this is not done properly, a smooth polished surface is impossible to obtain because the residual large pieces of polishing compound remove large pieces of material along with smaller pieces removed with the finer grain compound.

After the polishing technique was performed, the polished surface of the composite was examined under an SEM to verify a uniform, smooth surface was present.

Once the surface was polished, chemical etching was performed so that surface details could be easily seen. A solution of 10 gr NaOH and 90cc distilled H_2O at 150F was used for approximately 15 seconds to etch the specimen. The specimen was then rinsed and ultrasonically cleaned in distilled water followed by ultrasonic cleaning in MEK. The final step in preparation of the sample was to apply a thin (~100A) coating of gold by vacuum deposition. This is necessary to achieve a good image on the SEM. The SEM operates by having a voltage applied to the specimen. When the voltage is applied to the specimen, free electrons are released from the specimen. It is these electrons that are removed from the orbitals that are received by a sensor that forms the image. Light compounds have less free electrons, thus the image formed is not as sharp as an image of a heavy compound. Since gold is a heavy compound, a thin coating of it on the specimens provides an electron source, without losing surface detail.

After the specimens were sectioned, mounted in the conductive mount, polished, etched, and coated, the next step in the process was to examine them under the scanning electron microscope. A Joel JSM-25 II scanning electron microscope was used in this study.

Choosing an acceleration voltage for the specimens was a key consideration. If the voltage was too low not enough electrons were free to form an image. If too high, charging at interfaces and edges occurred leaving bright spots on the image and destroying detail. After experimentation a value of 25kv was used. Most pictures were taken at 2,000X. This magnification allowed details of the matrix, whiskers, and interfaces to be seen along with more macroscopic details such as large voids. The final product was a series of SEM photographs of the surfaces of orthogonal edges for specimens under both virgin, loaded, and failed condition (see Fig. 3). Along with SEM photographs of polished surfaces to reveal internal structure, photographs of fracture surfaces were taken to observe the effect of the whisker reinforcement.

Although this research is not complete at this time, the photographs are currently under study to determine the damage state at each load level. These data will then be fed into the damage model developed in Section 2.2.1 in order to evaluate the material constants and complete the model description for the

end view of composite (2000x)

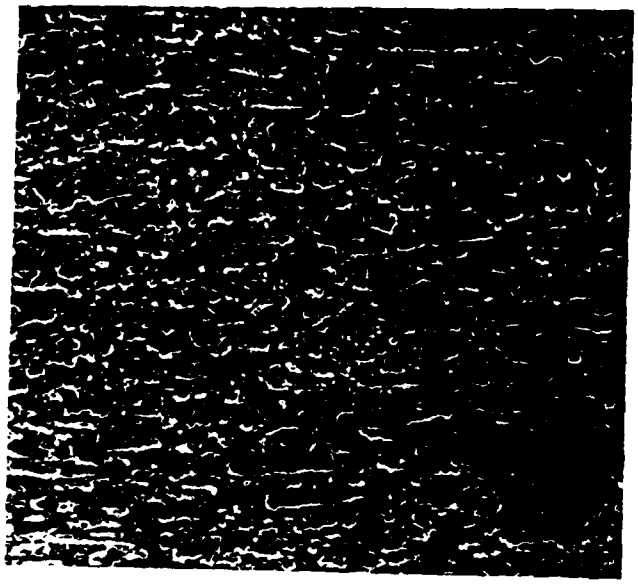

side view of composite (2000x)

damage resulting from rolling billet into sheet (2000x).

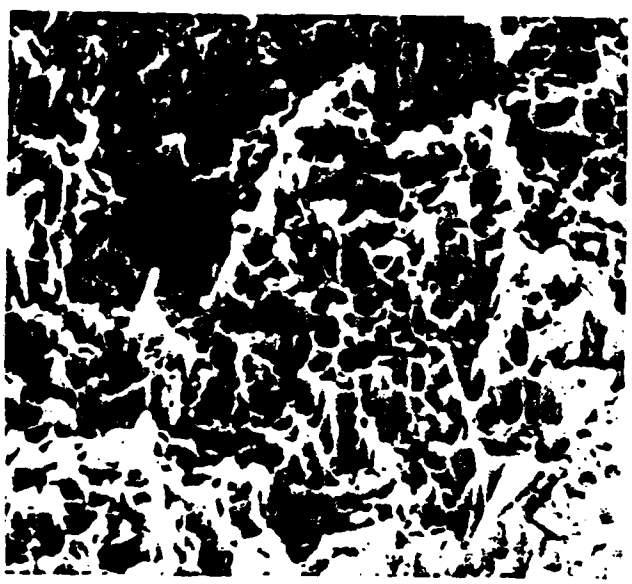

fracture surface (3000x)

Fig. 3. SEM Photographs of Chopped-Fiber Metal Matrix Composite.

chopped fiber metal matrix composite.

The above section details the M.S. thesis research of Mr. E. W. Nottorf.

2.3 Space Structural Response Due to Stiffness Loss

Fibrous composites are known to undergo a small but significant amount of stiffness loss due to load induced microcracking [3]. This stiffness loss usually occurs over several hundred thousand load cycles. Due to the stress dependent nature of the damage, the stiffness loss is spatially variable and concentrated in the areas of high stresses. This spatial change in the material properties of the structure results in appreciable changes in the dynamic response of the structure.

A part of the current research has been to develop approximate methods for determining this long term change in structural response (See Appendix 6.2.). The procedure developed here is to subject the structure to a dynamic load input which is in phase with one of the first few fundamental modes of the structure in the undamaged state. Utilizing the stress field calculated from this analysis, it is possible to estimate the spatial dependence in the stiffness loss that a space structure would undergo by approximating the constitutive equations which are designed to model long term material degradation. The approximation enters through the negligence of the actual long term history dependent nature of the damage process. This approximation is made for reasons of numerical economy. It is theoretically possible to obtain the actual history dependent response, but this would require many hours of computational time on a large mainframe computer for realistic space structures.

Because this procedure is approximate, the results should be considered as qualitative in nature. Consider, however, the case of a cantilevered space boom, as shown in Fig. 4. In Fig. 5 the displacement of the axial dimension of the boom is shown for the third mode as a function of damage induced stiffness loss in the second mode.

It is clear from Fig. 5 that damage induced by cyclic loading in fibrous composites will alter considerably the dynamic response of space structures even for small amounts of damage induced stiffness loss. Mode shapes are found to change dramatically, with node points shifting substantial distances in the structure. These results indicate that active control devices which are placed based on the initial undamaged mode shapes may require substantial relocation after the structure has been in operation for a few months or years.

2.3.1. Analysis of History Dependence of Structural Response of Simple Space Structures with Load Induced Stiffness Loss

Although it is not possible to construct a more precise history dependent structural algorithm for a representative space structure, a more accurate method is under development at this

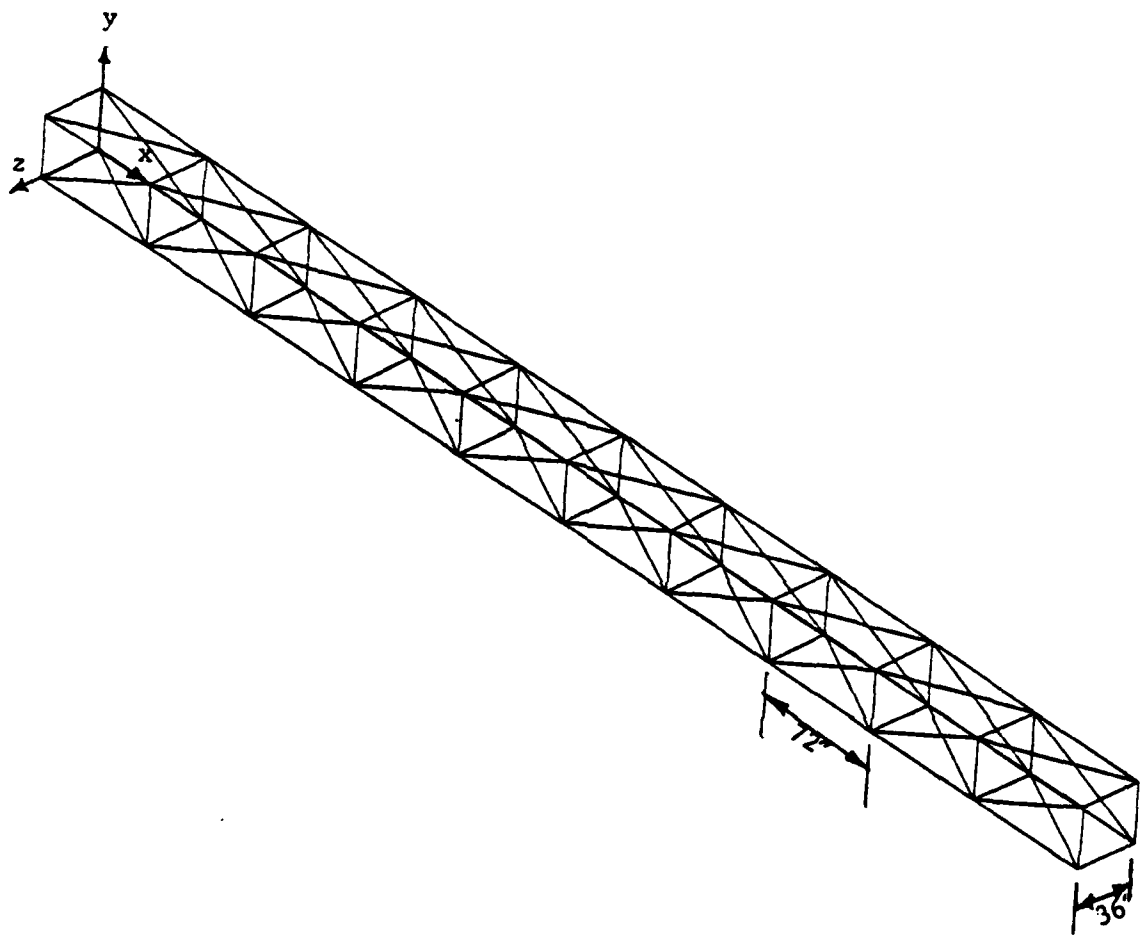

Fig. 4. Typical Beam-Like Space Structure.

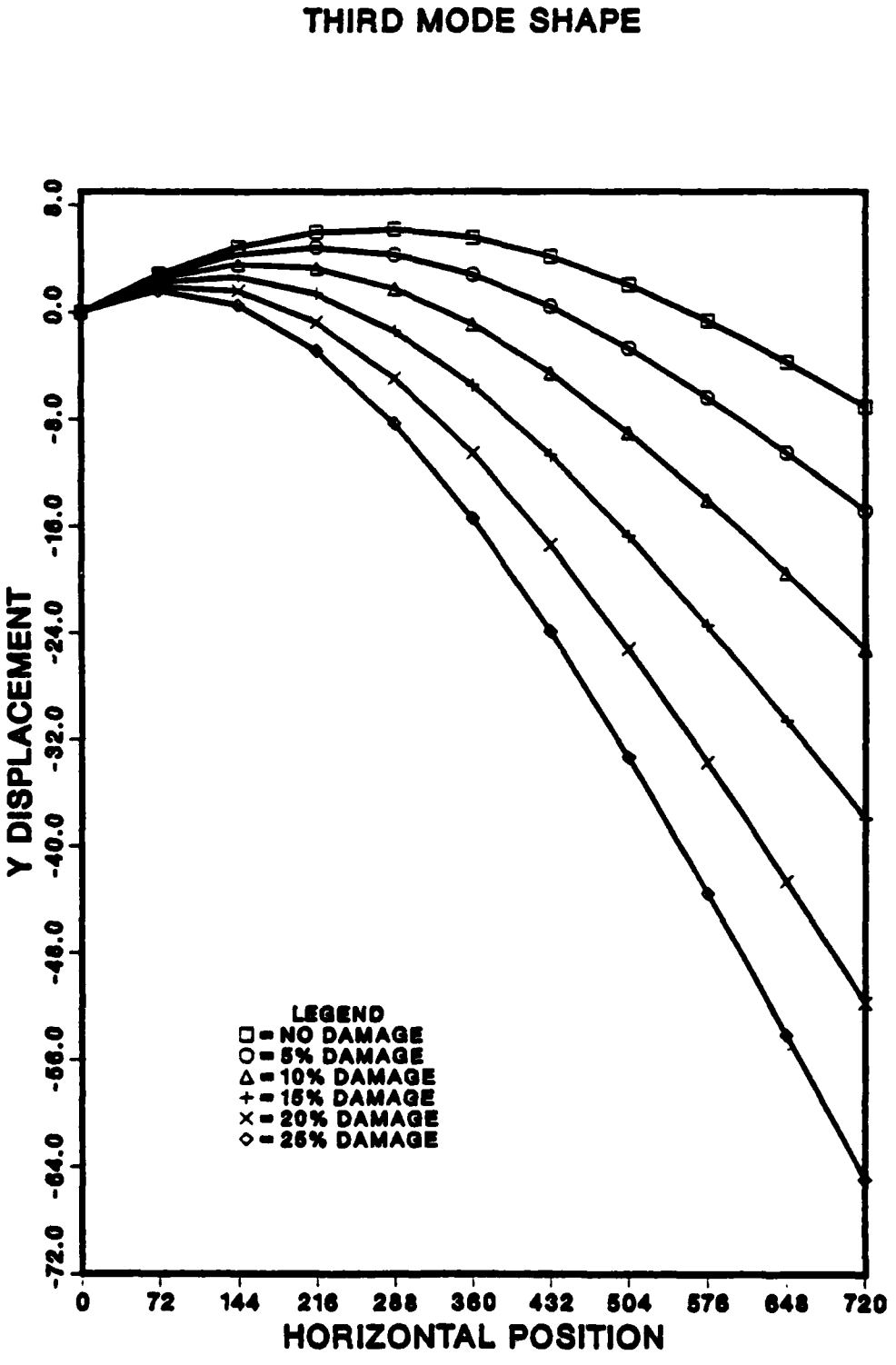

Fig. 5. Damage Dependent Modal Response of Structure shown in Fig. 4.

time for a single beam member with various boundary conditions. This model will carry out the actual time integration for the slowly degrading structure as damage accumulates for each cycle. Using this new model for simplified structures, it will be possible to determine the actual structural response for a load input of several hundred thousand cycles. The following is a brief description of this procedure.

The well known partial differential equation for the free vibration of a beam is

$$\frac{\partial^2}{\partial x^2}\left(EI\,\frac{\partial^2 y}{\partial x^2}\right)+\rho A\,\frac{\partial^2 y}{\partial t^2} \quad , \quad (3)$$

where E is Young's modulus, I is the moment of inertia of the cross-section, A is the cross-sectional area, ρ is the mass density, y is the transverse displacement, x is the axial coordinate, and t is time.

A number of solutions to the above differential equation are available in the literature for both uniform (constant cross-section) and nonuniform (variable cross-section) with different boundary conditions. Most of the solutions are for beams with homogeneous material properties. These solutions have been obtained by assuming that the stiffness of a structural element is constant in time and therefore independent of loading history. Neither material damage nor environmentally caused degradation are considered in these analyses.

Due to the occurrence of load induced and history dependent damage in composite materials, these previously obtained results represent unrealistic approximations of the actual structural behavior (See, for example, Appendix 6.2). In particular, the resonant frequencies and mode shapes of the structure can be severely altered by the introduction of spacially variable damage. These parameters in turn can have a substantial impact on the active control algorithm to be employed for control of flexible body modes. By introducing material damage and environmentally caused degradation, the stiffness of a structure is no longer a constant, since it will change substantially according to the stress distribution and the history of external loading. The stiffness loss may change the natural frequencies and mode shapes substantially. With the material damage and environmentally caused degradation involved, the differential equation becomes difficult if not impossible to solve in closed form.

The concept of internal state variables (ISV) is introduced to represent the history dependent change of stiffness. An internal state variable D is utilized as a local ISV representing the damage state. Together with the ISV growth law, the finite element solution technique can be modified to account for the history dependent stiffness of the beam element, with resulting field equations

$$[M]\{\ddot{y}\}+[K]\{y\}=\{0\} \quad , \quad (4)$$

where

$$m_{ij} = \int_0^L N_i N_j \rho A(x)\, dx$$

$$k_{ij} = \int_0^L E(\varepsilon, T, D) I(x) N_i'' N_j''\, dx \quad , \quad (5)$$

The above set of second order ordinary differential equations for each element is combined to represent the eigenvalue problem for the beam structure.

The occurrence of damage will cause the loss of stiffness, that is, the stiffness is history dependent. Experimental results indicate that the time scale for damage and degradation is very long compared to the first fundamental frequency of the structure. Therefore, the mathematical algorithm is treated as linear with slowly varying coefficients. In this research, particular interest is being placed on the natural vibration solution of a beam structure with history dependent stiffness and the investigation of the possible effect of material damage and stiffness reduction on the natural frequencies and mode shapes of planar beam structures with various boundary conditions (free-free, clamped-free, clamped-clamped and simply supported).

The research also focuses on the investigation of the internal state variable representation of the damage phenomenon. The damage in a composite material includes a sequence of microstructural and macrostructural events such as microvoid growth, matrix cracking, fiber matrix debonding, interior laminar cracking, edge delamination and fiber fracture. The most significant effect of damage on the material properties is that the stiffness will be substantially changed during the life of the component. The constitutive equation for a composite material could be represented as

$$\sigma = E(\varepsilon - \varepsilon^T) \quad , \quad (6)$$

where E is Young's modulus, which will change according to the damage D as

$$E = E_0(1 - D) \quad . \quad (7)$$

The subscript o represents the initial condition. The damage D is an internal state variable describing the damage phenomenon during the life of the composite structure, which is governed by the internal state variable growth law

$$\dot{D} = f(\varepsilon, T, D) \quad . \quad (8)$$

Since the damage phenomenon is not fully understood at this time some approximations to equation (8) will be made in the research in order to reasonably predict the damage behavior.

The above section details the Ph. D. thesis work of Mr. Y.

T. Chang.

2.3.2. Development of a Structural Model with Temperature Field Induced Damage

For many space structures the primary source of cyclic loading will be due to thermal strains induced by solar and earth radiation. The determination of the temperature field in this analysis comprises a difficult matter in itself. The following is a description of a model currently under development which will account for thermal effects on the damage process.

The anticipated construction of large space structures using composite materials has stimulated interest in the relationship between material damage and structural response. Early research concludes that during the normal life cycle of an LSS, damage, in the form of a reduction of stiffness up to 25%, should be expected. In addition, as little as 5% reduction in stiffness has been shown to significantly alter structural response. The current research attempts to study in more detail the relationship between damage and stress-strain distributions in a simplified space structure. Emphasis is placed on analyzing the structure under a set of accurate thermomechanically induced loads. The full impact of thermal loads has previously been largely ignored. Many studies have analyzed structures composed of truss type elements. This results in neglecting bending by the members themselves. For structures made with materials of high conductivity, this is not inaccurate. However, composite materials have low conductivities and therefore undergo large thermal gradients through their cross section. To incorporate these expected thermal moments, the models to be studied will be composed of beam type elements.

The outlined boundary value problem is complicated by several factors. First, a one way coupling between temperature and displacements exists. It is one way in that displacements depend on temperatures. Secondly, the problem is nonlinear due to the introduction of radiation boundary conditions. Thirdly, there are constantly changing thermal loading conditions due to varying earth-structure-sun orientation. Finally, geometrical factors such as shadowing and interelement radiation and conduction exist. These factors combine to create a highly complex problem (See Fig. 6.).

Several simplifying assumptions to the geometry and environment of the structure can be made without compromising the usefulness of the result. For a structure composed of long thin members which are sparsely placed, interelement contributions may be neglected. Each member can be treated as an isolated, independent body absorbing thermal radiation and in turn emitting its own radiation. For a structure in a geosychronous or other high earth orbit the effects of earth emitted radiation and earth reflected solar radiation are minimal. Furthermore, LSS such as solar collectors, antennas, and telescopes will have space-fixed orientations. This will result in steady-state thermal conditions due to solar radiation of nearly constant direction and intensity. This steady-state thermal condition also results in negligible axial temperature gradients (See Fig. 7.).

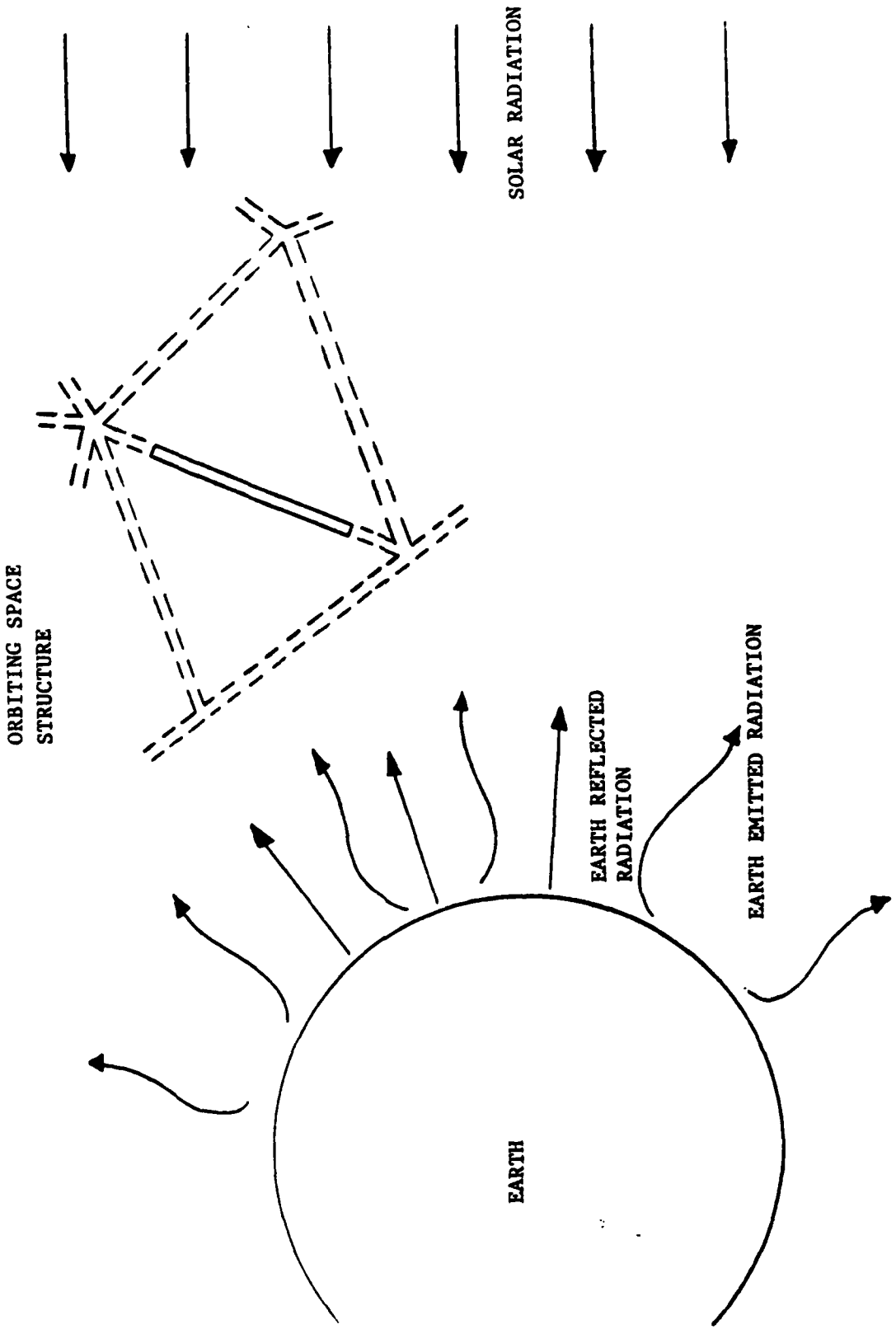

Fig. 6. Schematic of Typical Space Structural Component.

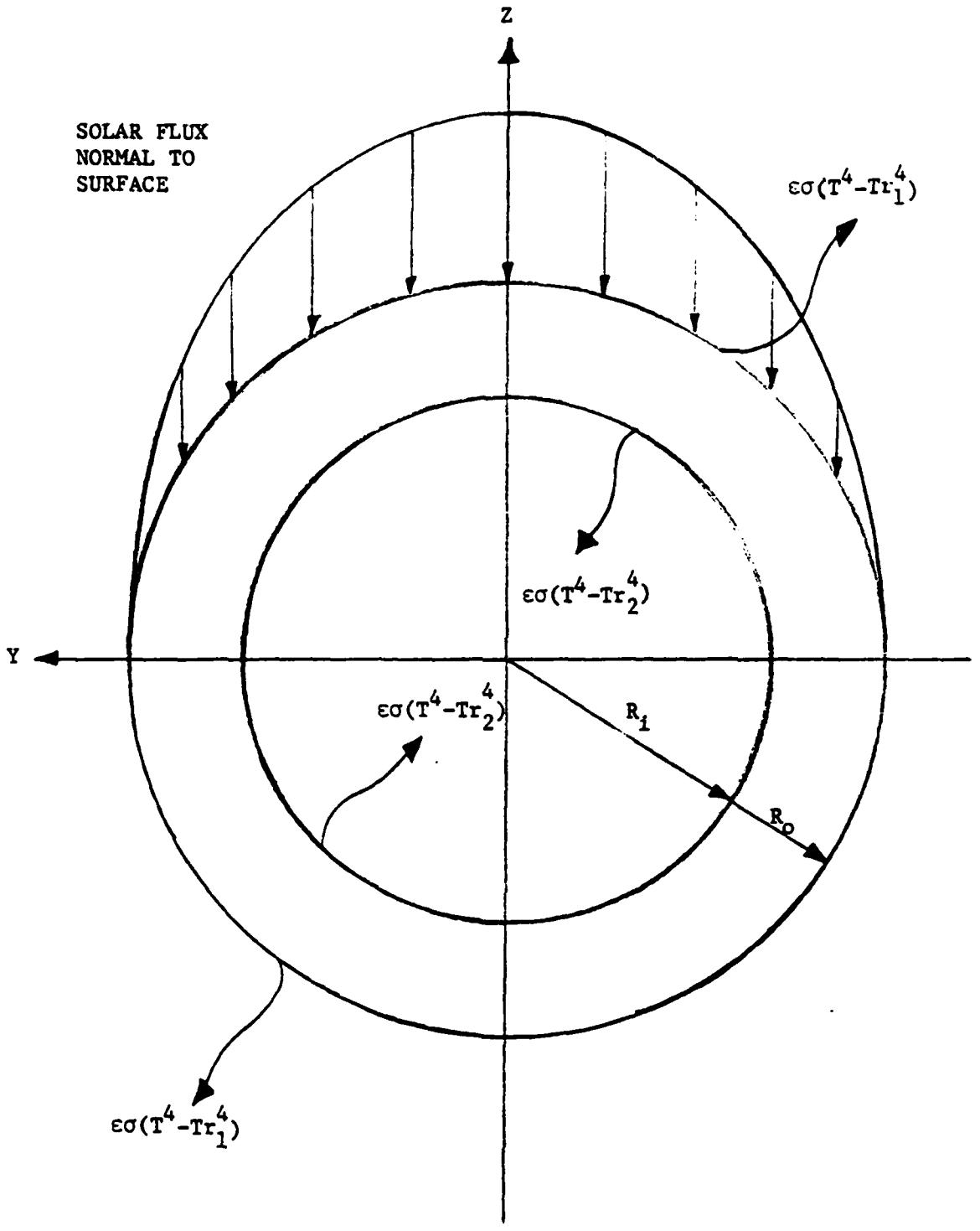

Fig. 7. Model of Thermal Problem for Space Structural Component.

The solution method to be outlined here is a completely numerical one. The algorithm consists of five parts, as shown in Fig. 8. Finite elements are used to construct the temperature field through the cross-section of a beam member. This temperature distribution is then converted to thermal forces and moments using the following equations:

$$P^T \equiv \int_A E\alpha_T \Delta T \, dA$$

$$M_y^T \equiv \int_A E\alpha_T \Delta T \, z \, dA$$

$$M_z^T \equiv \int_A E\alpha_T \Delta T \, y \, dA \qquad . \quad (9)$$

Here E represents Young's modulus, α_T is the coefficient of thermal expansion, A is cross-sectional area, ΔT is the change in temperature, and y and z are the distances to the geometric centroid. These loads are first calculated in the local coordinates of the cross-section and then transformed into the global coordinates of the structure. These global thermal forces and moments then serve as input to another finite element routine. The output from this is the stress and strain distribution in a beam member. The final step is to predict the distribution of damage in each member based on the stress history. Once the damage is known, a new stress-strain field may be generated for the current damage state.

The beam code is a standard transient one dimensional code and is the result of application of the standard finite element formulation to the governing differential equations:

$$\frac{d^2 v_0}{dx^2} = \frac{(M_z - M_z^T)}{E_1 I_{zz}^*}$$

$$\frac{d^2 w_0}{dx^2} = -\frac{(M_y + M_y^T)}{E_1 I_{yy}^*}$$

$$\frac{du_0}{dx} = \frac{(P + P^T)}{E_1 A^*} \qquad , \quad (10)$$

where u_0, v_0, w_0 = centroidal displacements in the x, y, and z coordinate directions,

P, M_y, M_z = axial force and moments,

P^T, M_y^T, M_z^T = thermally induced axial force and moments

E_1 = Young's modulus,

I_{yy}^*, I_{zz}^* = modulus weighted moments of inertia, and

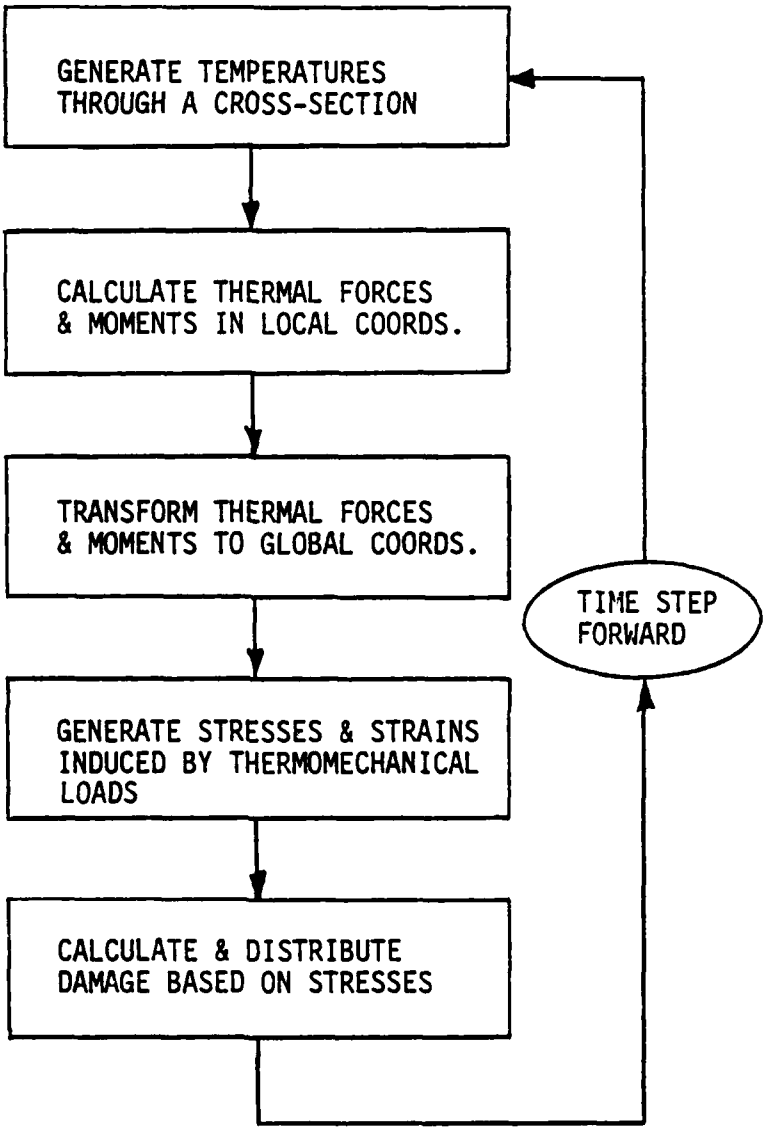

Fig. 8. Flowchart for Thermally Induced Damage Modeling.

A^* = modulus weighted cross-sectional area.

For more details about the above formulation see reference 8.

In order to place equations (10) in a variational form, each must be multiplied by a separate test function and integrated over the volume of a typical element. The resulting equations may then be discretized in the standard way.

The heat transfer code is less general. The code is developed from the general formulation for heat transfer in a plane geometry:

$$\rho c_v \dot{T} = \frac{\partial}{\partial x}\left(k_x \frac{\partial T}{\partial x}\right) + \frac{\partial}{\partial y}\left(k_y \frac{\partial T}{\partial y}\right) + Q \quad , \quad (11)$$

with boundary conditions

$$k_x \frac{\partial T}{\partial x} l_x + k_y \frac{\partial T}{\partial y} l_y = q_N \alpha + h(T_a - T) + \varepsilon\sigma(T_r^4 - T^4), \quad (12)$$

with variables defined as follows:

k_x, k_y = thermal conductivities,

Q = internal heat generation,

l_x, l_y = direction cosines,

q_N = flux normal to surface,

α = absorptivity,

h = film coefficient,

T_a = ambient temperature,

ε = emissivity,

σ = Boltzman's constant,

T_r = reference temperature,

ρ = density, and

C_v = specific heat.

Because of the steady-state conditions the governing equation reduces to the following:

$$0 = \frac{\partial}{\partial x}\left(k_x \frac{\partial T}{\partial x}\right) + \frac{\partial}{\partial y}\left(k_y \frac{\partial T}{\partial y}\right) + Q \quad . \quad (13)$$

All nonlinearity resides in the boundary conditions (12). To set up the finite element formulation, equation (11) is cast into its variational or weak form by multiplying by the test function δT

and integrating over an element volume Ω_e:

$$0 = \int_{\Omega_e} \left[\frac{\partial}{\partial x}\left(k_x \frac{\partial T}{\partial x}\right) + \frac{\partial}{\partial y}\left(k_y \frac{\partial T}{\partial y}\right) \right] \delta T \, d\Omega + \int_{\Omega_e} Q \delta T \, d\Omega \quad . \quad (14)$$

Integration by parts and the substitution of boundary conditions yields the following equilibrium equation in which B is the boundary of an element:

$$\int_{\Omega_e} \left[k_x \frac{\partial T}{\partial x} \frac{\partial \delta T}{\partial x} + k_y \frac{\partial T}{\partial y} \frac{\partial \delta T}{\partial y} \right] d\Omega = \int_{\Omega_e} Q \delta T \, d\Omega$$

$$+ \int_B \left[q_N \alpha + h(T_a - T) + \varepsilon \sigma (T_r^4 - T^4) \right] \delta T \, dB \quad . \quad (15)$$

Discretization of equation (15) results in the following set of equations for a single element:

$$\left([K_L^e] + [K_{NL}^e] \right) \{T^e\} = \{Q^e\} \quad . \quad (16)$$

K_{NLij} contains the unknown temperatures raised to the 3rd power. Because of this the solution of the equations requires that K_{NL} be approximated by a set of known temperatures and then updated through iteration until the correct temperature field is obtained.

Equation (16) may be recast in the following form:

$$\{f(T)\} = [K_L^e]\{T\} + [K_{NL}^e]\{T\} - \{Q\} = \{0\} \quad . \quad (17)$$

Newton Iteration can then be used to solve (17):

$$\left[\frac{\partial f^e}{\partial T} \right] \{\Delta T\} = -\{f^e(T)\} \quad , \quad (18)$$

where $$\frac{\partial f_i^e}{\partial T_j} = \sum_{k=1}^{N} \left(\frac{\partial K_{NL}^e}{\partial T_j} T_k \right) + K_{NL\,ij}^e + K_{L\,ij}^e$$

and n=number of degress of freedom per element and ΔT is the temperature correction on the Kth iteration. To increase the accuracy of the solution, load steps are used. Convergence of the solution is assumed if $[\partial f/\partial T]$ remains non-singular and the load steps are small. Equation (18) gives the final form of the equations to be solved:

$$\left[\frac{\partial f}{\partial T} \right]^k \{\Delta T\}^{k+1} = \{Q\}^k - \left([K_L] + [K_{NL}] \right)^k \{T\}^k \quad . \quad (19)$$

The process of ultimate failure in a composite is preceded by a series of events such as transverse cracking, delamination, fiber breakage, and fiber-matrix debonding. This sequence of

microstructural and macrostructural phenomena is termed damage. Global material properties such as stiffness and ultimate strength can be substantially altered by an accumulation of damage.

This research models damage as a load history dependent reduction in stiffness of the structural members. The distribution of the damage will be dependent on the resulting stress field. The members most heavily stressed will incur the greatest degree of damage. The intensity of the damage will be determined through the use of a power law degradation of stiffness. Therefore the degradation of the modulus is given by

$$E' = E_o \left[1 - \left(\sigma / \sigma_{MAX} \right)^n \right] \quad , \quad (20)$$

where E' is the reduced modulus, E_o is the initial modulus, σ is the stress in the member, σ_{max} is the ultimate strength, and n is some power.

The power law model is simplistic. In reality the models are expected to be quite complex. Work is currently being done to construct these models for future work in this area.

This research has two goals. The first is to investigate the sensitivity of stress-strain distributions in beams to damage induced by thermomechanically induced loads typical of their proposed environment. The second is to provide a numerical algorithm to be used in future research to provide thermal loadings for structural members. Expansion of the algorithm to include interelement contributions and transient thermal loads is suggested to enlarge the geometries and environments that can be studied.

The above section details the M.S. thesis research of Mr. J. D. Lutz.

2.4 Space Structural Response Due to Damping Change

In a vibrating structure mechanical energy is continuously converted to other forms of energy via irreversible thermodynamic processes, and this energy loss is partially exhibited in structural damping. The energy dissipation may be caused by thermal flux, material inelasticity, friction, creation of new boundaries via fracture, chemical processes, or other sources. The emphasis of this research is to develop a model capable of predicting this damping for composite materials undergoing load induced damage.

A damping measure which is commonly used is the quantity of energy D dissipated during one cycle of harmonic motion. The maximum potential energy V stored in the structure is related to the energy dissipated by the loss factor η given by

$$\eta = \frac{D}{2\pi V} \quad . \quad (21)$$

When the structure is built up from elements with known damping characteristics a proper damping matrix can be determined

yielding the fundamental structural dynamics problem

$$[M]\{\ddot{x}\} + [C]\{\dot{x}\} + [K]\{x\} = \{f(t)\} \quad , \quad (22)$$

in which x is the vector of discrete coordinates, f(t) is the vector of forcing functions, and [M], [C], and [K] are the system mass, damping, and stiffness matrices, assembled from the individual matrices of structural finite elements. The damping and stiffness depend on the damage in the structure.

For the LSS these matrices are very large, and the coordinates become highly coupled. Thus, the direct solution of the equations of motion becomes time-consuming and expensive. A very common way to analyze damped structures is to use a modal approach, which is permitted when only the response of the structure within a certain frequency range is of interest. Then the response can be expressed by means of a limited number of vibration modes. The reduction of the extent of the calculations is the advantage of this approach.

The modal matrix of eigenvectors can be calculated from the undamped free vibration problem

$$[M]\{\ddot{x}\} + [K]\{x\} = \{0\} \quad . \quad (23)$$

Modal equations can be obtained from the transformation

$$\{x\} = [\phi]\{q\} \quad , \quad (24)$$

where $[\phi]$ is the matrix of the eigenvectors and q is the vector of time dependent generalized coordinates. In general, the damping matrix in transformed coordinates is nondiagonal, so that the modal equations are coupled.

As an alternative to the assumption of modal damping, the equations of motion can be uncoupled without restrictions on the damping matrix [C], other than that it be symmetric. By selecting a different set of generalized coordinates, equation (22) can be reduced to

$$M^* \dot{q}(t) + K^* q(t) = Y(t) \quad , \quad (25)$$

where

$q(t) = [\dot{x}^T(t) : x^T(t)]^T$ is a 2N dimensional state vector, and

$Y(t) = [f^T(t) : 0^T]^T$ is a 2N dimensional generalized force vector.

Furthermore,

$$M^* = \begin{bmatrix} M & 0 \\ 0 & -K \end{bmatrix} \qquad K^* = \begin{bmatrix} C & K \\ K & 0 \end{bmatrix}$$

The associated eigenvalue problem becomes

$$\lambda M^* q + K^* q = 0 \quad , \quad (26)$$

which can be reduced to the form

$$Aq = \lambda q \quad , \quad (27)$$

where, assuming that M^* is nonsingular

$$A = -M^{*-1} K^* = \begin{bmatrix} -M^{-1}C & -M^{-1}K \\ I & 0 \end{bmatrix}$$

The solution consists of 2N eigenvalues λ_i and 2N eigenvectors. Because the matrices M^* and K^* are real, if λ_i is an eigenvalue, then $\bar{\lambda}_i$ is also an eigenvalue. The eigenvectors are orthogonal with respect to M^* and K^*.

The damping factor for composites has been observed to increase with damage. Plunkett [11] found that the damping factor could be calculated from the crack density as a function of strain level and the strain volume fraction.

If it is assumed that the energy dissipation in a material depends on the local strain state and its time history the damping factor can be of the form

$$\eta = f(D) \quad , \quad (28)$$

where D is the history dependent damage parameter. An internal state variable theory, [4] can then be utilized to relate the damping factor with a given damage state. Thus, response calculations can be made for large space structures.

The research detailed in the above section is the Ph. D. thesis work of Mr. S. Kalyanasundarum.

2.5 Temperature Change Due to Hysteretic Heating

It is envisioned that many space structural components will be fabricated from aluminum alloys. Furthermore, it has been suggested that utilizing these components in their post-yielded state can lead to enhanced passive damping of the structure due to hysteretic strain energy conversion to heat. For viscoplastic structures this is a complex nonlinear two-way coupled problem in that the conservation of energy is coupled via the temperature to the other field equations [9].

The purpose of this portion of the research has been to construct a model capable of predicting the structural response of a viscoplastic space structure to thermomechanical loading. The primary emphasis is placed on the prediction of the temperature rise accrued in typical viscoplastic members due to hysteretic loss during cyclic loading.

The general formulation of this problem was completed during the first year of research [10]. During the second year the model has been applied to a typical space truss structure made of aluminum members (See Appendix 6.4). The structure is assumed to be coated with special high emissivity materials, and is subjected to various levels of solar and earth radiation. The problem is complicated not only by the thermomechanical coupling, but also by the nonlinear constitutive equations and radiative boundary conditions.

As shown in Fig. 9, the predicted temperature rise for an input cyclic loading at 5 Hz can be very substantial in spite of the fact that the radiation boundary conditions provide a structural heat loss mechanism.

The algorithm developed in reference 10, although comprehensive in nature, is very computationally expensive to utilize. In fact, it is so costly as to preclude the analysis of the response of a structural member undergoing several thousand load cycles. Therefore, alternative procedures were considered for analyzing the temperature profile as a function of time. This research has resulted in the completion of the three part paper described in Appendices 6.5 through 6.7.

The principal result obtained from this research is the determination of upper and lower bounds for the hysteretically induced temperature rise as a function of load history, geometry, and material properties. As shown in Fig. 10, these bounds verify the results obtained in Appendix 6.4.

On the basis of these results it is concluded that material inelasticity in viscoplastic structural members should be used as a passive damping mechanism only with extreme caution. The temperature rises associated with this damping process can be so severe as to compromise the integrity of the structure.

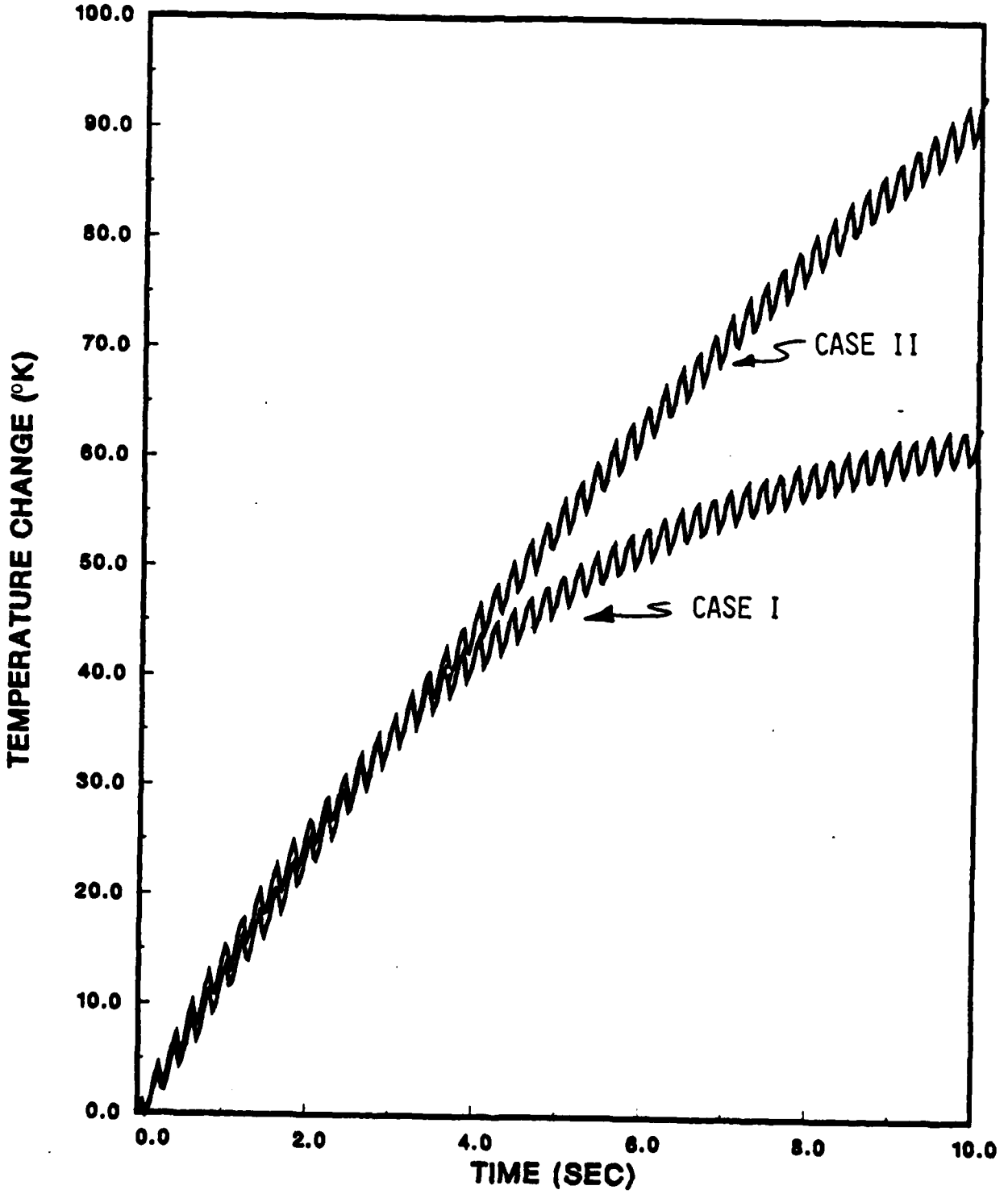

Fig. 9. Temperature Rise in a Typical Member Shown in Fig. 4 Subjected to Cyclic

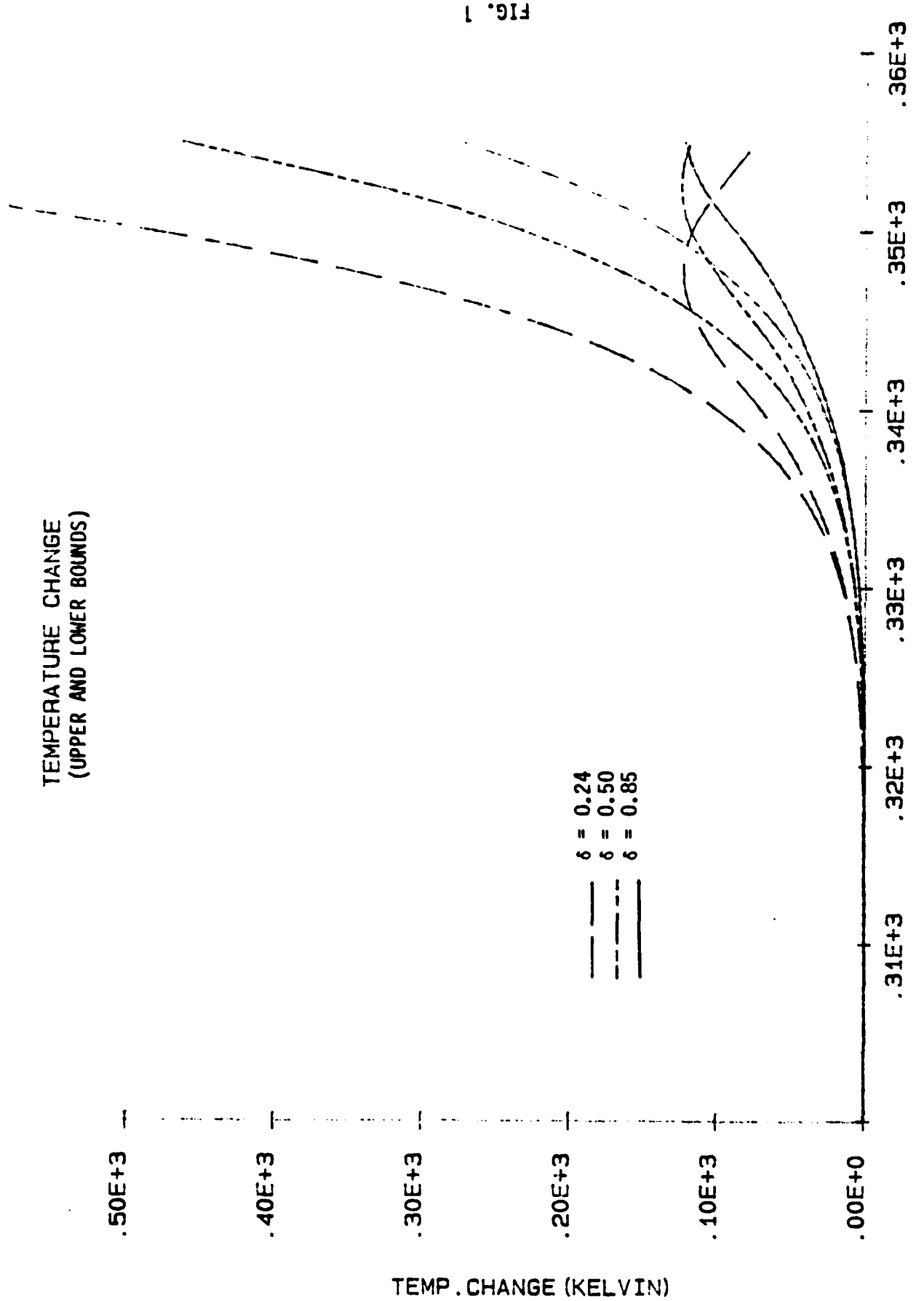

FIG. 1

Fig. 10. Temperature Bounds for Hysteretic Heating of

2.6 References

[1] Allen, D. H., and Haisler, W. E., "A model for Predicting Thermomechanical Response of Large Space Structures," Texas A&M University Research Foundation, Proposal No. 82-721, submitted to the Air Force Office of Scientific Research, June, 1982.

[2] Allen, D. H., and Haisler, W. E., "A Model for Predicting Thermomechanical Response of Large Space Structures - Annual Techanical Report," Texas A&M University Mechanics and Materials Center, Report No. MM-4875-84-16, June, 1984.

[3] Groves, S. E., and Allen, D. H., "A Survey of Damage in Continuous Fiber Composites," Texas A&M University Mechanics and Materials Center, MMC-5023-84-6, March, 1984.

[4] Allen, D. H., Groves, S. E., and Schapery, R. A., "A Damage Model for Continuous Fiber Composites - Part I: Theoretical Development," Texas A&M University Mechanics and Materials Center, MM-5023-84-17, August, 1984 (revised Feb. 1985).

[5] Coleman, B. D., and Gurtin, M. E., "Thermodynamics with Internal State Variables," Journal of Chemical Physics, Vol. 47, pp. 597-613, 1967.

[6] Hill, R., The Mathematical Theory of Plasticity, Oxford University Press, London, 1950.

[7] Kachanov, L. M., "On the Creep Fracture Time," Izv. AN SSR, Otd. Tekhn. Nauk, No. 8, pp. 26-31,1958 (in Russian).

[8] Allen, D. H., and Haisler, W. E., Introduction to Aerospace Structural Analysis, John Wiley and Sons, Inc., 1985.

[9] Allen, D. H., "Thermodynamic Constraints on the Constitution of a Class of Thermoviscoplastic Solids," Texas A&M University Mechanics and Materials Center, MMC 12415-82-10, December, 1982.

[10] Allen, D. H., "Predicted Axial Temperature Gradient in a Viscoplastic Uniaxial Bar Due to Thermomechanical Coupling," Texas A&M University Mechanics and Materials Center, Report No. MM-4875-84-15, Nov., 1984.

[11] Plunkett, R., "Damping in Fiber Reinforced Laminated Composites at High Strain," Journal of Composite Materials Supplement, Vol. 14, pp. 109-117, 1980.

3. PUBLICATIONS LIST

The following research has been published during the second research year:

1. Kalyanasundaram, S., Lutz, J. D., Haisler, W. E., and Allen, D. H., "Effect of Degradation of Material Properties on the Dynamic Response of Large Space Structures," Proceedings 26th AIAA/ASME/ASCE/AHS Structures, Dynamics, and Materials Conference, April, 1985 (Appendix 6.2).

2. Allen, D. H. and Haisler, W. E., "Predicted Temperature Gradient in a Thermomechanically Heated Viscoplastic Space Truss Structure," Proceedings 26th AIAA/ASME/ASCE/AHS Structures, Dynamics, and Materials Conference, April, 1985 (Appendix 6.4).

In addition, paper no. 1 listed above has been submitted for publication to the Journal of Spacecraft and Rockets, and paper no. 2 has been accepted for publication by the Journal of Spacecraft and Rockets.

The following paper has been submitted for publication:

1. Allen, D. H., "Predicted Axial Temperature Gradient in a Viscoplastic Uniaxial Bar Due to Thermomechanical Coupling," submitted to the International Journal for Numerical Methods in Engineering (Appendix 6.3).

The following papers are to be submitted for publication:

1. Allen, D. H., Nottorf, E. W., and Harris, C. E.,"A Fratographic Study of Damage Mechanisms in Short-Fiber Metal Matrix Composites," to be submitted to Fractography of Modern Engineering Materials, ASTM Special Technical Publication (Section 6.1).

2. Pilant, M. S. and Allen, D. H., "Analysis of a Thermoviscoplastic Uniaxial Bar Under Prescribed Stress," to be submitted to the SIAM Journal of Applied Mathematics (Appendices 6.5-6.7).

In addition, the following report not listed above has been completed during the second year of research:

1. Wren, G. and Allen, D. H., "Development of a Theoretical Framework for Constitutive Equations for Metal Matrix Composites with Damage," Texas A&M University Mechanics and Materials Center, Report No. MM 4875-85-9, June, 1985 (Appendix 6.1).

4. PROFESSIONAL PERSONNEL INFORMATION

4.1 Faculty Research Assignments

1. Dr. D. H. Allen (Co-principal Investigator) - development of constitutive equations for polymeric composites, metal matrix composites, and high strength metal alloys; development of variational principles and finite element methods for two-way coupled thermoviscoplastic media; experimental methods for material model development.

2. Dr. W. E. Haisler (Co-principal Investigator) - development of finite element algorithms for truss and beam structures with material property degradation; sensitivity studies for large space structures with material property degradation.

3. Dr. M. S. Pilant (Investigator) - development of solution algorithms for coupled thermoviscoplastic media.

4.2 Additional Staff

1. Mr. B. Harbert (Lab Technician) - experimental lab support.

2. Mrs. T. Marquez (Secretary) - secretarial support.

3. Mr. S. Kalyanasundaram (Ph.D. Research Assistant) - modeling of large space structures with damage induced stiffness loss and damping increase; expected completion date May 1986.

4. Mr. Y. T. Chang (Ph.D. Research Assistant) - modeling of history dependent behavior of beam-like structures with spacially and history dependent damage.

5. Mr. E. W. Nottorf (M.S. Research Assistant) - development of experimental techniques for determining load induced damage in metal matrix composites; expected completion date August 1985.

6. Mr. G. Wren (M.S. Research Assistant) - development of general theoretical model for constitutive equations for metal matrix composites with damage; expected completion date August 1985.

7. Mr. J. D. Lutz (M.S. Research Assistant) - modeling of damage dependent space structures in the presence of solar flux and radiation boundary conditions; expected completion date December 1985.

5. INTERACTIONS

5.1 Papers Presented

Presentations have been given during the second year at the following conferences:

1. D. H. Allen - 26th SDM Conference, April, 1985.
2. W. E. Haisler - 26th SDM Conference, April, 1985.
3. M. S. Pilant - SIAM Annual Spring Conference, June, 1985.

Papers have been accepted for presentation at the following conferences:

1. D. H. Allen - 3rd Forum on Large Space Structures, July, 1985.
2. W. E. Haisler - 3rd Forum on Large Space Structures, July, 1985.
3. D. H. Allen - 22nd Society of Engineering Science Meeting, October, 1985.
4. D. H. Allen - ASTM Symposium on Fractography of Modern Engineering Materials, November, 1985.

5.2 Awards and Achievements

1. Dr. Allen has been named Associate Editor of the Journal of Spacecraft and Rockets.

2. Dr. W. E. Haisler has been named Head of the Aerospace Engineering Department at Texas A&M University.

3. The textbook entitled Introduction to Aerospace Structural Analysis, co-authored by Drs. Allen and Haisler, has been published by John Wiley.

4. Dr. W. E. Haisler has been named to the Halliburton Chair at Texas A&M University.

5. Drs. Allen and Haisler have been named Texas Engineering Experiment Station Research Fellows for 1984-1985.

6. Dr. Allen has received the General Dynamics Award for Outstanding Teaching and Research in the College of Engineering at Texas A&M University.

7. Dr. Allen has been tenured and promoted to the rank of Associate Professor.

5.3 Other

1. Drs. Allen and Haisler have made a total of eleven research related trips during the past year.

6. APPENDIX

INTERIM TECHNICAL REPORTS

APPENDIX 6.1

Mechanics and Materials Center
TEXAS A&M UNIVERSITY
College Station, Texas

DEVELOPMENT OF A THEORETICAL FRAMEWORK FOR CONSTITUTIVE EQUATIONS FOR METAL MATRIX COMPOSITES WITH DAMAGE

G. WREN
AND
D.H. ALLEN

MM 4875-85-9

JUNE 1985

REPORT DOCUMENTATION PAGE

1a. REPORT SECURITY CLASSIFICATION: Unclassified	1b. RESTRICTIVE MARKINGS
2a. SECURITY CLASSIFICATION AUTHORITY	3. DISTRIBUTION/AVAILABILITY OF REPORT: Unlimited
2b. DECLASSIFICATION/DOWNGRADING SCHEDULE	
4. PERFORMING ORGANIZATION REPORT NUMBER(S): MM 4875-85-9	5. MONITORING ORGANIZATION REPORT NUMBER(S)
6a. NAME OF PERFORMING ORGANIZATION: Aerospace Engineering Dept; 6b. OFFICE SYMBOL (If applicable)	7a. NAME OF MONITORING ORGANIZATION: Air Force Office of Scientific Research
6c. ADDRESS (City, State and ZIP Code): Texas A&M University, College Station, TX 77840	7b. ADDRESS (City, State and ZIP Code): Bolling AFB, Washington D.C. 20332
8a. NAME OF FUNDING/SPONSORING ORGANIZATION: AFOSR; 8b. OFFICE SYMBOL (If applicable)	9. PROCUREMENT INSTRUMENT IDENTIFICATION NUMBER: F49620-83-C-0067
8c. ADDRESS (City, State and ZIP Code): Bolling AFB, Washington D.C. 20332	10. SOURCE OF FUNDING NOS. — PROGRAM ELEMENT NO. / PROJECT NO. / TASK NO. / WORK UNIT NO.
11. TITLE (Include Security Classification): Development of a Theoretical Framework for Constitutive Equations for Metal Matrix Composites with Damage	
12. PERSONAL AUTHOR(S): G. Wren and D.H. Allen	
13a. TYPE OF REPORT: Interim; 13b. TIME COVERED FROM _____ TO _____	14. DATE OF REPORT (Yr., Mo., Day): June 1985; 15. PAGE COUNT
16. SUPPLEMENTARY NOTATION	

17. COSATI CODES			18. SUBJECT TERMS (Continue on reverse if necessary and identify by block number)
FIELD	GROUP	SUB. GR.	composites constitutive equations plasticity metal matrix composites damage

19. ABSTRACT (Continue on reverse if necessary and identify by block number)

A continuum mechanics framework is utilized herein to construct constitutive equations for metal matrix composites with damage. Matrix plasticity and microcracking are modelled via the concept of internal state variables. Imposition of thermodynamic constraints results in a set of stress-strain relations which are dependent on damage and plastic strain. These equations are specialized to a one-dimensional case and it is then demonstrated how the material parameters may be determined experimentally.

20. DISTRIBUTION/AVAILABILITY OF ABSTRACT: UNCLASSIFIED/UNLIMITED ☒ SAME AS RPT. ☐ DTIC USERS ☐	21. ABSTRACT SECURITY CLASSIFICATION: Unclassified
22a. NAME OF RESPONSIBLE INDIVIDUAL: A. Amos	22b. TELEPHONE NUMBER (Include Area Code): (202) 767-4937; 22c. OFFICE SYMBOL: AFOSR/NA

DEVELOPMENT OF A THEORETICAL FRAMEWORK FOR CONSTITUTIVE EQUATIONS FOR METAL MATRIX COMPOSITES WITH DAMAGE

by

G. WREN

and

D.H. ALLEN

Aerospace Engineering Department

Texas A&M University

COLLEGE STATION TX 77843

DEVELOPMENT OF A THEORETICAL FRAMEWORK FOR CONSTITUTIVE EQUATIONS FOR METAL MATRIX COMPOSITES WITH DAMAGE

by

G. WREN

and

D.H. ALLEN

ABSTRACT

A continuum mechanics framework is utilized herein to construct constitutive equations for metal matrix composites with damage. Matrix plasticity and microcracking are modelled via the concept of internal state variables. Imposition of thermodynamic constraints results in a set of stress-strain relations which are dependent on damage and plastic strain. These equations are specialized to a one-dimensional case and it is then demonstrated how the material parameters may be determined experimentally.

INTRODUCTION

The characterization and modelling of matrix plasticity, cracks and other forms of microscopic damage in metal matrix composites is developed herein using the principles of continuum mechanics. The theory developed incorporates globally averaged, history dependent, thermodynamically constrained constitutive relations and utilizes tensor valued internal state variables to model history dependent energy dissipative (irreversible) phenomena.

The two primary energy dissipative phenomena considered are inelastic strain and damage. Depending on the complexity of the material under consideration, these internal state variables can be scalar or tensor valued functions. Since these phenomena are inherently history dependent, the specification of the internal state variables representing inelastic strain and damage and their associated growth laws introduces history dependence into the boundary value problem.

There exist many phenomena in the microstructure of a material which can be classified into energy dissipative/irreversible processes. These include crack formation, dislocation movement and arrangement, grain boundary

sliding, chemical changes and frictional losses due to rubbing of fractured surfaces. Therefore, some degree of clarification is required regarding how inelastic strain and damage are to be defined. In this paper, all damage will refer to cracks in the material microstructure.

Results obtained from previous research into the constitution of crystalline solids [1,2] indicate that for the class of materials into which metal matrix composites is classified, the inelastic strain tensor is treated as a second order tensor valued internal state variable. The primary mechanisms of inelastic strain are postulated as those of dislocation density (drag stress) and dislocation arrangement (back stress) which are themselves zero order (scalar) and second order tensor valued internal state variables respectively. Research into the kinematics of crack initiation and growth presented in this paper as well as reference [3] postulates damage to be a second order tensor valued internal state variable.

The damage is assumed to be statistically homogeneous within a representative volume element, which is assumed to be small in comparison to the body of interest. Under the condition of small scale statistical homogeneity, all continuum based conservation laws are assumed to be valid on a global scale in the sense that all changes in the continuum

problem resulting from internal damage are reflected only through alterations in the constitutive behavior. Therefore, microstructural phenomena such as cracks qualify as damage and their effects on the performance of a material can be reflected through the constitutive relations. However, macroscopic and/or nonhomogeneous damage states such as large scale surface cracks are treated as boundary effects which must be reflected in conservation laws via changes in the external boundary conditions rather than in the constitutive relations.

DEVELOPMENT OF THE CONSTITUTIVE RELATIONS

We now proceed to develop specific constraints on constitutive behavior. In this analysis the following assumptions are made:

a. thermomechanical coupling is non-zero,

b. electrical and magnetic effects can be neglected [4] as these can be either controlled or or their effect on the body of interest calculated,

c. infinitesimal deformations, and

d. in the absence of damage or at constant damage state the material behavior is initially linear thermoelastic and isotropic.

Field Parameters

Consider a body occupying a closed region V with material points $x_i = (x_1, x_2, x_3)$. In an analagous method to that proposed by Coleman and Gurtin [5], it is postulated that the following state variables are required to fully characterize the state of all material points x_j within a body at all times t:

a. displacement field $u_i = u_i(x_j, t)$ (1)

b. stress tensor $\sigma_{ij} = \sigma_{ij}(x_k, t)$ (2)

c. body force per unit mass $f_i = f_i(x_j, t)$ (3)

d. heat flux vector $q_i = q_i(x_j, t)$ (4)

e. internal energy per unit mass $u = u(x_j, t)$ (5)

f. heat supply per unit mass $r = r(x_j, t)$ (6)

g. entropy per unit mass $s = s(x_j,t)$ (7)

h. absolute temperature $T = T(x_j,t)$ (8)

and

i. $\alpha_{ij}^{\ k} = \alpha_{ij}^{\ k}(x_m,t) \qquad k = 1.....,n$ (9)

where $\alpha_{ij}^{\ k}$ are a set of n second order tensor valued internal state variables necessary to model inelastic deformation and damage.

Field Equations

The following pointwise field equations , written in differential form, are assumed to hold for all media undergoing infinitesimal strains:

a. conservation of linear momentum

$$\sigma_{ij,j} + \rho f_i = \rho \ddot{u}_i \tag{10}$$

b. conservation of angular momentum (assuming negligible body moments):

$$\sigma_{ij} = \sigma_{ji} \tag{11}$$

c. kinematics:

$$\varepsilon_{ij} = 1/2\ (u_{i,j} + u_{j,i}) \tag{12}$$

d. conservation of mass:

$$d\rho/dt = 0 \tag{13}$$

e. conservation of energy:

$$\rho\dot{u} = \sigma_{ij}\dot{\varepsilon}_{ij} - q_{j,j} + \rho r \tag{14}$$

f. second law of thermodynamics

$$\rho\gamma \equiv \rho\dot{s} - \rho r/T + (q_j/T)_{,j} \tag{15}$$

where γ is the specific entropy production rate. Equation (15) together with the Clausius-Duhem inequality:

$$\gamma \geq 0 \tag{16}$$

is assumed to hold for all processes. It should be noted that although equation (15) introduces one additional equation, it

simultaneously introduces a new variable, namely Υ. Therefore, equation (15) alleviates no degrees of freedom. However, although inequality (16) cannot itself specify any degrees of freedom, it will impose constraints on the allowable form of the constitutive equations.

In the foregoing analysis the body force vector, inertial effects and body moments will be assumed to be negligible and the conservation of mass is trivially satisfied.

Helmholtz Free Energy

We now define the Helmholtz free energy per unit mass:

$$h \equiv u - Ts \tag{17}$$

where h is the arithmetic sum of the total internal energy (u) of a body and the internal entropy production (irrecoverable energy loss) (Ts) dissipated during a process. Thus, the Helmholtz free energy represents the net available internal energy within a body following any process.

It follows that:

$$\dot{u} = \dot{h} + \dot{T}s + T\dot{s} \tag{18}$$

Equation (18) can be substituted into equation (14) and this result then combined with equation (15) and inequality (16) to give:

$$\rho T\gamma = -\rho h - \rho\dot{T}s + \sigma_{kl}\dot{\varepsilon}_{kl} - q_j g_j/T \geq 0 \tag{19}$$

where

$$g_j = T_{,j} \tag{20}$$

The field equations (10), (11), (14), (15) and (16) are combined with conditions applied on the boundary B of a body to specify the complete field problem.

Constitutive Relations

Suppose that the displacements u and temperature T are specified. Then the method of Coleman and Noll [6] can be used to obtain the spatial and time distribution of the body force vector (f) and the heat supply (r) from the conservation of linear momentum and energy equations respectively, assuming that the displacement and temperature fields are specified.

Constitutive relations can then be constructed [7] from the remaining state variables and their spatial derivatives. The form of the constitutive relations used including internal state variables and their associated growth is postulated as follows:

$$\sigma_{ij} = \sigma_{ij}(\varepsilon_{kl}, T, g_k, \alpha_{kl}{}^p) \tag{21}$$

$$u = u(\varepsilon_{kl}, T, g_k, \alpha_{kl}{}^p) \tag{22}$$

$$s = s(\varepsilon_{kl}, T, g_k, \alpha_{kl}{}^p) \tag{23}$$

$$q_i = q_i(\varepsilon_{kl}, T, g_k, \alpha_{kl}{}^p) \tag{24}$$

and

$$\alpha_{kl}{}^q = \Omega_{kl}{}^q(\varepsilon_{kl}, T, g_k, \alpha_{kl}{}^p) \tag{25}$$

The form of equations (21) through (24) implies that all constitutive equations are evaluated in the specified state (x_j, t). For this reason σ_{ij}, u, s and q_i are termed observable state variables since they can be determined from equations of state for all times t even though there is implicit history dependence via the internal state variables $\alpha_{kl}{}^p$. In addition, from the definition (17) and the form of equations (22) and (23) it follows that:

$$h = h(\varepsilon_{kl}, T, g_k, \alpha_{kl}{}^p) \tag{26}$$

Note that:

1) the constitutive relations (21) through (24) are equations of state and therefore cannot contain time rates of change of state variables;

2) the principles of local action and equipresence [8,9] hold for equations (21) through (24), but need not be satisfied in the growth laws [equation (25)];

3) the superscripts p and q in equation (25) range from one to the number of internal state variables required to fully characterize the inelastic response and the damage state of the body;

4) the growth laws by their definition embody time dependence and can therefore contain both spatial and time derivatives of state variable arguments. If equations (25) are at all times integrable in time then the following is an equivalent expression to (25):

$$\alpha_{ij}{}^{k}(x_m,t) = \int_{-\infty}^{t} \Omega_{ij}{}^{k}(x_m,t')\, dt' \qquad (26a)$$

where t is the time of interest and t' is a dummy variable of integration. Therefore, it is apparent that $\alpha_{ij}{}^{k}$ are not directly observable at any time and must be considered as internal or hidden state variables.

Internal State Variables Considered

When a body denoted by B is subjected to some traction or deformation history as shown in Figure 1, it will undergo a thermodynamic process which will in general be irreversible to some degree.

This irreversibility is introduced by such phenomena as dislocation movement and growth, fracture (both micro- and macroscale), friction (due to rubbing of fractured surfaces), grain boundary sliding, deformation twinning and chemical changes. However, due to the relative magnitudes of these energy dissipative processes the two primary internal state variables postulated to be of interest in this analysis are those of inelastic strain (α_{1ij}) representing dislocation phenomena and damage (α_{4ij}) representing microcracking. Although there may exist some interrelationship between these variables, they are considered to be independent as they represent different physical phenomena.

The two microstructural mechanisms which are considered to have the greatest prominence [10] at temperatures less than one half the melting temperature of the material under consideration are:

a. Drag Stress (α_2): representing locally averaged

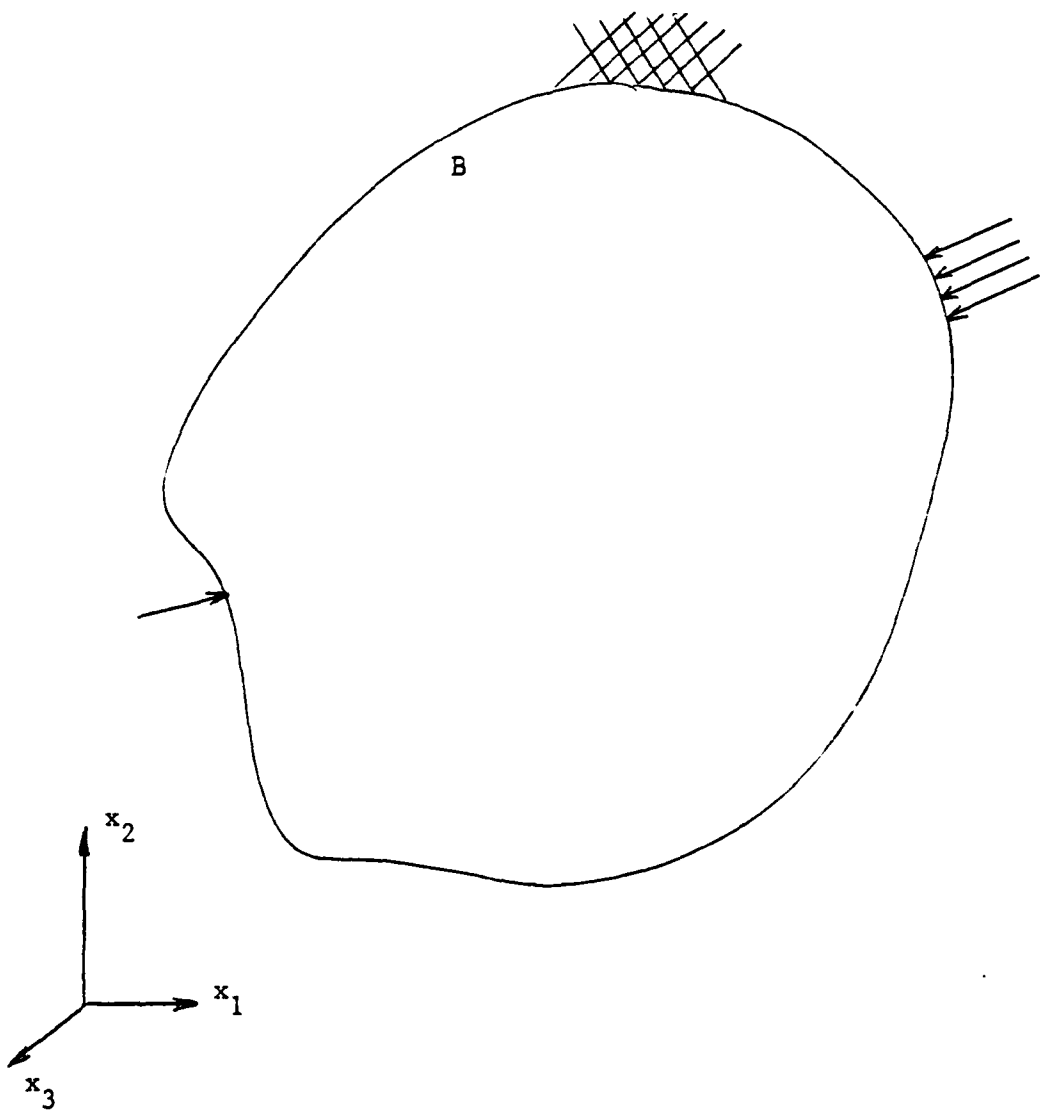

Figure 1

Arbitrary Body Subjected to Applied Tractions

dislocation density and producing isotropic hardening; and

b. Back Stress (α_{3ij}): representing the locally averaged dislocation arrangement and producing kinematic hardening (Bauschinger effect).

Factors Influencing the Growth of Inelastic Strain.

The primary independent internal state variables influencing the growth of damage are considered to be the historical inelastic strain and damage states, back stress and drag stress. The growth law for the inelastic strain is therefore postulated as follows [11]:

$$\dot{\alpha}_{1ij} = \dot{\lambda}(\varepsilon_{kl}, T, \alpha_{1kl}, \alpha_2, \alpha_{3kl}, \alpha_{4kl})\sigma_{ij}' \tag{27}$$

where:

$$\dot{\alpha}_2 = \dot{\alpha}_2(\varepsilon_{kl}, T, \alpha_{1kl}, \alpha_2, \alpha_{3kl}, \alpha_{4kl}) \tag{28}$$

$$\dot{\alpha}_{3ij} = \dot{\alpha}_{3ij}(\varepsilon_{kl}, T, \alpha_{1ij}, \alpha_2, \alpha_{3ij}, \alpha_{4kl}) \tag{29}$$

$\dot{\lambda}$ = scalar valued function of state

and σ_{ij}' = deviatoric stress tensor

It should be noted that the back stress and drag stress represent mechanisms which physically exist. However, dislocation arrangement and density are microstructural phenomena. Although they influence the growth of the inelastic strain, they do not directly enter into the stress-strain relations because they are not kinematic quantities.

Factors Influencing the Growth of Damage.

Damage is defined in this analysis as intergranular mechanisms such as grain boundary sliding, microvoid growth and microstructural cracks.

As the arrangement, density and growth of dislocations will effect the growth parameters (rate, direction) of any damage existing in the microstructure, the primary internal state variables influencing the growth of damage are considered to be inelastic strain, the previous damage state, back stress and drag stess. Therefore, the growth law for damage is postulated as:

$$\dot{\alpha}_{4ij} = \dot{\alpha}_{4ij}(\varepsilon_{kl}, T, \alpha_{1kl}, \alpha_2, \alpha_{3kl}, \alpha_{4kl}) \qquad (30)$$

for isotropic conditions:

$$\dot{\alpha}_{4ij} = f(\varepsilon_{kl}, T, \alpha_{1kl}, \alpha_2, \alpha_{3kl}, \alpha_{4kl})\delta_{ij} \tag{31}$$

It should be noted that although damage is obviously a directionally related quantity and therefore tensorial in nature, it is difficult to distinguish phenomenologically between damage and drag stress since both can interpreted as stiffness reducing mechanisms.

Functional Form of the Helmholtz Free Energy.

As the inelastic strain and damage are postulated to be the primary independent internal state variables affecting the constitution of the materials considered herein and both are functions of the back stress and drag stress, the Helmholtz free energy is postulated to have the following form:

$$h = h\,(\varepsilon_{kl}, T, g_k, \alpha_{1kl}, \alpha_{4kl}) \tag{32}$$

Thermodynamic Constraints.

Thermodynamic constraints on the form of the constitutive relations [equations (21) through (24)] can be accomplished using the Coleman-Mizel procedure [12] under the assumption of the Clausius-Duhem inequality [equation (16)]. In this procedure, the Helmholtz free energy [equations (32)] is implicitly differentiated with respect to its arguments as follows:

$$\begin{aligned} h = {} & \partial h/\partial \varepsilon_{kl}\dot{\varepsilon}_{kl} + \partial h/\partial T\,\dot{T} + \partial h/\partial g_m \dot{g}_m \\ & + \partial h/\partial \alpha_{1ij}\dot{\alpha}_{1ij} + \partial h/\partial \alpha_{4ij}\dot{\alpha}_{4ij} \end{aligned} \tag{33}$$

Substitution of equation (33) into the inequality (19) results in:

$$\begin{aligned} \rho T\Upsilon = {} & [\sigma_{kl}(\varepsilon_{mn},T,g_m,\alpha_{mn}{}^i) - \rho\partial h/\partial \varepsilon_{kl}(\varepsilon_{mn},T,g_m,\alpha_{mn}{}^i)]\dot{\varepsilon}_{kl} \\ & - [\rho\partial h/\partial T(\varepsilon_{mn},T,g_m,\alpha_{mn}{}^i) + \rho s(\varepsilon_{mn},T,g_m,\alpha_{mn}{}^i)]\dot{T} \\ & - \rho\partial h/\partial g_i(\varepsilon_{mn},T,g_m,\alpha_{mn}{}^i)\dot{g}_i \\ & - \rho\partial h/\partial \alpha_{ij}{}^k(\varepsilon_{mn},T,g_m,\alpha_{mn}{}^i)\ \Omega_{ij}{}^k(\alpha_{mn},Tg_m,\alpha_{mn}{}^i) \\ & - q_j(\varepsilon_{mn},T,g_m,\alpha_{mn}{}^i)g_j/T \geq 0 \end{aligned} \tag{34}$$

where i assumes the values of 1 and 4 representing the inelastic strain and damage respectively. On the basis of this technique it can be shown that the satisfaction of the First and Second Laws of Thermodynamics will lead to the following conclusions [2]:

$$h = h(\varepsilon_{kl}, T, \alpha_{1kl}, \alpha_{4kl}) \tag{35}$$

$$\sigma_{ij} = \rho \partial h / \partial \varepsilon_{ij} \tag{36}$$

$$s = - \partial h / \partial T \tag{37}$$

$$u = h + Ts \tag{38}$$

and $$\dot{\alpha}_{ij}{}^{q} = \Omega_{ij}{}^{q}(\varepsilon_{kl}, T, \alpha_{1kl}, \alpha_{2}, \alpha_{3kl}, \alpha_{4kl}) \tag{39}$$

Note that:

1) thermodynamically constraining the constitutive relations removes the dependence of the Helmholtz free energy on the temperature gradient g_k.

2) the above thermodynamically constrained forms of the constitutive relations [equations (36) through (38)] show an intrinsic dependence of stress, entropy and internal energy on the Helmholtz free energy.

Following the Coleman-Mizel procedure, inequality

(34) reduces to:

$$\rho T\gamma = -\rho \partial h/\partial \alpha_{ij}{}^{k}\, \Omega_{ij}{}^{k} - q_j g_j/T \geq 0 \qquad (40)$$

where the first term is called the internal dissipation and the last term is dissipation due to heat conduction.

Coleman and Gurtin [5] utilize inequality (40) to prove that:

$$q_i = k_{ij} g_j + 0(|g_j|) \qquad (41)$$

at an asymptotically stable equilibrium state where k_{ij} is the positive semidefinite thermal conductivity tensor. It will be assumed herein that these conditions hold and the higher order terms in equations (41) will be neglected.

Therefore, the specification of the Helmholtz free energy function [equations (35)] will completely define the constitutive equations (21) through (23) and equations (41) will define the constitutive equations (24). Thus, if the internal state variable growth laws (39) can be determined the field problem will be completely specified.

The Local Averaging Process

Constitutive relations (21) through (24) are theoretically pointwise in nature; that is, they are applicable to fixed infinitesimal material points. However, there is no practical method to construct experiments on material points since at the microscopic level the continuum assumption becomes invalid. Therefore, to obtain constitutive relations which are applicable to a continuum, it is considered acceptable to construct constitutive equations by subjecting local specimens to surface deformations or tractions which lead to spatially homogeneous stress and strain fields so that some local average of the pointwise observable state variables can be determined directly from the effects on the boundaries of the specimen.

As shown in Figure 2, the scale of the smallest dimension of a local specimen is generally constructed to be at least an order of magnitude larger than the scale of the largest material inhomogeneity. This sizing assists in preserving the continuum assumption while still averaging out the effects of point defects such as crystal lattice dislocations. Conversely, the scale of the largest dimension of a typical specimen should be small compared to the scale of the boundary value problem of interest. This constraint is necessary in order to preserve the notion that the constitutive equations are indeed pointwise in nature.

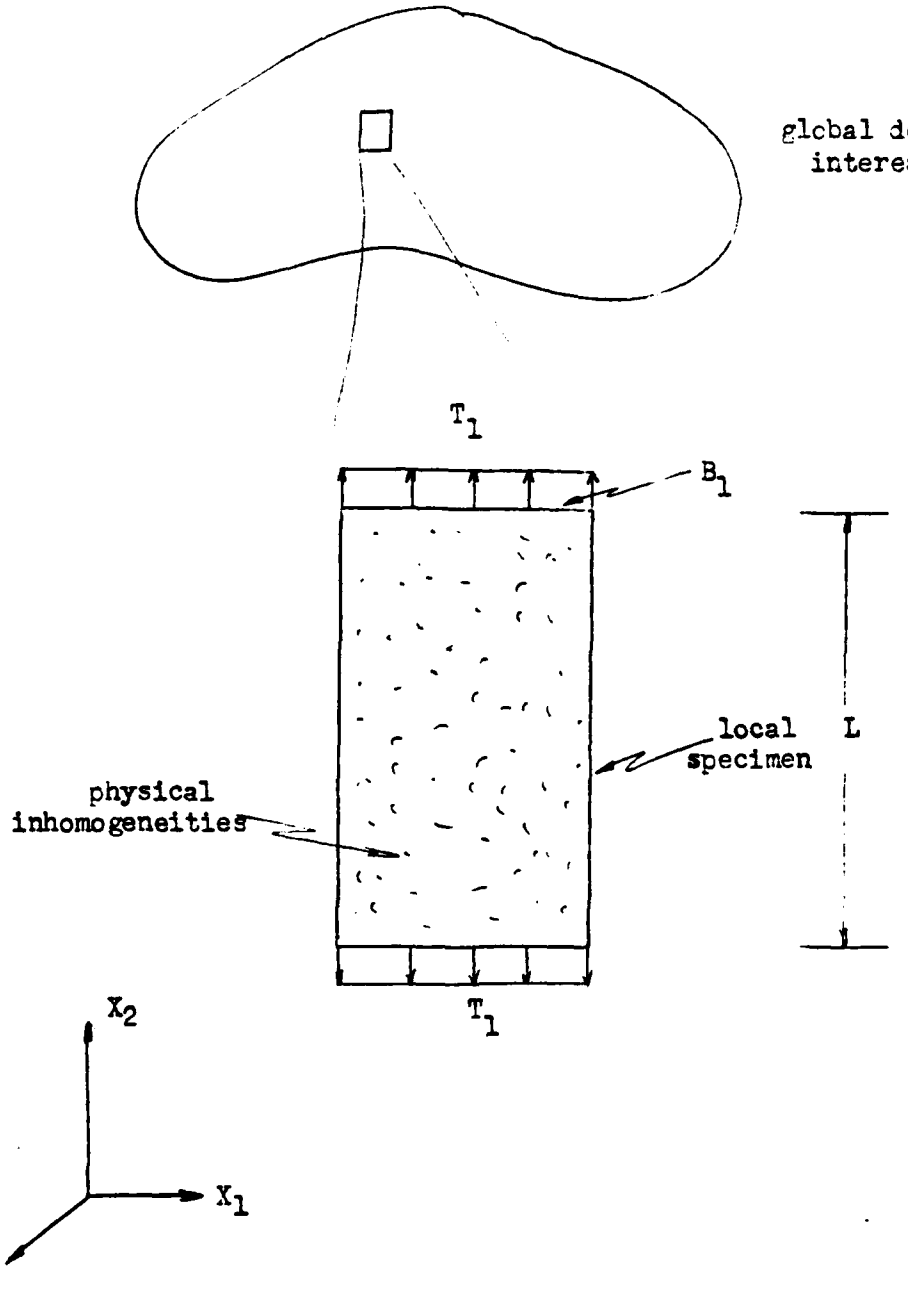

Figure 2

Dimension of Local Specimen

The local rather than pointwise constitutive equations that result from experimentation are assumed to be of the same form as pointwise equations (21) through (25). For example, in the uniaxial test described in Figure 2 it is customary to define the following:

$$\bar{\sigma}_{11} = 1/A \int_{B_1} \sigma_{11} dx_2 dx_3 \tag{42}$$

$$\bar{\varepsilon}_{11} = 1/L \int_{L} \varepsilon_{11} dx_1 \tag{43}$$

and

$$\bar{T} \equiv T(a_1, a_2, a_3) \tag{44}$$

where L is the local specimen gage length, A is the cross-sectional area in the x_2-x_3 plane, and (a_1, a_2, a_3) is some arbitrary point on the surface of the specimen. Utilizing these quantities, it is then hypothesized that:

$$\sigma_{11}(\varepsilon_{11}, T, \alpha_{kl}{}^{p}) = \bar{\sigma}_{11}(\bar{\varepsilon}_{11}, \bar{T}, \bar{\alpha}_{kl}{}^{p}) \tag{45}$$

where

$$\bar{\alpha}_{kl}{}^{p} = 1/V \int_{V} \alpha_{kl}{}^{p} dx_1 dx_2 dx_3 \tag{46}$$

and all quantities with bars represent the locally measured state variables.

Although equations (45) represent an often used way

of relating pointwise to experimental results, the local averaging process is nevertheless prone to shortcomings since the definitions (42) through (44) all represent nonunique relations between pointwise state variables and σ_{ij}, ε_{ij}, T, $\alpha_{ij}{}^{k}$ and their locally defined counterparts $\bar{\sigma}_{ij}$, $\bar{\varepsilon}_{ij}$, $\bar{T}$, $\bar{\alpha}_{ij}{}^{k}$. There are in fact an infinite number of distributions $\alpha_{kl}{}^{p}(x_1,x_2,x_3)$ which will result in identical values for $\bar{\alpha}_{kl}{}^{p}$. However, assuming that the scale of any inhomegeneities is small and that the distribution of $\alpha_{kl}{}^{p}$ is random, the specimen will be statistically homogeneous and the relation between $\bar{\alpha}_{kl}{}^{p}$ and $\alpha_{kl}{}^{p}$ will be approximately one to one. Note that for clarity the overbar will be excluded from expressions.

Determination of the Constitutive Equation Form.

To evaluate the constitutive form of the stress tensor and the entropy from the equalities given in equations (36) and (37), the pointwise Helmholtz free energy per unit mass is expressed as a second order Taylor Series expansion in the independent state variable arguments as follows:

$$h = A + B_{ij}\varepsilon_{ij} + 1/2C_{ijkl}\varepsilon_{ij}\varepsilon_{kl} + D\Delta T + 1/2E\Delta T^2$$

$$+ F_{ij}\alpha_{1ij} + 1/2G_{ijkl}\alpha_{1ij}\alpha_{1kl} + H_{ij}\alpha_{4ij}$$

$$+ \ 1/2J_{ijkl}\alpha_{4ij}\alpha_{4kl} + K_{ij}\varepsilon_{ij}\Delta T + L_{ij}\alpha_{1ij}\Delta T \qquad (47)$$

$$+ \ M_{ij}\alpha_{4ij}\Delta T + N_{ijkl}\varepsilon_{ij}\alpha_{1kl} + O_{ijkl}\varepsilon_{ij}\alpha_{4kl}$$

$$+ \ P_{ijkl}\alpha_{1ij}\alpha_{4kl}$$

If second order effects are neglected then the stress tensor can be evaluated from equation (36) by differentiating equations (47) with respect to the strain tensor as follows:

$$\sigma_{ij} = \rho\partial h/\partial\varepsilon_{ij}$$

$$\text{ie} \quad \sigma_{ij} = \rho(B_{ij} + C_{ijkl}\varepsilon_{kl} + K_{ij}\Delta T \qquad (48)$$

$$+ N_{ijkl}\alpha_{1kl} + O_{ijkl}\alpha_{4kl})$$

Now define:

$$\rho B_{ij} = \sigma_{ij}^{R}$$

$$-\rho K_{ij}\Delta T = C_{ijkl}\varepsilon_{kl}^{T}$$

(48a)

$$-\rho N_{ijkl}\alpha_{1kl} = C_{ijkl}\alpha_{1kl}$$

$$-\rho O_{ijkl}\alpha_{4kl} = C_{ijkl}\alpha_{4kl}$$

Substitution of equations (48a) into equations (48) yields:

$$\sigma_{ij} = \sigma_{ij}^{R} + C_{ijkl}(\varepsilon_{kl} - \alpha_{1kl} - \alpha_{4kl} + \varepsilon_{kl}^{T}) \qquad (49)$$

where σ_{ij}^{R} = residual stress tensor, and

ε_{ij}^{T} = thermal strain tensor.

The expression for entropy can be readily obtained by differentiating equation (47) with respect to temperature.

A coupled heat equation can also be obtained by substituting equation (18) into (14), imposing the conditions of equations (35) through (37) and then subtituting the Helmholtz free energy expression into the result [3].

Description of the Internal State.

Consider an arbitary region denoted by B as shown in Figure 3. (The body B is assumed to be small on a scale to a boundary value problem of interest). Now consider an arbitary local element denoted as L with external surfaces S1 which are chosen normal to a set of Cartesian coordinate axes (x_1, x_2, x_3) as shown in Figure 4. Although the element L is an intrinsic part of the body B, it can be thought of as being removed from B and the

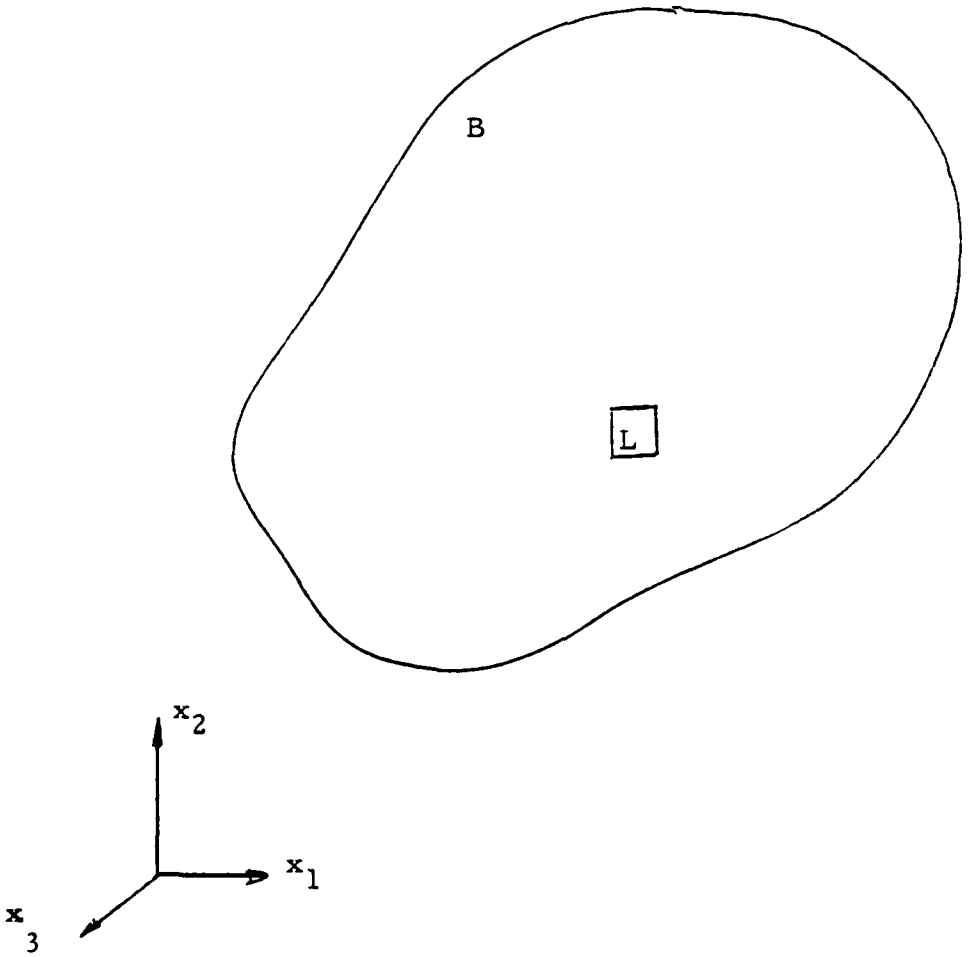

Figure 3

General Bounded Continuum of Interest

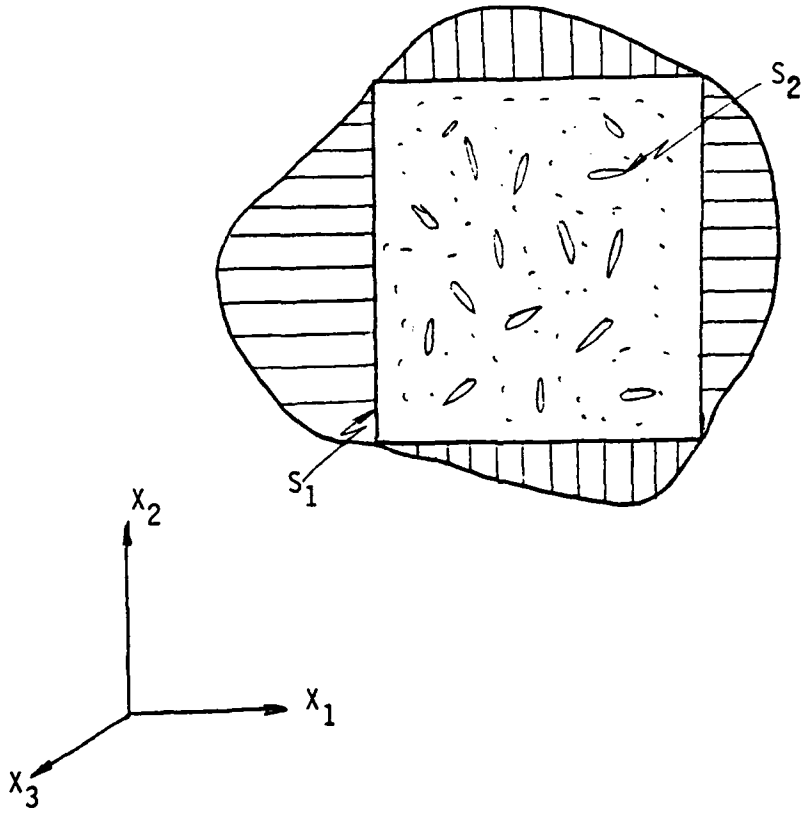

Figure 4

Local Volume Element V

newly created surfaces subjected to appropriate boundary conditions so that the response of the element L to an imposed boundary condition is identical to that of the element when it is located in B. The scale of L is chosen so that its dimensions are small compared to the dimensions of B. However, the dimensions of L are also large enough to guarantee statistical homogeneity of the material properties and existing defects even though the total surface area of the defects may be the same order of magnitude as S1.

Internal surfaces resulting from fracture are labelled S2. The volume of the element is defined to be V, which includes the volume of any damage (cracks and/or voids) denoted as V_c.

In order to describe the internal state, we first consider the kinematics of a typical point O with neighboring points A and B as shown in Figure 5. Before deformation lines OA and OB are orthogonal as shown in Figure 5a. After deformation we imagine that the lines joining O',A' and B' are as shown in Figure 5b and just at the instant that deformation is completed, a crack forms normal to the plane of AOB through point O' as shown in Figure 5c. Furthermore, point O' becomes two material points O' and O'' on opposite crack faces and points A' and B' deform further to points A'' and B''. It is assumed that all displacements, including crack opening are infinitesimal so that

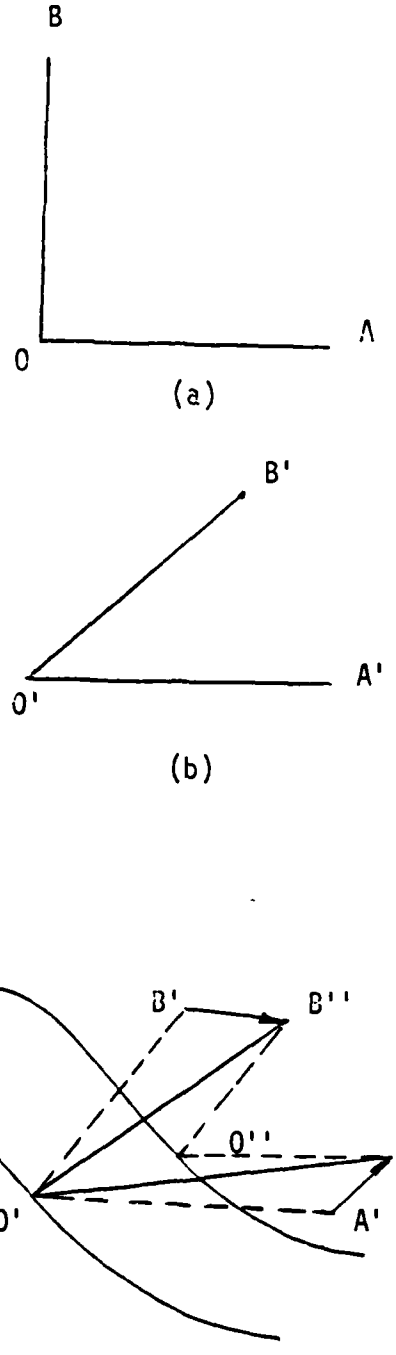

Figure 5

Kinematics of the Damage Process

a) Point O Prior to Deformation,

b) Point O After Deformation and Prior to Fracture Process,

c) Point O After Fracture.

the observer at an appropriate observation distance from point O sees only the deformation A'' O' B''. The strain associated with this deformation is appropriately called an observable state variable. However, the strain of interest is associated with A''O''B''. Therefore, it is essential to construct an internal state variable which will relate these two strain descriptions.

We therefore construct the vectors u^c connecting O' and O'' and n^c describing the normal to the crack face at O' as shown in Figure 6. It should be noted that u^c can be used to construct a pseudo-strain representing the difference in rotation and extension of lines A''O''B''.

The rate of change of surface energy released per unit local volume due to cracking in L [3] is given by:

$$u_L{}^c = -1/\rho_L V_L \int_{S_2} \sigma_{ij} u_i n_j \, dS \tag{50}$$

Assuming that any cracks in the body recover elastically, that is, close upon the removal of the load, then we further assume that this process is reversible and that tractions $\dot{T}$ can be applied at point O' which will close the crack:

$$u_L{}^c = 1/\rho_L V_L \int_{S_2} T_i{}^c u_i{}^c \, dS \tag{51}$$

Using Cauchy's formula Equation (46) can be placed in the form:

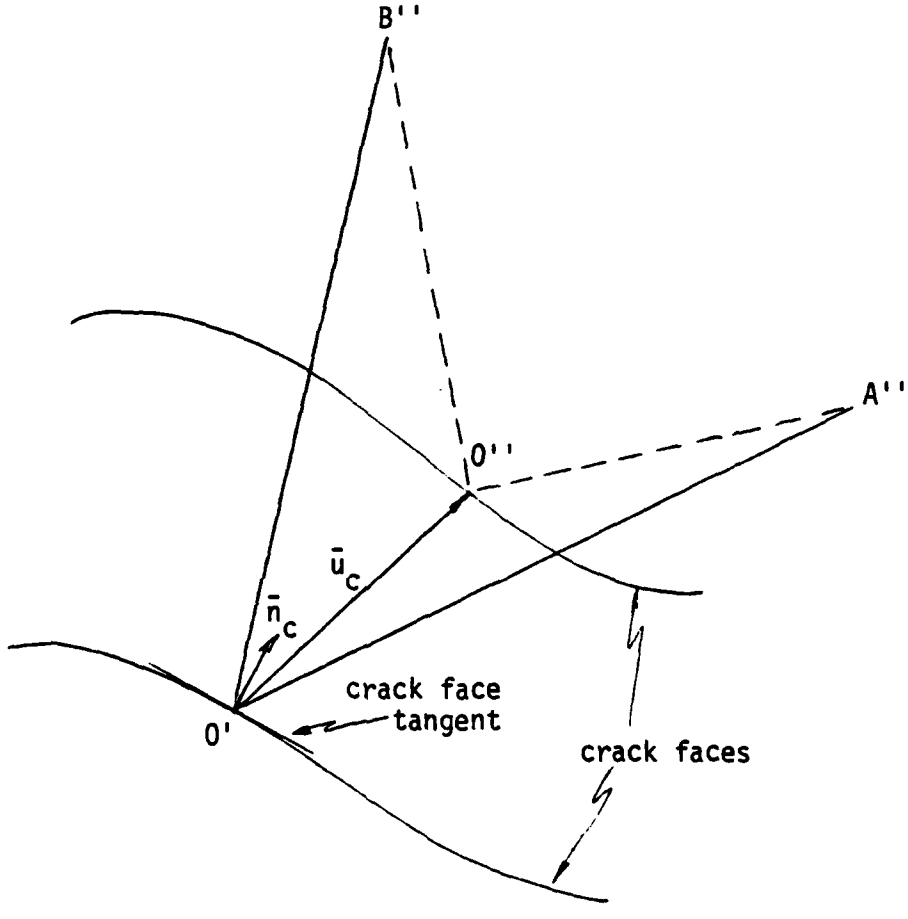

Figure 6

Description of the Internal State at O

$$u_L^c = 1/\rho_L V_L \int_{S_2} \sigma_{ij}{}^c u_i{}^c n_i{}^c \, dS \tag{52}$$

where the subscripts denote quantities associated with the actual crack geometry.

Guided by the fact that u^c and n^c describe the kinematics of the cracking process at point 0, we now define the following second order tensor valued internal state variable to describe damage:

$$\alpha_{ij} = u_i{}^c n_j{}^c \tag{53}$$

We now define the locally averaged internal state variable describing damage to be:

$$\alpha_{4ij} = k/\rho_L V_L \int_V u_i n_j \, dS \tag{54}$$

where Sc = surface area of cracks, and

k = a constant resulting from the simplification of equations (48) to equations (49).

Mathematical Model for Damage

The damage model considered in this paper classifies damage as a displacement related mechanism; current models [13] classify damage as a stiffness reducing mechanism. For the case of infinitesimal strains, the following section demonstrates that the model proposed herein is consistent with these existing models.

Kachanov's reduced stiffness model [13] is given by:

$$\sigma_{ij} = B_{ij} + C_{ijkl}'(\varepsilon_{kl} - \alpha_{1kl} - \varepsilon_{kl}^{T}) \tag{55}$$

Equations (55) can be shown to be equivalent to equations (48a) by first equating as follows:

$$C_{ijkl}(\varepsilon_{kl} - \alpha_{1kl} - \alpha_{4kl} - \varepsilon_{kl}^{T}) = C_{ijkl}'(\varepsilon_{kl} - \alpha_{1kl} - \varepsilon_{kl}^{T}) \tag{55a}$$

Now let:

$$C_{ijkl}' = C_{ijkl} - \Psi_{ijklmn}\alpha_{4mn} \tag{56}$$

then (55a) becomes:

$$C_{ijkl}(\varepsilon_{kl} - \alpha_{1kl} - \alpha_{4kl} - \varepsilon_{kl}^{T}) = (C_{ijkl} - \Psi_{ijklmn}\alpha_{4mn})(\varepsilon_{kl} - \alpha_{1kl} - \varepsilon_{kl}^{T})$$

$$\Rightarrow \quad C_{ijkl}\alpha_{4kl} = \Psi_{ijklmn}\alpha_{4mn}(\varepsilon_{kl} - \alpha_{1kl} - \varepsilon_{kl}^{T})$$

$$\Rightarrow \quad C_{ijkl}\alpha_{4kl} = \Psi_{ijmnkl}\alpha_{4kl}(\varepsilon_{mn} - \alpha_{1mn} - \varepsilon_{mn}^{T})$$

$$\Rightarrow \quad [C_{ijkl} - \Psi_{ijmnkl}(\varepsilon_{mn} - \alpha_{1mn} - \varepsilon_{mn}^{T})]\alpha_{4kl} = 0$$

Therefore,

$$\Psi_{ijmnkl}(\varepsilon_{mn} - \alpha_{1mn} - \varepsilon_{mn}^{T}) = C_{ijkl} \tag{57}$$

UNIAXIAL FORM OF THE MODEL

For the purpose of this analysis, the temperature field is assumed to be significantly less than 1/2Tm. Therefore, if thermal strain is neglected, the uniaxial isothermal form of equation (44) is given by:

$$\sigma = \sigma^{R} + E(\varepsilon - \alpha_{1} - \alpha_{4}) \tag{58}$$

Consider the input strain profile shown in Figure 7. The stress-strain curve resulting from a uniaxial tension test of a metal matrix coupon using this strain profile is given in Figure 8. Denote the slope of the elastic portion of the load-up curve as (E) and the slope of the unloading curve as (E_t).

The slope (E_t) is defined as:

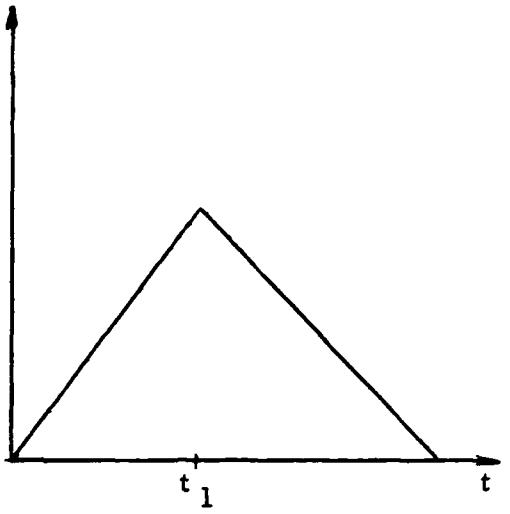

Figure 7

Input Strain Profile

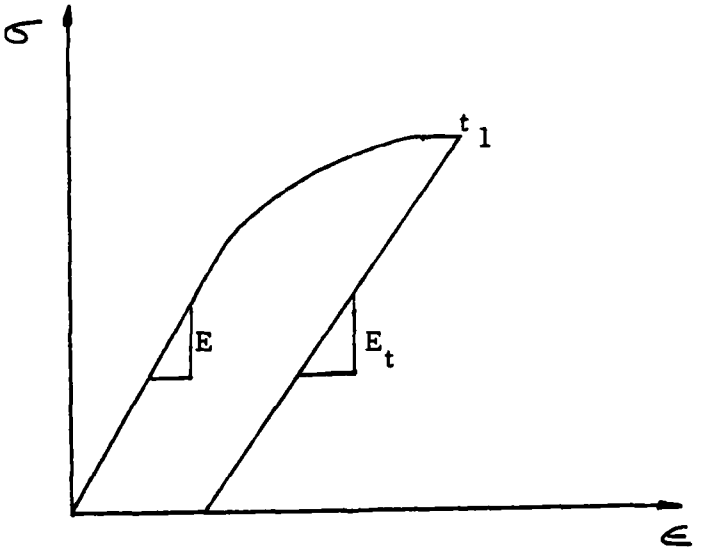

Figure 8

Stress-Strain Curve

$$E_t = \partial\sigma/\partial\varepsilon \tag{59}$$

Thus, differentiating Equation (58) with respect to the strain tensor gives:

$$E_t = E(1 - \partial\alpha_1/\partial\varepsilon - \partial\alpha_4/\partial\varepsilon) \tag{60}$$

If the specimen is unloaded following the application of a traction or deformation field the inelastic strain remains constant as the strain energy ($\sigma\varepsilon$) has substantially decreased due to the decrease in the applied stress (σ). This is shown diagramatically in in Figure 9.

Therefore, for unloading:

$$\partial\alpha_1/\partial\varepsilon = 0 \tag{61}$$

and Equation (60) becomes:

$$E_t = E(1 - \partial\alpha_4/\partial\varepsilon) \tag{62}$$

Now, if the aluminium matrix is linear elastic on unloading then E_t is constant on unloading and the implication is that:

$$\partial\alpha_4/\partial e = \text{constant (on unloading)} \tag{63}$$

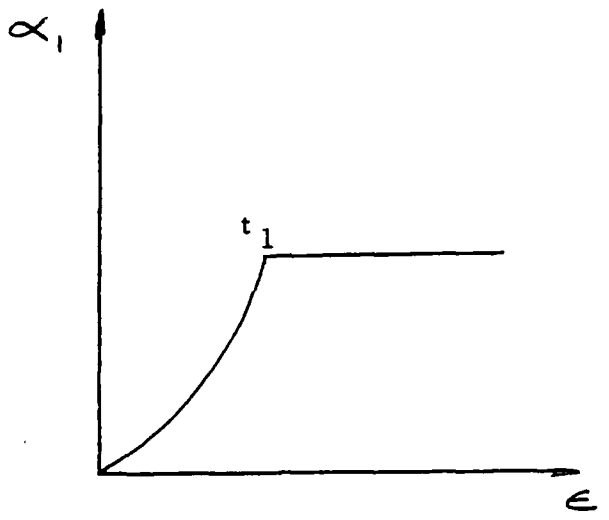

Figure 9

Inelastic Strain vs Input Strain Curve

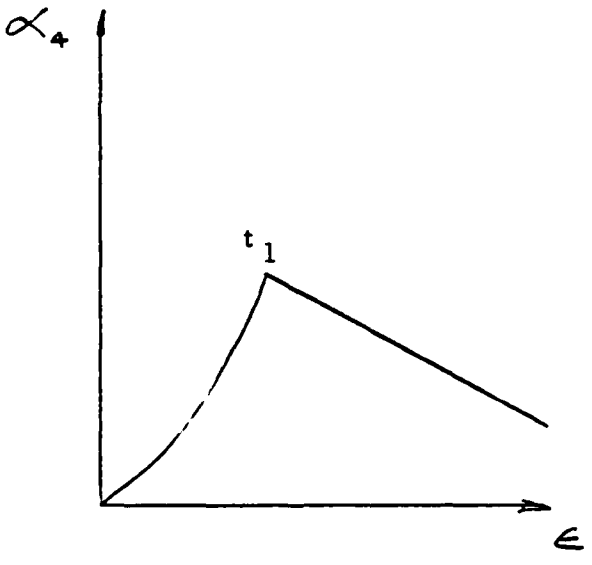

Figure 10

Damage vs Input Strain Curve

The curve corresponding to this result is given at Figure 10.

EXPERIMENTAL VERIFICATION OF MODEL

In order to qualitatively verify the supposition that the inelastic strain tensor (α_{1ij}) can be regarded to be an internal state variable, consider the example of a uniaxial bar subjected to applied displacements such that the end tractions will be evenly distributed. It is customary to deduce the inelastic strain in an experiment of this type by utilizing the output from a loadcell to determine the stress and then make use of equations (58) to determine the elastic strain. However, equations (58) entail the damage tensor (α_{4ij}). Therefore an experimental procedure is required to distinguish between deformation due to inelastic strain (back stress and drag stress) and that due to damage. The procedure proposed is demonstrated by equations (61) and (63) and illustrated in Figures 9 and 10.

Therefore, it is proposed that the inelastic strain and damage resulting from an applied stress or deformation field can be distinguished experimentally; the inelastic strain is obtained from the unrecovered strain and the damage is related to the change in slope between the loadup and unloading portions of

the stress-strain curve.

CONCLUSIONS

The foregoing analysis has developed a constitutive model for the inelastic deformation of a continuum with damage. Following the application of thermodynamic constraints on the form of the constitutive relations and a kinematically justifiable definition of the Helmholtz free energy, a constitutive equation relating the stress tensor to the total strain tensor, the inelastic strain tensor and the damage tensor was developed. Experimental results from uniaxial tests carried out on aluminium matrix material with silicon carbide fibres has determined that a global measure of microstructural damage could be directly related to the slope differential between the load-up and unloading curves on the uniaxial stress-strain plot [14].

ACKNOWLEDGEMENT

The authors gratefully acknowledge the support provided for this research by the Air Force Office of Scientific Research under contract no. F49620-83-0067.

REFERENCES

1. Hill, R., "The Mathematical Theory of Plasticity," Oxford University Press, 1950.

2. Allen D.H., "Thermodynamic Constraints on the Constitution of a Class of Thermoviscoplastic Solids," Texas A&M Mechanics and Materials Center, Report No. MM12415-82-10, December 1982.

3. Allen, D.H., Haisler, W.E. and Harris, C.E., "Research on Damage Models for Continuous Fibre Composites," Texas A&M University Report No. MM 5023-85-4, February 1985.

4. Kratochvil, J., and Dillon, O.W., Jr., "Thermodynamics of Crystalline Elastic-Visco-Plastic Materials," Journal of Applied Physics, Vol. 41, pp. 1470-1479, 1970.

5. Coleman, B.D. and Gurtin, M.E., "Thermodynamics with Internal State Variables," Journal of Chemical Physics, Vol. 47, pp.597-613, 1967.

6. Coleman, B.D. and Noll, W., "The Thermodynamics of Elastic Materials with Heat Conduction and Viscosity," Archive for Rational Mechanics and Analysis, Vol. 13, p.167, 1963.

7. Allen, D.H., "Development of a Thermdynamically Consistent Coupled Heat Conduction Equation for a Class of Thermoviscoplastic Crystalline Solids," Texas A&M Mechanics and Materials Center, Report No. MM 12415-82-3, May 1982.

APPENDIX 6.2

Mechanics and Materials Center
TEXAS A&M UNIVERSITY
College Station, Texas

EFFECT OF DEGRADATION OF MATERIAL PROPERTIES ON THE DYNAMIC RESPONSE OF LARGE SPACE STRUCTURES

S. KALYANASUNDARAM
J. D. LUTZ
W. E. HAISLER
D. H. ALLEN

MM4875-85-3

FEBRUARY 1985

SECURITY CLASSIFICATION OF THIS PAGE

REPORT DOCUMENTATION PAGE

1a. REPORT SECURITY CLASSIFICATION: unclassified	1b. RESTRICTIVE MARKINGS: NA
2a. SECURITY CLASSIFICATION AUTHORITY: NA	3. DISTRIBUTION/AVAILABILITY OF REPORT: unlimited
2b. DECLASSIFICATION/DOWNGRADING SCHEDULE: NA	
4. PERFORMING ORGANIZATION REPORT NUMBER(S): MM-4875-85-3	5. MONITORING ORGANIZATION REPORT NUMBER(S): NA
6a. NAME OF PERFORMING ORGANIZATION: Aerospace Engr. Dept. / 6b. OFFICE SYMBOL (If applicable): NA	7a. NAME OF MONITORING ORGANIZATION: Air Force Office of Scientific Research
6c. ADDRESS (City, State and ZIP Code): Texas A&M University, College Station, Texas	7b. ADDRESS (City, State and ZIP Code): Bolling AFB, Washington, D.C. 20332
8a. NAME OF FUNDING/SPONSORING ORGANIZATION: Air Force Office of Scien. Res. / 8b. OFFICE SYMBOL (If applicable):	9. PROCUREMENT INSTRUMENT IDENTIFICATION NUMBER: NA
8c. ADDRESS (City, State and ZIP Code): Bolling AFB, Washington, DC 20332	10. SOURCE OF FUNDING NOS.

PROGRAM ELEMENT NO.	PROJECT NO.	TASK NO.	WORK UNIT NO.
F49620-83-C-0067			

11. TITLE (Include Security Classification): Effect of Degrad. of Material Properties on the Dynamic Response of Large Space Structures

12. PERSONAL AUTHOR(S): S. Kalyanasundaram, J.D. Lutz, W.E. Haisler, D.H. Allen

13a. TYPE OF REPORT	13b. TIME COVERED	14. DATE OF REPORT (Yr., Mo., Day)	15. PAGE COUNT
Interim	FROM _____ TO _____	February 1985	

16. SUPPLEMENTARY NOTATION

17. COSATI CODES			18. SUBJECT TERMS (Continue on reverse if necessary and identify by block number)
FIELD	GROUP	SUB. GR.	

19. ABSTRACT (Continue on reverse if necessary and identify by block number)

In this paper the effect of degradation of material properties on structural frequencies and mode shapes of Large Space Structures (LSS) is investigated. The difficulty and cost maintenance of LSS make it a necessity to design these structures to operate with a certain amount of load-induced damage. This damage is commonly observed in fibrous composite media.

Sensitivity studies conducted on representative space truss structures indicate that degradation of material properties may have a significant effect on the structural mode shapes and frequencies. For even small amounts of reduction in stiffness (10%), frequencies and modal locations may change significantly. It is clear that these effects must be taken into consideration when designing control systems for Large Space Structures.

20. DISTRIBUTION/AVAILABILITY OF ABSTRACT	21. ABSTRACT SECURITY CLASSIFICATION
UNCLASSIFIED/UNLIMITED ☒ SAME AS RPT. ☐ DTIC USERS ☐	unclassified

22a. NAME OF RESPONSIBLE INDIVIDUAL	22b. TELEPHONE NUMBER (Include Area Code)	22c. OFFICE SYMBOL
David H. Allen	(409) 845-1669	

DD FORM 1473, 83 APR EDITION OF 1 JAN 73 IS OBSOLETE. unclassified

SECURITY CLASSIFICATION OF THIS PAGE

EFFECT OF DEGRADATION OF MATERIAL PROPERTIES ON THE DYNAMIC RESPONSE OF LARGE SPACE STRUCTURES

S. Kalyanasundaram*, J. D. Lutz*, W. E. Haisler**, and D. H. Allen***
Texas A&M University
College Station, Texas 77843

Abstract

In this paper the effect of degradation of material properties on structural frequencies and mode shapes of Large Space Structures (LSS) is investigated. The difficulty and cost of maintenance of LSS make it a necessity to design these structures to operate with a certain amount of load-induced damage. This damage is commonly observed in fibrous composite media.

Sensitivity studies conducted on representative space truss structures indicate that degradation of material properties may have a significant effect on the structural mode shapes and frequencies. For even small amounts of reduction in stiffness (10%), frequencies and nodal locations may change significantly. It is clear that these effects must be taken into consideration when designing control systems for Large Space Structures.

Introduction

Due to economic constraints, it is projected that advanced high strength-to-weight ratio aerospace materials will be utilized in future generation space structures. Such materials include polymer and metal matrix fibrous composites, which are known to undergo a certain amount of load induced damage.[5,6] These materials are also expected to undergo a certain amount of environmentally induced damage or degradation, thus resulting in significant stiffness losses.

Experimental research on advanced composite materials indicates that the material may undergo up to 15 percent loss in stiffness due to thermomechanical fatigue, which causes a variety of damage modes in the structure. Additional loss of stiffness may be attributed to elevated temperature and chemical changes due to solar radiation and other environmental effects. This reduction in stiffness affects the dynamic response which in turn is critical in the development of control systems for LSS. In this paper, sensitivity studies will be presented which investigate the effect of stiffness loss on structural frequencies and mode shapes.

The advent of the space shuttle has made possible the development of LSS. Control systems for stabilizing and maneuvering these very large space structures, especially those for precise pointing, will require extension of current technology.

Although large size by itself does not arouse concern, structural flexibility resulting from minimizing the structural weight in non-gravitational fields may present problems. Extremely large structural flexibility may result in large amplitudes and low frequencies (.01 to 10 Hz) which may create new complications for control designers.

As an example of the precision required[1], a typical radiometry application may utilize a 200 meter antenna with an effective beam width of 0.01 degrees and have requirements limiting the vibratory beam shift to less than 0.005 degrees and dynamic surface distortions to less than 1mm. Maneuvering or maintaining the altitude of such a satellite leads to flexible body motion which must be well predicted and controlled.

The importance of interaction between control systems and vibratory response has caused considerable research in LSS control systems.[2-4] The current practice of guaranteeing a large separation between modal frequencies and the bandwidth of control will not be adequate in future applications. The combination of large size and payload-weight restrictions will drive structural frequencies down and the need for more accurate pointing will drive the control system bandwidth up. When sufficient frequency separation becomes impossible, there exists a need for adaptive control systems. This leads to further research in the design of structural control systems actuator/sensor placement, and distributed sensing and actuation as opposed to co-located sensors and actuators.

Techniques for achieving modal control of LSS will require a more accurate knowledge of modal characteristics. Optimum sensor and actuator placement will be greatly influenced by modal effects which must be known to a greater degree of precision.

Problem Summary

In order to investigate the possible effects of material degradation on the dynamic response of LSS, a representative space truss structure has been selected in the shape of a long boom as shown in Fig. 1. Using several loading histories, stress distributions have been obtained for each truss member. The resulting stress distributions can be used in a material damage model to define material degradation and resultant stiffness reductions. Using the reduced stiffness properties, modal analyses have been conducted on the structure to show the effect of material degradation on natural frequencies, mode shapes and nodes. Details of the finite element model, material degradation model, and numerical results are presented below.

* Research Assistant, Aerospace Engineering
** Professor and Head, Aerospace Engineering
Associate Fellow AIAA
*** Assistant Professor, Aerospace Engineering
Member AIAA

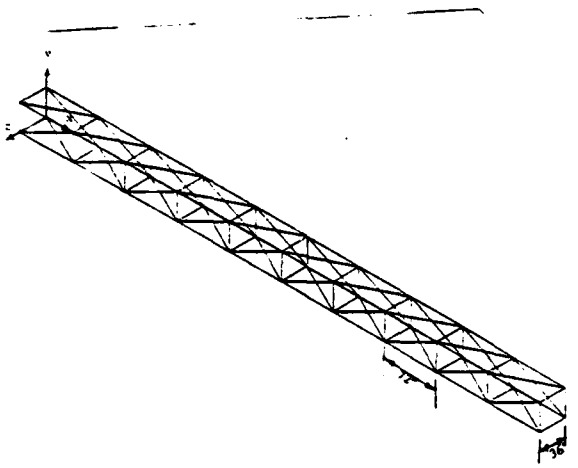

Fig. 1 Space Truss Structure

Model Description

Material Degradation Model

The process of ultimate failure of composite materials is preceded by a sequence of microstructural and macrostructural events which are termed as damage. These events may be due to transverse cracking, delamination, fiber breaking and fiber-matrix debonding.[5-11] The mechanical response of the structure is affected by this damage. Global material properties like stiffness and residual strength may be substantially altered during the life of the structural components.[5-6] Some of the analytical studies for modeling damage include a shear lag concept,[10] fracture based concepts,[12-14] and internal state variable theories.[12-14] Although important progress has been made, current understanding of damage is not complete.

Damage in polymeric composites is modelled in this paper as a load history-dependent reduction in stiffness in each structural element. The internal state variable theory (ISV) is used for modeling mechanical behavior and the stress strain relationship is of the form,[12-13]

$$\sigma_{ij} = C'_{ijkl} (\varepsilon_{kl} - \varepsilon_{kl}^{T}) \qquad (1)$$

In this case, the ISV are assumed to be second order tensor valued and to enter only through the modulus tensor. C'_{ijkl} is the effective modulus tensor given by

$$C'_{ijkl} = C_{ijkl} - {}^{p}P_{mnklij}\,\alpha^{p}_{mn}\,, \quad p=1,\ldots,r \qquad (2)$$

where α^{p}_{mn} are a set of r internal state variables[12] which are given by the following set of ISV growth laws,

$$\dot{\alpha}^{p}_{mn} = \Omega^{p}_{mn}(\varepsilon_{kl}, T, \alpha_{kl}^{q}) \qquad (3)$$

At low homologous temperatures these materials are assumed to be rate insensitive so that the above model will result in quasi-elastic (rate independent) equations in which inelasticity is reflected only through the slowly degrading modulus tensor. Experimental evidence[6,10] indicates that the time scale for degradation of C'_{ijkl} is very long compared to the frequencies and mode shapes of representative structures. It is therefore sufficient for many space structural applications to treat equations (1) in the degraded state only.

The stress-strain relationship for the truss elements is a one-dimensional approximation of equations (2) given by

$$\sigma_{xx} = E'(\varepsilon_{xx} - \varepsilon^{T}_{xx}) \qquad (4)$$

where σ_{xx} and ε_{xx} are the uniaxial stress and strain, ε^{T}_{xx} is the thermal strain, and E' is the axial stiffness of the truss element given by

$$E' = E\,(1 - \alpha) \qquad (5)$$

where E is the undegraded axial stiffness and α is a scalar valued parameter representing the integrated effect of all damage modes such as matrix cracking, interlaminar fracture, fiber breakage, and fiber-matrix debonding.

Experimental research on composite materials indicates a power law degradation of axial stiffness as a function of stress history.[11,13] Hence the damage ISV growth law is assumed to be of the form

$$\dot{\alpha} = k_1\,(\sigma/\sigma_{max})^{n} \qquad (6)$$

where k_1 and n are material parameters, σ_{max} is the maximum stress in the structure, and σ is the axial stress in each truss element. For constant stress amplitude, equation (6) may be integrated in time to give the following approximation

$$\alpha(t_1) = k'_1\,[\sigma(t_1)/\sigma_{max}]^{n'} \qquad (7)$$

where k'_1 and n' are material parameters which may be time dependent.

A power law form of damage is used herein for simplicity and for an initial attempt at modeling the structural response with damage. In reality the damage laws will be more complex and are currently being developed for future work.[12]

Finite Element Model

Figure 1 illustrates the geometry of the representative space truss used to simulate an antenna boom. This structure is sixty feet long with 10 bays, six feet long by three feet wide. The finite element model has 124 space truss elements and 44 nodes. In the initial undegraded configuration, the material properties are the same for all members with the following values:

Material type: Graphite epoxy (Hexel)
Young's modulus E = 21.5×10^6 psi
Cross sectional area = 1.0 in^2
Density = 0.065 lb/in^3
Coefficient of thermal expansion = 2×10^{-6} $in/in/^oF$
Reference temperature = 89.6^oF

Each truss member is idealized with a standard six degree of freedom truss element of constant cross section. Because the structure is idealized as linear with slowly varying material properties, conventional linear finite element methodology may be used to write global equations of equilibrium of the form[16-17]

$$[M]\{\ddot{q}\} + [K]\{q\} = \{Q\} \qquad (8)$$

where [M] is the mass matrix, [K] is the stiffness matrix, {q} is the nodal displacement vector, and {Q} is the nodal force vector. The stiffness matrix [K] is dependent on the spatially variable damage state α which varies from element to element. Standard eigenvalue extraction may be performed; in this case, subspace iteration was used to obtain the first five frequencies and mode shapes.

Spatial Distribution of Degradation

The spatial distribution of degradation and stiffness reduction of LSS will be complex and dependent on loading and environmental history. For the present investigation, wherein material degradation is assumed to be a function of stress history, it was necessary to make some assumptions about the corresponding stress history and spatial distribution of stresses within the LSS.

Two approaches were used to obtain candidate stress histories/distributions for predicting the stiffness degradation. In one case, the stress distribution was obtained for an assumed thermal load history/distribution. Secondly, a modal approach was used wherein it was assumed that primary degradation occurred in the first two bending modes of the structure. After computing the mode shapes for the first two undegraded bending modes, the nodal displacements were used to compute a corresponding stress distribution.

In each case, the degradation model given by equation (7) was then used to obtain degraded properties for each truss member assuming that the element stressed the most was degraded a specified percentage. The resultant structure with degraded properties has spatially variable stiffness that varies from element to element. Mode shapes and frequencies were then computed with varying maximum percentages of degraded properties.

Discussion of Results

Natural frequency and mode shape responses have been obtained for several stress-induced degradation test cases as described above for the representative space truss structure shown in Fig. 1. This particular truss structure geometry, representing a segment of a boom, is similar to ones being used for other PACOSS related work. Assuming the boom is fixed on one end (at x=0), the five lowest frequencies (for the virgin structure) are equal to 3.4 Hz, 4.5 Hz, 4.6 Hz, 19.2 Hz, and 20.3 Hz. The first mode is a combined torsion-inplane shear mode, the next two modes are bending modes about the z and y axes, respectively, and the fourth mode is a pure torsion mode.

The first case considers the boom structure shown in Fig. 1 (which is assumed to be fixed on one end) with a thermal gradient over the cross-section. It is likely that one surface of the space structure will become significantly hotter than the other surface due to solar heating, attitude of the structural elements and shadowing effects. To investigate the effect of this thermal gradient through the depth of the truss, the stresses in each element were calculated by specifying a temperature of 122^oF for the members on the top surface, 80.6^oF for the members on the bottom surface and 100^oF for the diagonal members connecting the top and bottom surface. With this thermally-induced stress distribution, the axial stiffness of each element was degraded by using equation (7). The maximum level of degradation (loss of stiffness) was set to a prescribed percentage for the element with the highest stress and remaining elements were degraded according to their stress level by using equation (7). The value of n' in equation (7) was assumed to be 0.75.

In Fig. 2 the first three natural frequencies are plotted for different levels of damage. The effect of damage on the natural frequencies is clear. Increasing the level of damage reduces the stiffness of the space truss and this in turn drives the natural frequencies down significantly even for modest damage states. For a maximum loss of 25% in axial stiffness (for the highest stressed members), the first three natural frequencies are reduced by about 8%. Since mode shapes are

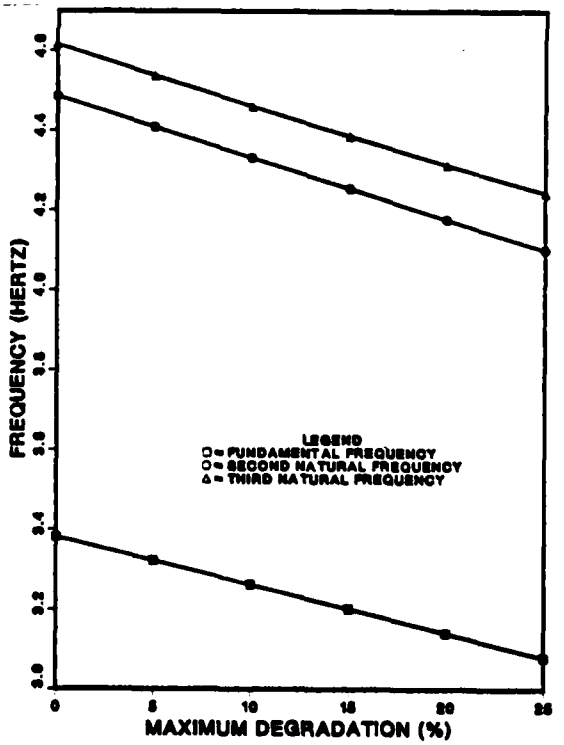

Fig. 2 Effect of Damage on Natural Frequencies

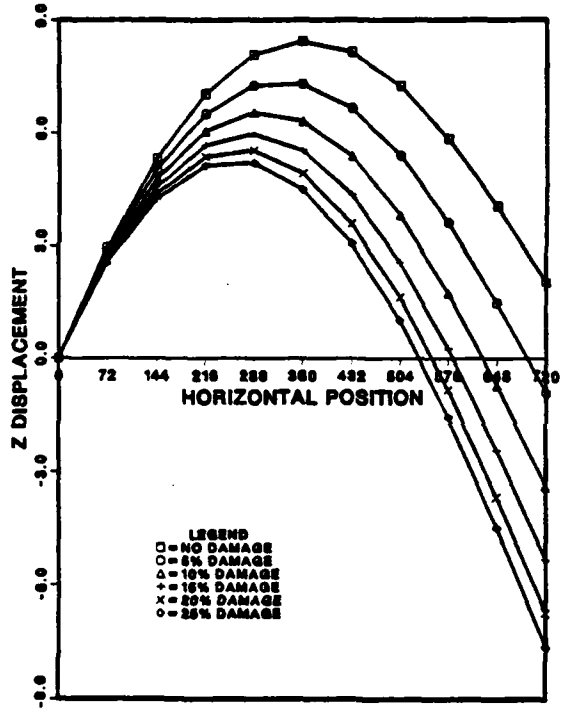

Fig. 3 Effect of Degradation on Second Mode

important for designing the control systems of the large space structures, it is desirable that they be constant with time. Although it was found that there was no appreciable change in the first mode shape between the undegraded and degraded cases, higher modes were altered due to material degradation. Figure 3 is a plot of the z displacement for the second mode shape along the length of the space truss (z=0, y=0). Significant changes in the mode shape and node locations as a function of percent degradation are observed. The sign of the modal displacement is reversed near the free edge for the degraded and undegraded cases and the location of the node (zero displacement) changes appreciably. Figure 4 is a similar plot of the y displacement along the length of the space truss for the third mode.

The value of n' in equation (7) was varied from 0.25 to 1.0 to study its effect on the mode shapes. It was found that the trend in mode shape changes was similar for different n'. Figure 5 illustrates this point. Here the z displacement for the second mode is plotted along the length of the space truss for different values of n' (maximum reduction in axial stiffness was 20%). The plot indicates that increasing n' (i.e., decreasing the nonlinearity of the degradation model) tends to increase the changes in the modal displacements. Such nonlinearity becomes increasingly important when stresses vary spatially over the structure, i.e., some members are highly stressed compared to others.

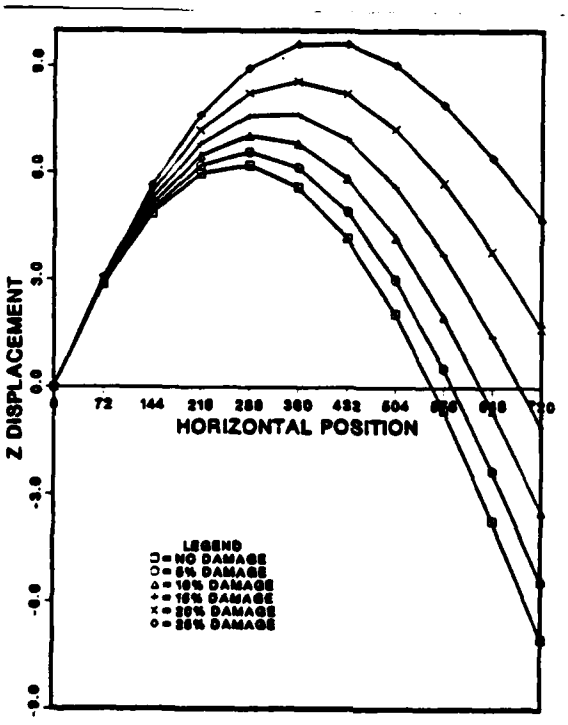

Fig. 4 Effect of Degradation on Third Mode

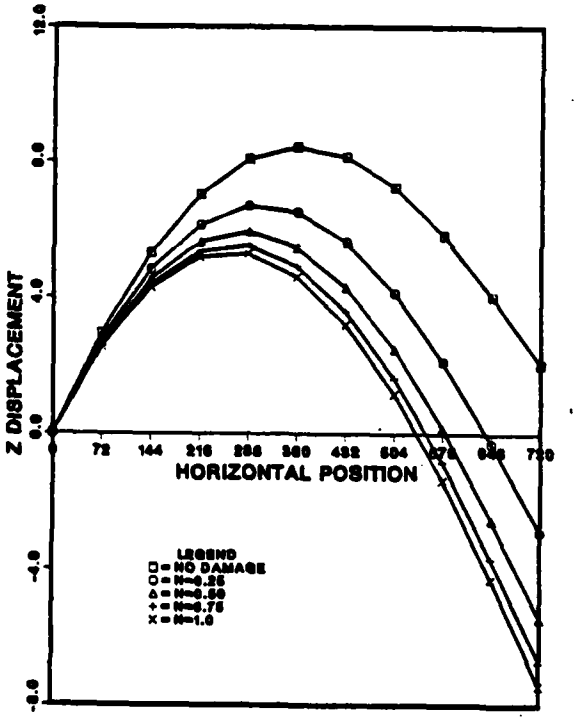

Fig. 5 Effect of Material Degradation Exponent on Second Mode Shape

The next two sample cases consider the situation where we assume that primary degradation occurs in the first two bending modes. For simplicity, it is assumed that damage occurring in one mode does not affect the damage in any others, i.e., no damage induced coupling of modes. In reality, this may not be the case and will be considered in future research.

In the first case, we consider the case where degradation has occurred in the first bending mode, i.e., degradation is based on stresses calculated from the modal displacements corresponding to the second mode shape. Figure 6 shows the resulting first three natural frequencies for different levels of damage. For a maximum reduction in stiffness of 25% the first three natural frequencies decrease by 8.6%, 9.2% and 7.6%, respectively. There is little change in the first mode shape for the degraded and undegraded cases. Figure 7 is a plot of the z displacement for the second mode shape along the length of the space truss and shows that the modal displacements change quite drastically for the degraded structure. The displacement at the free edge is nearly 30 times the magnitude of the undegraded case for a maximum damage of 25% (the sign of the displacement is also reversed) and the location of nodes also change considerably. Figure 8 indicates similar changes in the y displacement for the third mode shape. The fourth mode (torsional) is relatively unaffected by the degradation of material stiffness properties. This is as expected because the present analysis assumed that primary degradation occurred in the first two bending modes. Different results would be expected if significant stiffness reduction occurred in the primary torsion mode.

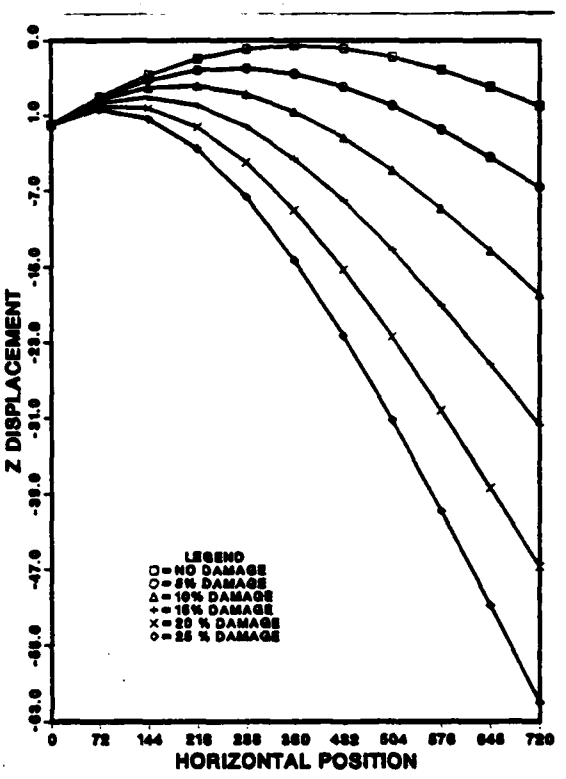

Fig. 7 Effect of Degradation on Second Mode Assuming Second Mode Damage State

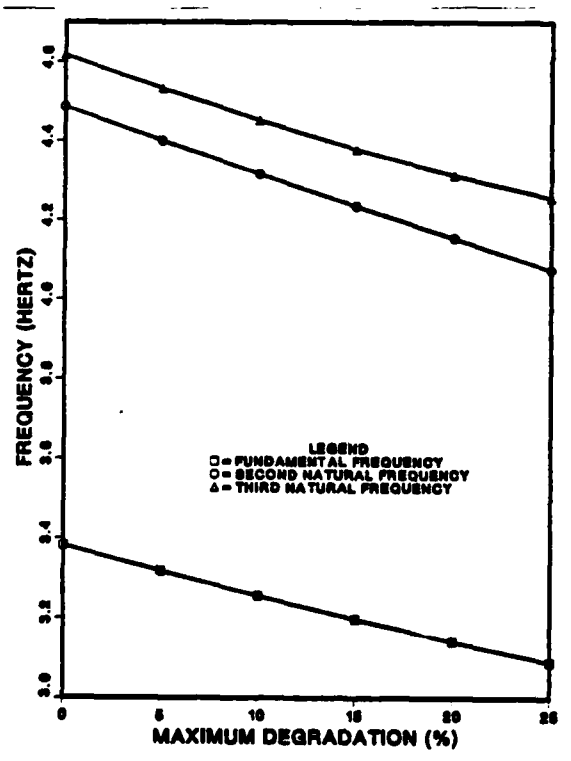

Fig. 6 Effect of Damage on Natural Frequencies

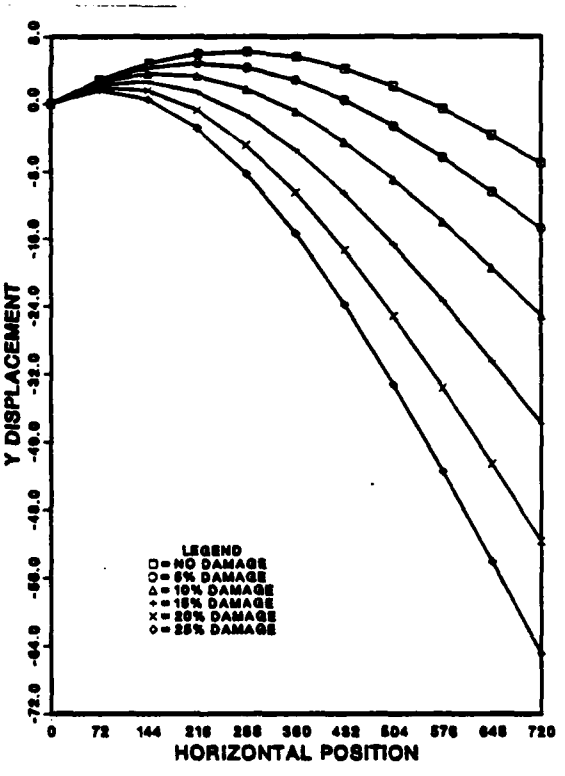

Fig. 8 Effect of Degradation on Third Mode Assuming Second Mode Damage State

Results have also been obtained for the case where damage is assumed to occur in the third mode (second bending mode). As in the previous examples there is no appreciable change in the first mode shape between the undegraded and degraded cases. The z displacement corresponding to the second mode shape is plotted in Fig. 9 for different levels of damage. The displacement at the free edge is very large in the damaged states as compared to the undegraded state. Figure 10 illustrates similar results for the third mode shape. These results show that the mode shapes and node points may change significantly for even small damage amounts.

Conclusions

This study has attempted to investigate the possible effects of material damage and stiffness reduction on the modal response of LSS. Large space structures constructed of fibrous composites will experience some stiffness reductions produced by load-induced and environmentally-induced damage of the material. To what extent this will occur is uncertain at this point but even small damage amounts appear to be significant.

The present work has shown that load-induced degradation of material properties may have a significant effect on the structural frequencies and mode shapes. For the representative boom structure considered here, even small amounts of material stiffness degradation (10%) produce frequency and node shifts which appear to be significant. It is not inconceivable that mode shapes, node locations, and frequency distributions will change over the plant design life in such a way that the structure response is very much different from the virgin structure. Such changes in plant response would require "robust" control of a nature which may not be possible with present technology. Consequently, it is important that these effects be taken into consideration when designing the control systems for large space structures.

Although preliminary, this study suggests the need for a more accurate knowledge of the physical nature of material degradation in fibrous composites, its influence on structure stiffness, and how material degradation will affect the long-term modal characteristics for large space structures.

Acknowledgement

This work was sponsored by the Air Force Office of Scientific Research under Contract No. F49620-83-C-0067.

References

1. Herzberg R.J., Johansen K.F., and Stroud R.C., "Dynamics and Control of Large Satellites," Astronautics and Aeronautics, Vol. 16, Oct., 1978 pp. 35-39.
2. Skelton R.E., "Algorithm Development for the Control Design of Flexible Structures," NASA-CP-2258, 1982.
3. Skelton R.E., "Large Space System Control Technology Model Order Reduction Study," NASA-CP-2118, 1979.

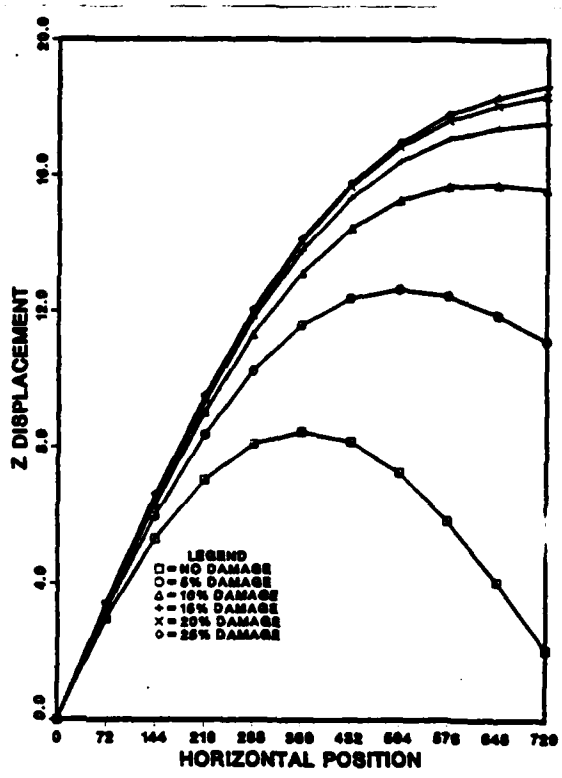

Fig. 9 Effect of Degradation on Second Mode Assuming Third Mode Damage State

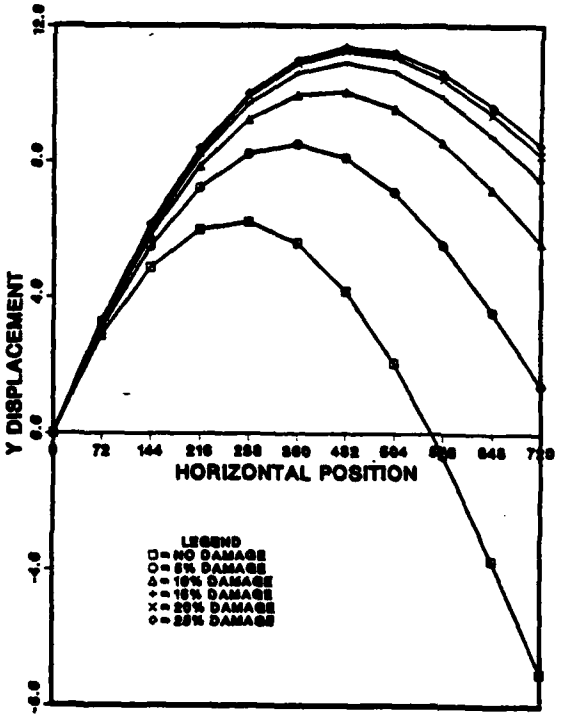

Fig. 10 Effect of Degradation on Second Mode Assuming Third Mode Damage State

4. Hroner G.C.,"Optimum Damper Location for a Free-Free Beam," NASA-CP-2168.
5. Reifsnider K.L., Schultz K., and Duke J.C., "Long-Term Fatigue Behavior of Composite Materials," Long-Term Behavior of Composites, ASTM STP 813, 1983, pp. 136-159.
6. Reifsnider K.L., and Jamison K., "Fracture of Fatigue-Loaded Composite Laminates," Int. J. Fatigue, pp. 187-197, October 1982.
7. Masters J.E., and Reifsnider K.L., "An Investigation of Cumulative Damage Development in Quasi-Isotropic Graphite/Epoxy Laminates," Damage in Composite Materials, ASTM STP 775, 1982, pp. 40-62.
8. O'Brien T.K., "Characterization of Delamination Onset and Growth in a Composite Laminate," Damage in Composite Materials, ASTM-STP 775, 1982, pp. 140-167.
9. Whitney J.M., "Fatigue Characterization of Composite Materials," Fatigue of Fibrous Composite Materials, ASTM-STP 723, 1981, pp. 133-151.
10. Highsmith A.L., Stinchcomb W.W., and Reifsnider K.L., "Stiffness Reduction Resulting from Transverse Cracking in Fiber-Reinforced Composite Laminates," VPI-E-81.33, Virginia Polytechnic Institute, November 1982.
11. Chou P.C., Wang A.S.D., and Miller H., "Cumulative Damage Model for Advanced Composite Materials," Material Laboratory Air Force Wright Aeronautical Laboratories, Report No. AFWAL-TR-82-4089.
12. Allen D.H., Groves S.E., and Schapery R.A., "A Damage Model for Continuous Fiber Composites - Part I: Theoretical Development," Texas A&M Mechanics and Materials Center, Report No. MM 5023-84-17, Feb. 1985.
13. Groves, S.E., Allen, D.H., and Schapery, R.A., "A Damage Model for Continuous Fiber Composites - Part II: Model Applications, "Texas A&M Mechanics and Materials Center, in preparation.
14. Schapery, R.A., "On Constitutive Equations for Viscoelastic Composite Materials with Damage," National Science Foundation Damage Workshop, May 4-7, 1980.
15. Mikulas M.M., Bush H.G., and Card M.F., "Structural Stiffness, Strength and Dynamic Characteristics of Large Tetrahedral Space Truss Structures," NASA TM X-74001, March 1977.
16. Bathe K.J., and Wilson E.L., "Numerical Methods in Finite Element Analysis," Prentice-Hall Inc., 1976.
17. Zienkiewicz, O.C., "The Finite Element Method," Third Edition, McGraw-Hill Book Company, 1978.

APPENDIX 6.3

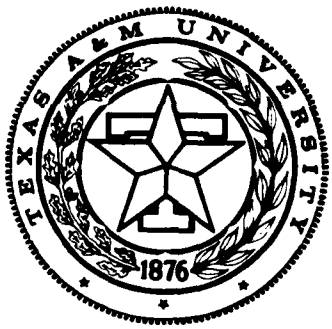

Mechanics and Materials Center
TEXAS A&M UNIVERSITY
College Station, Texas

PREDICTED AXIAL TEMPERATURE GRADIENT IN A VISCOPLASTIC UNIAXIAL BAR DUE TO THERMOMECHANICAL COUPLING

BY

D. H. ALLEN

MM 4875-84-15

NOVEMBER 1984

SECURITY CLASSIFICATION OF THIS PAGE

REPORT DOCUMENTATION PAGE

1a. REPORT SECURITY CLASSIFICATION: unclassified	1b. RESTRICTIVE MARKINGS: NA
2a. SECURITY CLASSIFICATION AUTHORITY: NA	3. DISTRIBUTION/AVAILABILITY OF REPORT: Unlimited
2b. DECLASSIFICATION/DOWNGRADING SCHEDULE: NA	
4. PERFORMING ORGANIZATION REPORT NUMBER(S): MM 4875-84-15	5. MONITORING ORGANIZATION REPORT NUMBER(S): NA
6a. NAME OF PERFORMING ORGANIZATION: Aerospace Engineering Dept. / 6b. OFFICE SYMBOL (If applicable): NA	7a. NAME OF MONITORING ORGANIZATION: Air Force Office of Scientific Research
6c. ADDRESS (City, State and ZIP Code): College Station, TX 77843	7b. ADDRESS (City, State and ZIP Code): Washington, D.C. 20332
8a. NAME OF FUNDING/SPONSORING ORGANIZATION: Air Force Office of Scientific Research / 8b. OFFICE SYMBOL (If applicable)	9. PROCUREMENT INSTRUMENT IDENTIFICATION NUMBER: NA
8c. ADDRESS (City, State and ZIP Code): Washington, D.C. 20332	10. SOURCE OF FUNDING NOS. — PROGRAM ELEMENT NO. / PROJECT NO. / TASK NO. / WORK UNIT NO.
11. TITLE (Include Security Classification): Predicted Axial Temp. Gradient in a Viscoplastic Uniaxial Bar Due	
12. PERSONAL AUTHOR(S): David H. Allen	
13a. TYPE OF REPORT: Interim / 13b. TIME COVERED: FROM _____ TO _____	14. DATE OF REPORT (Yr., Mo., Day): November 1984 / 15. PAGE COUNT
16. SUPPLEMENTARY NOTATION	
17. COSATI CODES — FIELD / GROUP / SUB. GR.	18. SUBJECT TERMS (Continue on reverse if necessary and identify by block number)

19. ABSTRACT (Continue on reverse if necessary and identify by block number)

The thermomechanical response of a uniaxial bar with thermoviscoplastic constitution is predicted herein using the finite element method. After a brief review of the governing field equations, variational principles are constructed for the one dimensional conservation of momentum and energy equations. These equations are coupled in that the temperature field affects the displacements and vice versa.

Due to the differing physical nature of the temperature and displacements, first order and second order elements are utilized for these variables, respectively. The resulting semi-discretized equations are then discretized in time using finite differencing. This is accomplished by Euler's method, which is utilized due to the stiff nature of the constitutive equations.

The model is utilized in conjunction with with stress-strain relations developed by Bodner and Partom to predict the axial temperature field in a bar subjected to cyclic mechanical end displacements and temperature boundary conditions. It is found that

20. DISTRIBUTION/AVAILABILITY OF ABSTRACT: UNCLASSIFIED/UNLIMITED ☒ SAME AS RPT. ☐ DTIC USERS ☐	21. ABSTRACT SECURITY CLASSIFICATION: Unclassified
22a. NAME OF RESPONSIBLE INDIVIDUAL: David H. Allen	22b. TELEPHONE NUMBER (Include Area Code) / 22c. OFFICE SYMBOL

DD FORM 1473, 83 APR EDITION OF 1 JAN 73 IS OBSOLETE.

SECURITY CLASSIFICATION OF THIS PAGE

spacial and time variation of the temperature field is significantly affected by the boundary conditions.

AD-A162 139 A MODEL FOR PREDICTING THERMOMECHANICAL RESPONSE OF LARGE SPACE STRUCTURE..(U) TEXAS A AND M UNIV COLLEGE STATION MECHANICS AND MATERIALS RE.. D H ALLEN ET AL. 2/3

UNCLASSIFIED JUN 85 MM-4875-85-11 AFOSR-TR-85-1016 F/G 22/2 NL

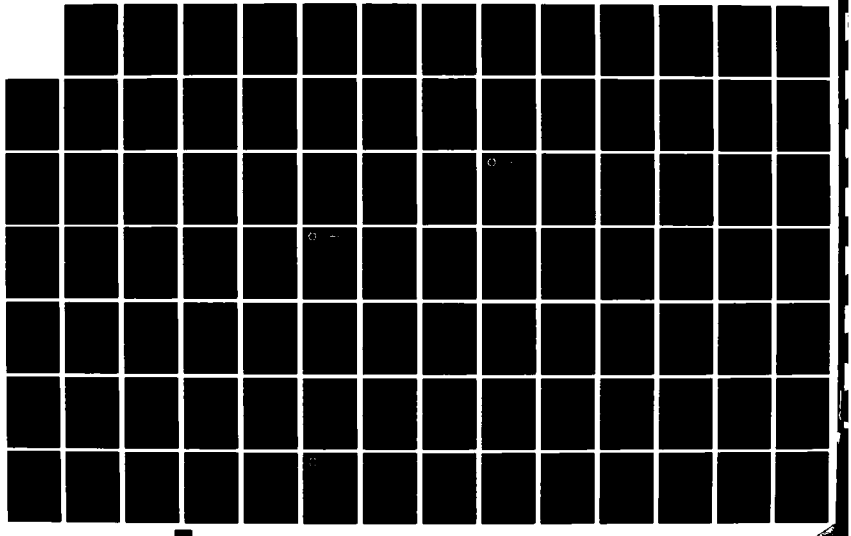

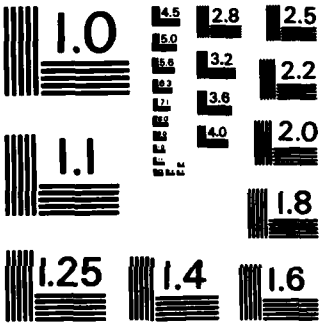

PREDICTED AXIAL TEMPERATURE GRADIENT IN A VISCOPLASTIC UNIAXIAL BAR DUE TO THERMOMECHANICAL COUPLING

by

D.H. Allen
Assistant Professor
Aerospace Engineering Department
Texas A&M University
College Station, TX 77843

MM 4875-84-15

November 1984

ABSTRACT

The thermomechanical response of a uniaxial bar with thermoviscoplastic constitution is predicted herein using the finite element method. After a brief review of the governing field equations, variational principles are constructed for the one dimensional conservation of momentum and energy equations. These equations are coupled in that the temperature field affects the displacements and vice versa.

Due to the differing physical nature of the temperature and displacements, first order and second order elements are utilized for these variables, respectively. The resulting semi-discretized equations are then discretized in time using finite differencing. This is accomplished by Euler's method, which is utilized due to the stiff nature of the constitutive equations.

The model is utilized in conjunction with stress-strain relations developed by Bodner and Partom to predict the axial temperature field in a bar subjected to cyclic mechanical end displacements and temperature boundary conditions. It is found that spacial and time variation of the temperature field is significantly affected by the boundary conditions.

TABLE OF SYMBOLS

t - time

P - axial internal resultant force

p_x - axial externally applied force per unit length

x - axial coordinate dimension

σ - axial stress component

A - cross-sectional area

T_x - end traction in units of force per unit area

s - surface area

Table of Symbols (cont.)

S_c - area of the longitudinal surface of the bar

ε - axial strain component

u - axial displacement component

α_1 - internal state variable representing axial inelastic strain

E - Young's modulus in the axial coordinate direction

α - coefficient of thermal expansion in the axial coordinate direction

T - temperature

T_R - reference temperature at which no deformation is observed at zero load

α_2 - internal state variable representing drag stress

q - axial component of heat flux

k - coefficient of axial thermal conductivity

C_v - specific heat at constant elastic strain

ρ - mass density

r - internal heat source per unit mass

L - length of the bar

INTRODUCTION

It is well known that mechanical and thermodynamic coupling are significant in metallic solids [1-11]. The author has recently developed a model capable of predicting this coupling effect in thermoviscoplastic metals [12]. In the previous paper a cyclic strain control loading on a sample of IN100 at 1005°K (1350°F) was used to predict a temperature rise of approximately 3.7°K per cycle when the strain amplitude was 2% and the specimen was adiabatically insulated.

The focus of the current research is to consider the effect of thermal boundary conditions on this same process. The introduction of these

conditions causes the strain and temperature fields to be inhomogeneous even though the stress field is homogeneous if the bar is prismatic. This spacial variation in the field variables causes the process to be difficult to model because the thermomechanical constitutive equations are highly nonlinear stiff differential equations. In this paper the finite element method is utilized to spatially discretize the dependent variables displacement and temperature, and the finite difference method is employed for timewise discretization. This process results in a set of highly nonlinear algebraic equations.

Since the thrust of this research is to obtain accurate results without regard to numerical efficiency, the results are obtained via the relatively inefficient but accurate method of simply utilizing successively smaller time steps along with refined spatial mesh to obtain a convergent and therefore accurate solution for the temperature and displacement fields both spatially and as a function of time for a cyclically imposed end displacement.

The physical interest in the problem is to determine the effect of temperature boundary conditions on the predicted temperature rise in a bar subjected to cyclic mechanical loading. It is found from the analysis that the introduction of these nonadiabatic boundary conditions causes significant axial temperature gradients. Since nonadiabatic conditions cannot be avoided in experimental research, it is concluded that experimental tests of this type should be viewed with caution when their purpose is to construct constitutive relations.

PROBLEM SOLUTION

Field Problem Description

The following field equations are given:

a) equilibrium [13],

$$\frac{\partial P}{\partial x} = -p_x(x) \quad , \tag{1}$$

where the axial resultant P is defined by

$$P \equiv \int_A \sigma dA \quad , \qquad \text{and} \quad (2)$$

$$p_x \equiv \oint_{S_c} T_x ds \quad ; \qquad (3)$$

b) strain-displacement relation

$$\varepsilon = \frac{\partial u}{\partial x} \quad ; \qquad (4)$$

c) thermomechanical constitution,

$$\sigma = E[\varepsilon - \alpha_1 - \alpha(T - T_R)] \quad , \qquad (5)$$

$$\frac{\partial \alpha_i}{\partial t} = \Omega_i(\varepsilon, T, \alpha_j) \quad , \quad i = 1,z \quad , \qquad \text{and} \quad (6)$$

$$q = -k \frac{\partial T}{\partial x} \quad ; \qquad (7)$$

where z is the total number of internal state variables; and

d) conservation of energy

$$\left[(E\varepsilon - E\alpha_1 + E\alpha T_R) \frac{\partial \alpha_1}{\partial t} + E\alpha^2 T \frac{\partial T}{\partial t}\right] - E\alpha T \frac{\partial \varepsilon}{\partial t} - \rho C_v \frac{\partial T}{\partial t} - \frac{\partial q}{\partial x} + \rho r = 0 \quad . \qquad (8)$$

The conservation of mass is satisfied trivially and the second law of thermodynamics has been previously shown to be satisfied by the above equations [14-16]. It should be noted that equilibrium equation (1) satisfies equilibrium in the axial coordinate direction only in an average sense over the cross-section.

The above 6+Z equations (excluding definition (3)) define a nonlinear initial-boundary value problem (together with appropriate thermal and mechanical initial and boundary conditions) in which the following dependent variables are sought as functions of x and t: σ, ε, u, q, T, P, and α_i.

For convenience the domain is defined to be of length L, so that boundary and initial conditions are of the form:

$$\left.\begin{array}{l} u(x,0) \equiv u_0^x = \text{known} \\ T(x,0) \equiv T_0^x = \text{known} \end{array}\right\} \quad \text{initial conditions} \quad ; \tag{9}$$

and

$$\text{essential boundary conditions} \left\{\begin{array}{ll} u(0,t) \equiv u_t^0 = \text{known or } P(0,t) \equiv P_t^0 = \text{known} & \\ u(L,t) \equiv u_t^L = \text{known or } P(L,t) \equiv P_t^L = \text{known} & \\ T(0,t) \equiv T_t^0 = \text{known or } q(0,t) \equiv q_t^0 = \text{known} & \\ T(L,t) \equiv T_t^L = \text{known or } q(L,t) \equiv q_t^L = \text{known} & \end{array}\right\} \text{natural boundary conditions.} \tag{10}$$

It is now assumed that $\sigma = \sigma(x)$ so that equation (2) reduces to

$$P = \sigma A \quad . \tag{11}$$

Therefore, substituting (4) into (5) and this result into (11) gives

$$P = EA\left[\frac{\partial u}{\partial x} - \alpha_1 - \alpha(T - T_R)\right] \quad . \tag{12}$$

The above result is now substituted into (1) to obtain

$$\frac{\partial}{\partial x}\left\{EA\left[\frac{\partial u}{\partial x} - \alpha_1 - \alpha(T - T_R)\right]\right\} = -p_x(x) \quad , \tag{13}$$

which represents the differential equation relating displacements and temperature to the applied load $p_x(x)$.

Equations (4) and (7) are next substituted into energy balance law (8) and this result is integrated over the cross-sectional area A to obtain

$$A\left[\left(E\frac{\partial u}{\partial x} - E\alpha_1 + E\alpha T_R\right)\frac{\partial \alpha_1}{\partial t} + E\alpha^2 T\frac{\partial T}{\partial t}\right] - AE\alpha T\frac{\partial^2 u}{\partial t \partial x} - A\rho C_v\frac{\partial T}{\partial t}$$

$$+ A\frac{\partial}{\partial x}\left(k\frac{\partial T}{\partial x}\right) = -A\rho r \quad , \tag{14}$$

where it has been assumed that all field variables depend on x and t only.

Now define

$$Q \equiv \int_A q\, dA = -\int_A k\frac{\partial T}{\partial x}\, dA = -k\frac{\partial T}{\partial x}A \quad . \tag{15}$$

Careful inspection of equations (13) and (14) will indicate that these equations, together with internal state variable growth laws (6) and initial and boundary conditions (9) and (10), represent a well-posed boundary value problem in terms of the 2+z dependent variables u, T, and α_i.

Solution Procedure

The field problem is to be solved analytically using the semi-discretized finite element technique with timewise finite differencing. In order to accomplish this, differential equations (13) and (14) must first be written in a suitable variational form.

Variational Equations

Consider first equation (13). This governing equation is integrated against a suitably smooth test function $v = v(x)$ over the domain of some element Ω_e: $x_e < x < x_{e+1}$:

$$\int_{x_e}^{x_{e+1}} v \left[\frac{\partial}{\partial x} \left\{ EA \left[\frac{\partial u}{\partial x} - \alpha_1 - \alpha(T - T_R) \right] \right\} + p_x \right] dx = 0 \quad . \tag{16}$$

Integrating by parts results in

$$- \int_{x_e}^{x_{e+1}} EA \frac{\partial v}{\partial x} \left[\frac{\partial u}{\partial x} - \alpha_1 - \alpha(T - T_R) \right] dx = - \left| v \, EA \left[\frac{\partial u}{\partial x} - \alpha_1 - \alpha(T - T_R) \right] \right|_{x_e}^{x_{e+1}}$$

$$- \int_{x_e}^{x_{e+1}} v \, p_x dx \quad . \tag{17}$$

Substituting equation (12) into the boundary term thus results in

$$- \int_{x_e}^{x_{e+1}} EA \frac{\partial v}{\partial x} \left[\frac{\partial u}{\partial x} - \alpha_1 - \alpha(T - T_R) \right] dx =$$

$$-v(x_{e+1}) \, P(x_{e+1}) + v(x_e) \, P(x_e) - \int_{x_e}^{x_{e+1}} v \, p_x dx \quad . \tag{18}$$

Now consider equation (14). Once again the governing equation is integrated against a suitably smooth test function $w = w(x)$ over the domain of the element Ω_e:

$$\int_{x_e}^{x_{e+1}} w \left\{ A \left[\left(E \frac{\partial u}{\partial x} - E\alpha_1 + E\alpha T_R \right) \frac{\partial \alpha_1}{\partial t} + E\alpha^2 \, T \frac{\partial T}{\partial t} \right] \right.$$

$$\left. -AE\alpha T \frac{\partial^2 u}{\partial t \partial x} - A\rho C_v \frac{\partial T}{\partial t} + A \frac{\partial}{\partial x} \left(k \frac{\partial T}{\partial x} \right) + A \, \rho r \right\} dx = 0 \quad . \tag{19}$$

Integrating the heat flux term by parts results in

$$\int_{x_e}^{x_{e+1}} \left\{ -kA \frac{\partial w}{\partial x} \frac{\partial T}{\partial x} + wA \left[\left(E \frac{\partial u}{\partial x} - E\alpha_1 + E\alpha T_R \right) \frac{\partial \alpha_1}{\partial t} + E\alpha^2 T \frac{\partial T}{\partial t} \right.\right.$$

$$\left.\left. -E\alpha T \frac{\partial^2 u}{\partial t \partial x} \right] \right\} dx = w(x_{e+1})\, Q(x_{e+1}) - w(x_e)\, Q(x_e)$$

$$+ \int_{x_e}^{x_{e+1}} wA \left(\rho C_v \frac{\partial T}{\partial t} - \rho r \right) dx \quad , \tag{20}$$

where equation (15) has been substituted into the boundary terms.

Finite Element Spacial Discretization

Quadratic displacement and linear temperature fields are now chosen within each element:

$$u(x,t) = \sum_{i=1}^{3} u_i^e \psi_i^e \quad , \quad x_e < x < x_{e+1} \quad , \text{ and} \tag{21}$$

$$T(x,t) = \sum_{i=1}^{2} T_i^e \phi_i^e \quad , \quad x_e < x < x_{e+1} \quad , \tag{22}$$

where $u_i^e = u_i^e(t)$ and $T_i^e = T_i^e(t)$ are the nodal displacements and temperatures, respectively, and $\psi_i^e = \psi_i^e(x)$ and $\phi_i^e = \phi_i^e(x)$ are quadratic and linear shape functions, respectively [17].

Appropriately, v and w are endowed with the properties of u and T, respectively, so that

$$v \equiv \psi_i^e \quad i = 1,2,3$$

$$w \equiv \phi_i^e \quad i = 1,2 \quad . \tag{23}$$

Substitution of equations (12) and (21) through (23) into variational principle (18) results in

$$-\int_{x_e}^{x_{e+1}} EA \frac{d\psi_i^e}{dx} \left[\frac{\partial}{\partial x} \left(\sum_{j=1}^{3} u_j^e \psi_j^e \right) - \alpha_1 \right.$$

$$\left. -\alpha \left(\sum_{j=1}^{2} T_j^e \phi_j^e - T_R \right) \right] dx = - \psi_i^e(x_{e+1}) P(x_{e+1}) + \psi_i^e(x_e) P(x_e)$$

$$- \int_{x_e}^{x_{e+1}} \psi_i^e p_x dx \quad , \quad i = 1,2,3 \quad . \tag{24}$$

The above may be written in the following compact form

$$\sum_{j=1}^{3} K_{ij}^e u_j^e + \sum_{j=1}^{2} S_{ij}^e T_j^e = F_i^e \quad , \quad i = 1,2,3, \tag{25}$$

where

$$K_{ij}^e \equiv - \int_{x_e}^{x_{e+1}} EA \frac{d\psi_i^e}{dx} \frac{d\psi_j^e}{dx} dx \qquad i = 1,2,3; \; j = 1,2,3 \quad ; \tag{26}$$

$$S_{ij}^e \equiv \int_{x_e}^{x_{e+1}} EA\alpha \frac{d\psi_i^e}{dx} \phi_j^e dx \qquad i = 1,2,3; \; j = 1,2 \quad ; \tag{27}$$

$$F_i^e \equiv \int_{x_e}^{x_{e+1}} EA \frac{d\psi_i^e}{dx} \left(-\alpha_1 + \alpha T_R\right) dx$$

$$-P(x_i) - \int_{x_e}^{x_{e+1}} \psi_i^e \, p_x dx \quad , \qquad i = 1,2,3. \tag{28}$$

Similarly, substitution of equations (21) through (23) into equation (20) results in

$$\int_{x_e}^{x_{e+1}} \left\{ -kA \frac{d\phi_i^e}{dx} \frac{\partial}{\partial x}\left(\sum_{j=1}^{2} T_j^e \phi_j^e\right) + A\,\phi_i^e \left[\left(E \frac{\partial}{\partial x}\left(\sum_{j=1}^{3} u_j^e \psi_j^e\right) - E\alpha_1 \right.\right.\right.$$

$$\left. + E\alpha T_R\right) \frac{\partial \alpha_1}{\partial t} + E\alpha^2 \left(\sum_{j=1}^{2} T_j^e \phi_j^e\right) \frac{\partial}{\partial t}\left(\sum_{m=1}^{2} T_m^e \phi_m^e\right)$$

$$\left.\left. - E\alpha \left(\sum_{j=1}^{2} T_j^e \phi_j^e\right) \frac{\partial^2}{\partial t \partial x}\left(\sum_{m=1}^{3} u_m^e \psi_m^e\right)\right]\right\} dx =$$

$$\phi_i^e(x_{e+1})\, Q(x_{e+1}) - \phi_i^e(x_e)\, Q(x_e) + \int_{x_e}^{x_{e+1}} \phi_i^e A \left[\rho C_v \frac{\partial}{\partial t}\left(\sum_{m}^{2} T_m^e \phi_m^e\right) - \rho r\right] dx,$$

$$i = 1,2. \tag{29}$$

Equations (29) may be written in the following form:

$$\sum_{j=1}^{3} \overline{K}_{ij}^e u_j^e + \sum_{j=1}^{2} \overline{S}_{ij}^e T_j^e + \int_{x_e}^{x_{e+1}} \phi_i^e A \left[E\alpha^2 \left(\sum_{j=1}^{2} T_j^e \phi_j^e\right)\left(\sum_{m=1}^{2} \frac{dT_m^e}{dt} \phi_m^e\right)\right.$$

$$-E\alpha\left(\sum_{j=1}^{2} T_j^e \phi_j^e\right)\left(\sum_{m=1}^{3} \frac{du_m^e}{dt}\frac{d\psi_m^e}{dx}\right) - \rho C_v\left(\sum_{m=1}^{2} \frac{dT_m^e}{dt}\phi_m^e\right) + \rho r\Bigg] dx$$

$$= -\int_{x_e}^{x_{e+1}} \phi_i^e A(-E\alpha_1 + E\alpha T_R)\frac{\partial \alpha_1}{\partial t} - Q(x_i) \quad , \qquad i = 1,2, \tag{30}$$

where

$$\bar{K}_{ij}^e \equiv \int_{x_e}^{x_{e+1}} AE\, \phi_i^e \frac{d\psi_j^e}{dx}\frac{\partial \alpha_1}{\partial t}\, dx \qquad i = 1,2;\ j = 1,2,3; \text{ and} \tag{31}$$

$$\bar{S}_{ij}^e \equiv -\int_{x_e}^{x_{e+1}} kA \frac{d\phi_i^e}{dx}\frac{d\phi_j^e}{dx}\, dx \quad ; \quad i = 1,2;\ j = 1,2. \tag{32}$$

Finite Difference Timewise Discretization

Time dependence in equations (6) and (30) is handled via finite differencing. Although higher order approximations may be used, Euler forward difference approximations are now entered for the time rate of change of α_k^e, T_m^e, and u_m^e.

$$\frac{\partial \alpha_k^e}{\partial t}(x,t) \cong [\alpha_k^e(x,t+\Delta t) - \alpha_k^e(x,t)]/\Delta t, \qquad k = 1, \ldots, z \tag{33}$$

$$\frac{dT_m^e}{dt}(t) \cong [T_m^e(t+\Delta t) - T_m^e(t)]/\Delta t, \qquad m = 1,2\ , \quad \text{and} \tag{34}$$

$$\frac{du_m^e}{dt}(t) \cong [u_m^e(t+\Delta t) - u_m^e(t)]/\Delta t, \qquad m = 1,2,3. \tag{35}$$

Substitution of (33) through (35) into finite element equations (30) gives

$$\sum_{j=1}^{3} \overline{K}_{ij}^{e} u_j^e + \sum_{j=1}^{2} \overline{S}_{ij}^{e} T_j^e$$

$$+ \int_{x_e}^{x_{e+1}} A\phi_i^e \left\{ E\alpha^2 \left[\sum_{j=1}^{2} T_j^e \phi_j^e \right] \left[\sum_{m=1}^{2} \left(\frac{T_m^e(t + \Delta t) - T_m^e(t)}{\Delta t} \right) \phi_m^e \right] \right.$$

$$- E\alpha \left[\sum_{j=1}^{2} T_j^e \phi_j^e \right] \left[\sum_{m=1}^{3} \left(\frac{u_m^e(t + \Delta t) - u_m^e(t)}{\Delta t} \right) \frac{\partial \psi_m^e}{\partial x} \right]$$

$$\left. - \rho C_v \left[\sum_{m=1}^{2} \left(\frac{T_m^e(t + \Delta t) - T_m^e(t)}{\Delta t} \right) \phi_m^e \right] + \rho r \right\} dx$$

$$= - \int_{x_e}^{x_{e+1}} A\phi_i^e \left[-E\alpha_1(t) + E\alpha T_R \right] \frac{\partial \alpha_1}{\partial t} (t)$$

$$- Q(x_i) \quad , \qquad i = 1,2 \, . \tag{36}$$

The above may be written as follows:

$$\sum_{j=1}^{3} \overline{K}_{ij}^{e} u_j^e + \sum_{j=1}^{2} \overline{S}_{ij}^{e} T_j^e$$

$$+ \sum_{k=1}^{2} \sum_{j=1}^{2} C_{ijk} T_j^e T_k^e + \sum_{j=1}^{2} D_{ij} T_j^e$$

$$+ \sum_{k=1}^{2} \sum_{j=1}^{3} E_{ikj} T_k^e u_j^e + \sum_{j=1}^{2} G_{ij} T_j^e$$

$$+ \sum_{j=1}^{2} H_{ij} T_j^e = \overline{F}_i^e \quad , \qquad i = 1,2, \tag{37}$$

where

$$C_{ijk} \equiv \int_{x_e}^{x_{e+1}} A\phi_i^e \frac{E\alpha^2}{\Delta t} \phi_j^e \phi_k^e \, dx \quad , \qquad i = 1,2;\ j = 1,2;\ k = 1,2 \ , \tag{38}$$

$$D_{i1} \equiv - \int_{x_e}^{x_{e+1}} A\phi_i^e \frac{E\alpha^2}{\Delta t} [T_1^e(t)(\phi_1^e)^2 + T_2^e(t)\ \phi_1^e\phi_2^e] \, dx, \qquad i = 1,2 \ , \tag{39}$$

$$D_{i2} \equiv - \int_{x_e}^{x_{e+1}} A\phi_i^e \frac{E\alpha^2}{\Delta t} [T_1^e(t)\phi_1^e\phi_2^e + T_2^e(t)(\phi_2^e)^2] \, dx, \qquad i = 1,2 \ , \tag{40}$$

$$E_{ikj} \equiv - \int_{x_e}^{x_{e+1}} A\phi_i^e \frac{E\alpha}{\Delta t} \phi_k^e \frac{\partial \psi_j^e}{\partial x} \, dx \quad , \qquad i = 1,2,;\ k = 1,2;\ j = 1,2,3 , \tag{41}$$

$$G_{i1} \equiv \int_{x_e}^{x_{e+1}} A\phi_i^e \frac{E\alpha}{\Delta t} \left[u_1^e(t)\ \phi_1^e \frac{\partial \psi_1^e}{\partial x} + u_2^e(t)\ \phi_1^e \frac{\partial \psi_2^e}{\partial x} + u_3^e(t)\ \phi_1^e \frac{\partial \psi_3^e}{\partial x} \right] dx, \ i = 1,2 \ , \tag{42}$$

$$G_{i2} \equiv \int_{x_e}^{x_{e+1}} A\phi_i^e \frac{E\alpha}{\Delta t} \left[u_1^e(t)\phi_2^e \frac{\partial \psi_1^e}{\partial x} + u_2^e(t)\phi_2^e \frac{\partial \psi_2^e}{\partial x} + u_3^e(t)\phi_2^e \frac{\partial \psi_3^e}{\partial x} \right] dx \ , \ i = 1,2 \ , \tag{43}$$

$$H_{ij} \equiv - \int_{x_e}^{x_{e+1}} A\phi_i^e \frac{\rho C_v}{\Delta t} \phi_j^e \, dx \quad , \qquad i = 1,2;\ j = 1,2; \qquad \text{and} \tag{44}$$

$$\overline{F}_i^e \equiv - \int_{x_e}^{x_{e+1}} A\phi_i^e \left[\frac{\rho C_v}{\Delta t} \left(\sum_{j=1}^{2} T_j^e(t)\phi_j^e \right) + \rho r \right] dx$$

$$- \int_{x_e}^{x_{e+1}} A\phi_i^e \left[-E\alpha_1(t) + E\alpha T_R \right] \frac{\partial \alpha_1}{\partial t}(t) \, dx$$

$$- Q(x_i) \qquad i = 1,2 \ . \tag{45}$$

Equations (37) may be written equivalently as follows:

$$\sum_{j=1}^{3} \bar{\bar{K}}^e_{ij} u^e_j + \sum_{j=1}^{2} \bar{\bar{S}}^e_{ij} T^e_j = \bar{F}^e_i \quad , \tag{46}$$

where K^e_{ij} and $\bar{F}^e_i$ are as defined previously, and

$$\bar{\bar{K}}^e_{ij} \equiv \bar{K}^e_{ij} + \sum_{k=1}^{2} E_{ikj} T^e_k \quad , \quad \text{and} \tag{47}$$

$$\bar{\bar{S}}^e_{ij} \equiv \bar{S}^e_{ij} + \sum_{k=1}^{2} C_{ijk} T^e_k + D_{ij} + G_{ij} + H_{ij} \quad . \tag{48}$$

The above equations may be adjoined with equations (25) to obtain the following set of nonlinear equations for each element.

$$\underbrace{\left[\begin{array}{c|c} K^e & S^e \\ \hline \bar{\bar{K}}^e & \bar{\bar{S}}^e \end{array}\right]}_{5\times 5} \left\{\begin{array}{c} u^e \\ \hline T^e \end{array}\right\} = \left\{\begin{array}{c} F^e \\ \hline \bar{F}^e \end{array}\right\} \tag{49}$$

2x3 2x2 5x1 5x1

where all nonlinearity is contained in $[\bar{\bar{S}}]$, $\{F^e\}$, and $\{\bar{F}^e\}$.

Global Assembly and Boundary Conditions

Global assembly is accomplished in the standard way using the Boolean matrix [17]. Interelement continuity is guaranteed by setting

$$P^e_2 + P^{e+1}_1 = 0 \quad , \quad \text{and} \tag{50}$$

$$\phi^e_2 + \phi^{e+1}_1 = 0 \quad . \tag{51}$$

Boundary conditions are implemented in the standard way: 1) essential boundary conditions are handled by placing one on the diagonal of the

appropriate row and zeros off diagonal in the stiffness matrix, and the specified value of the essential variable on the right hand side; and 2) natural boundary conditions are implemented directly to the right hand side.

Solution of the Nonlinear Algebraic System

Initial conditions are used for the first time step. The time step Δt is supplied for each load increment and boundary conditions are incremented directly from supplied input functions.

The internal state variable α_1 is handled in equations (23) and (45) by using equations (35). α_1 is initialized according to reference 18. The nonlinear stiffness matrix $[\bar{\bar{S}}]$ is initialized using nodal temperatures and displacements from the previous time step. The displacements and temperatures at time $t+\Delta t$ are then estimated directly and without iteration by utilizing equations (49) for very small time steps.

EXAMPLE PROBLEMS

In order to completely define an example problem it is necessary to specify internal state variable growth laws (6). Numerous models have been proposed for crystalline metals [18,19]. Since it is not the purpose of this research to compare these models, a relatively established model proposed by Bodner and Partom [20] has been chosen. This model contains two internal state variables: the inelastic strain (α_1) and the drag stress (α_2). The growth laws for these variables are given by

$$\dot{\alpha}_1 = \frac{2}{\sqrt{3}} D_o \frac{\sigma}{|\sigma|} \exp\left[-\left(\frac{n+1}{2n}\right)\left(\frac{\alpha_2}{\sigma}\right)^{2n}\right] \tag{52}$$

and

$$\dot{\alpha}_2 = m(Z_1 - \alpha_2)\,\sigma\dot{\alpha}_1 - A_1 Z_1 \left(\frac{\alpha_2 - Z_I}{Z_1}\right)^r , \tag{53}$$

where D_0, n, m, Z_I, Z_1, and r are experimentally determined material constants.

For the purpose of modeling the temperature gradient in a specific component, a hypothetical problem has been chosen using material properties representative of Inconel 100 at 1005°k (1350°F). The material and geometric properties are given in Table I. The geometry is representative of a cylindrical uniaxial bar which is 2.50 inches long and 0.25 inches in diameter. It has previously been shown that Bodner and Partom's model accurately predicts the stress-strain behavior of IN100 under uniaxial loading conditions for both monotonic and cyclic strain controlled loadings [12,18].

ρC_v = 5.032 MPa/°K

α = 13.14 x 10^{-6} in/in/°K

k = 21.0 x 10^{-6} $\frac{\text{MPa m}^2}{\text{sec °K}}$

E = 146.86 x 10^3 MPa

A = 7.12557 x 10^{-5} m^2

T_R = 1005°K

L = .06350 m

D_0 = 10 x 10^3 in/in

n = 0.70

m = 2.57

Z_1 = 1015.0

Z_I = 600.0

r = 2.66

A_1 = 0.0019

Table I. Material Properties for IN 100 at 1005°K (1350°F)

Utilizing the material properties described above, the following effects have been studied using the model developed herein:

1) the effect of variation of strain rate on the time dependence of temperature at the midpoint of a monotonically extended uniaxial bar which is insulated on the longitudinal boundaries [Figs. 1-4];

2) the spacial variation of temperature for the case above [Fig. 5];

and

3) the effect of end temperature boundary conditions on the temperature at the center of a uniaxial bar which is held at fixed temperature at the end points and subjected to cyclically imposed end displacements [Figs. 6 and 7].

Examples 1 and 2 are constructed primarily to determine the effects of thermomechanical heating on the stress-strain behavior of uniaxial constitutive specimens. It is found in examples 1 and 2 that if a specimen is mounted in an experimental apparatus which has massive grips simulating a fixed temperature boundary condition there can be substantial axial temperature gradients induced in a time dependent boundary layer near the ends of the specimen. On the other hand, these boundary conditions do not appear to substantially affect the predicted stress-strain behavior, especially when the strain measurement is taken between the thermal boundary layers near the grips. Therefore, it would appear that the standard procedure for obtaining stresses and strains in uniaxial bars is not substantially affected by mechanically induced, axial temperature gradients when the grips are at fixed temperature equivalent to the initial specimen temperature and the bar is loaded monotonicalaly. However, it should be noted that massive grips which are mounted outside a furnace could, by their much lower temperature

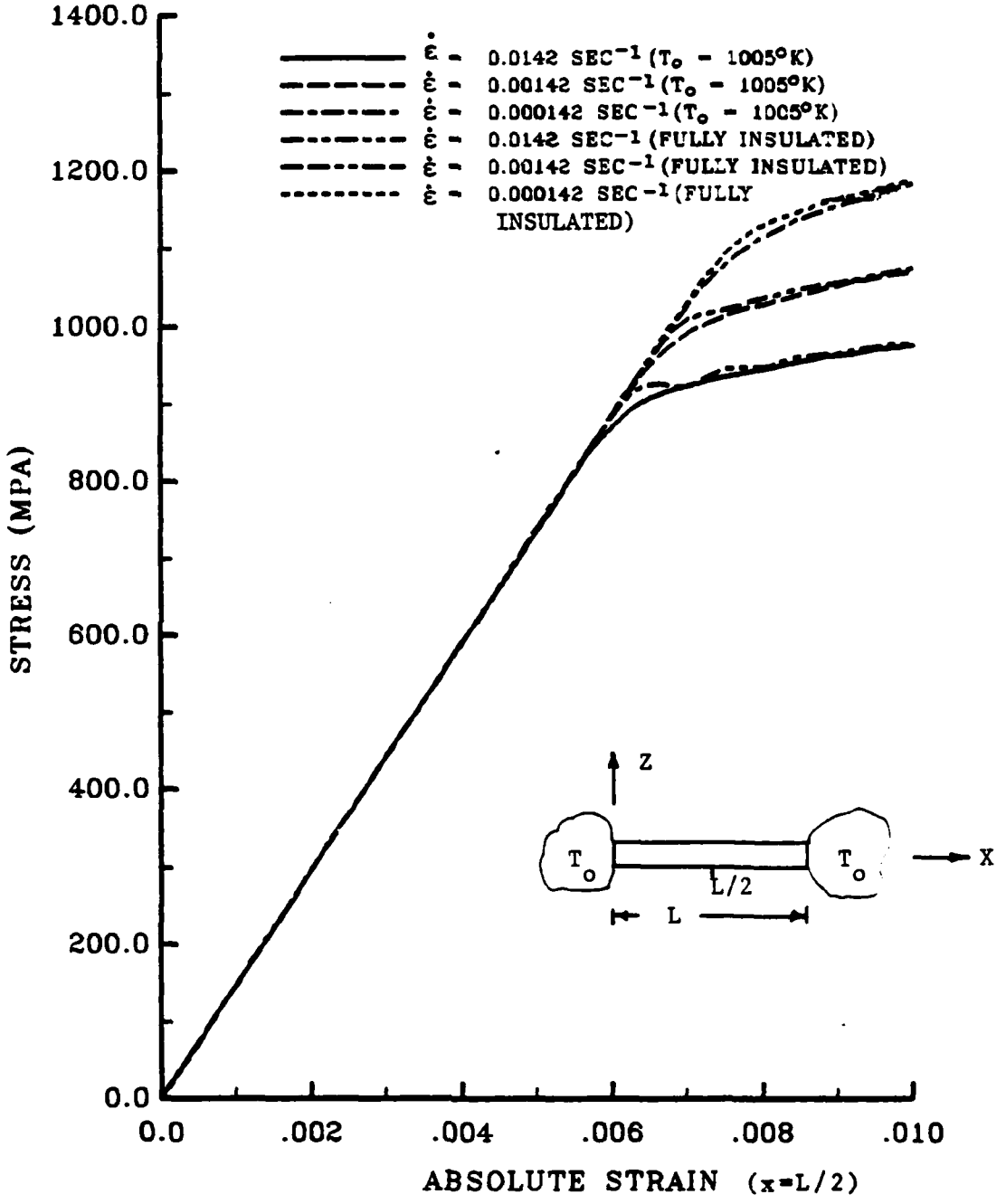

Fig. 1. Predicted Stress vs. Strain for a Uniaxial Bar Pulled at Various Constant Strain Rates.

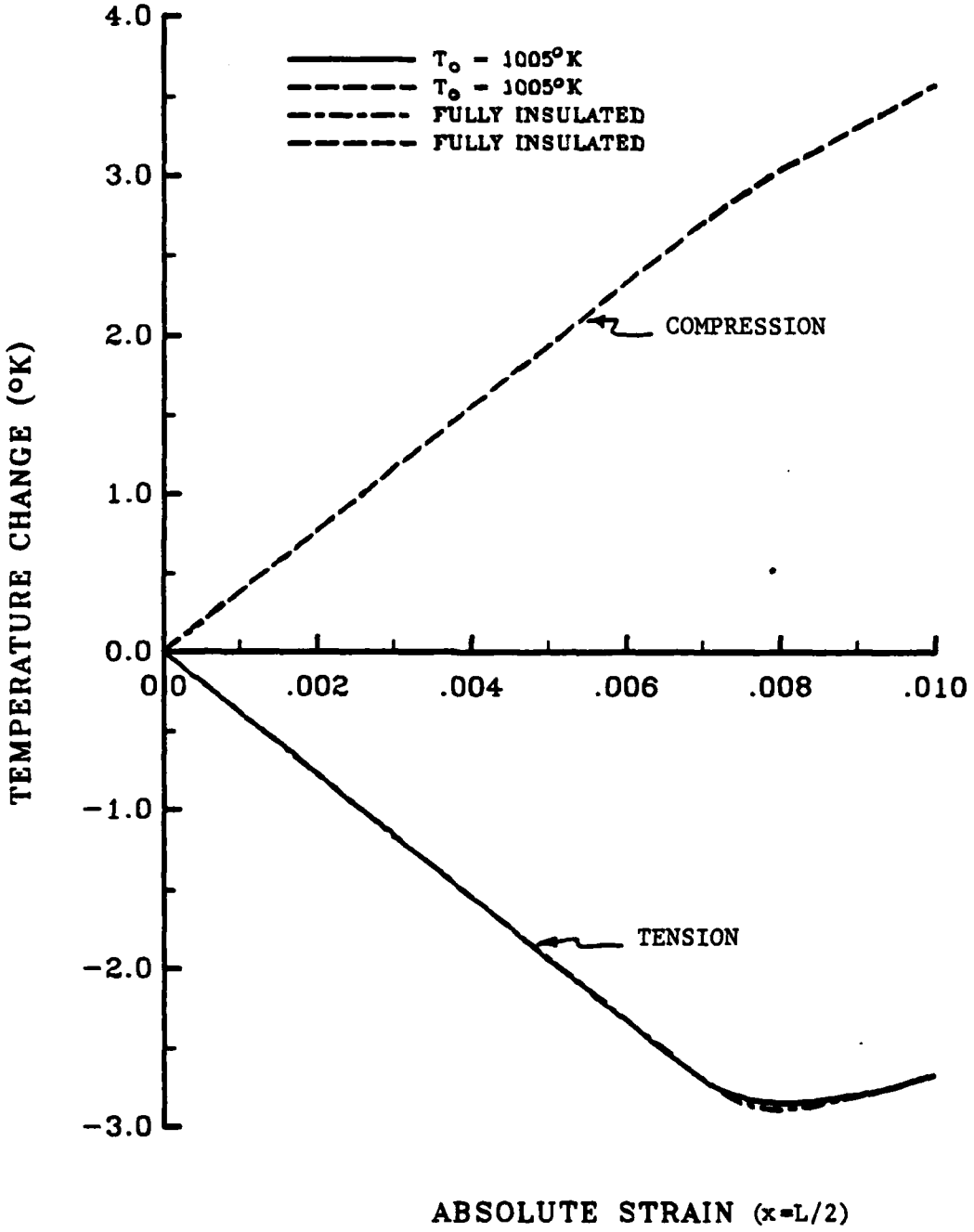

Fig. 2. Predicted Temperature vs. Absolute Strain for Monotonic Deformation Histories Described in Fig.1. ($\dot{\varepsilon} = \pm .0142$ sec^{-1})

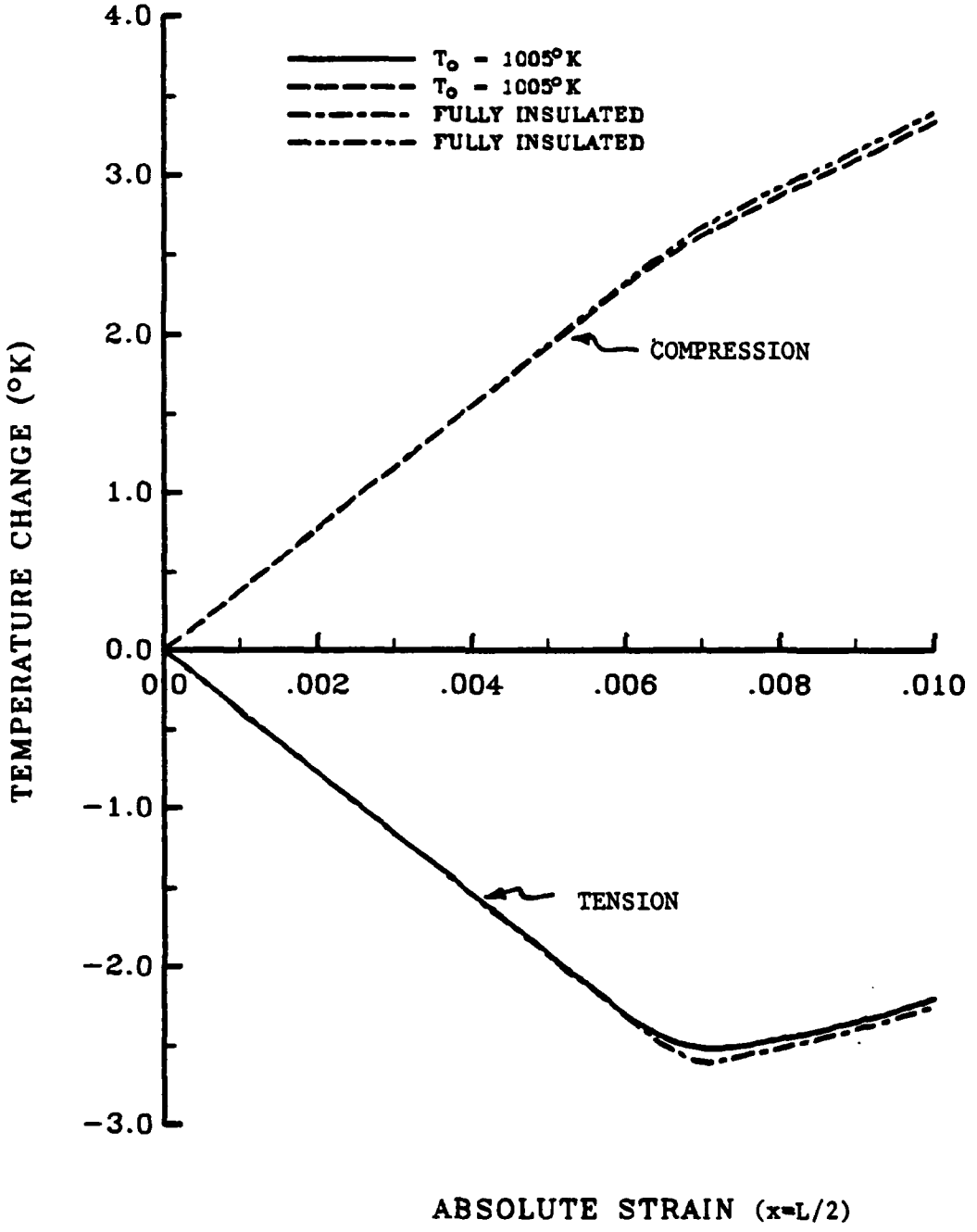

Fig. 3. Predicted Temperature vs. Absolute Strain for Monotonic Deformation Histories Described in Fig. 1. ($\dot{\varepsilon} = \pm .00142$ sec^{-1})

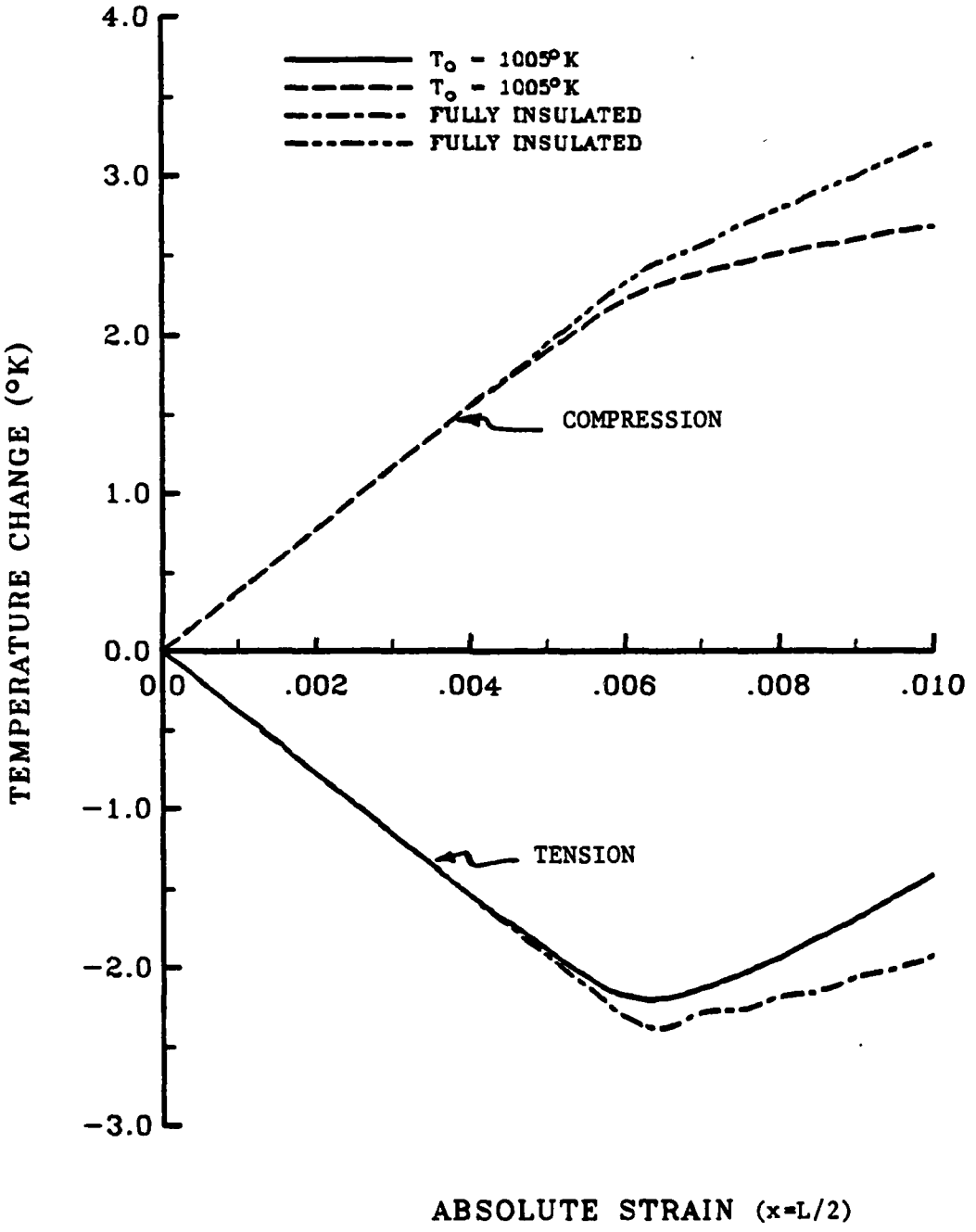

Fig. 4. Predicted Temperature vs. Absolute Strain for Monotonic Deformation Histories Described in Fig. 1. ($\dot{\varepsilon} = \pm .000142$ sec^{-1})

than the initial speciman temperature, may induce significant error in predicted strains if the strain is measured by dividing relative displacement by some gage length.

The final example demonstrates that under cyclic loading conditions the above conclusions may not necessarily be true, especially when the specimen is subjected to high-cycle fatigue and at high strain rates. There is definitely a trend towards an increasing mean temperature in the bar, and this mean temperature is strongly affected by the thermal boundary conditions as well as the loading rate. Although it would be interesting to determine the mean temperature rise in a cyclic fatigue test, the current algorithm precludes this analysis due to the extremely large computer times necessary to predict only a few cycles of response (approximately 43.8 CPU minutes on an Amdahl 470/V6 for the example demonstrated in Figs. 6 and 7).

Example 3 also demonstrates another interesting phenomenon which may be significant in large space structures. If the bar is perfectly insulated the mean temperature rise per cycle for the relatively slow loading rate shown in Fig. 6 is 3.7°K, whereas if the ends of the bar are held at a fixed temperature of 1005°K, the mean rise is 1.0°K per cycle. Faster loading rates show less difference between the adiabatic result and the fixed end temperature result. Since many of these structures are expected to be extremely flexible truss-like configurations, a typical metallic member which undergoes some yielding (which might be desirable in order to induce natural damping) might in fact undergo substantial enough heating during vibrational response such that the material properties could be adversely affected, thus resulting in a material related failure of the structure. However, further investigation is needed on this last issue since it is expected that the primary form of heat flux off of space structures will be via radiation on the longitudinal surfaces of the truss member. Since the current analysis

has treated these surfaces as insulated, no general statements can be made at this time regarding thermomechanical heating in space structures.

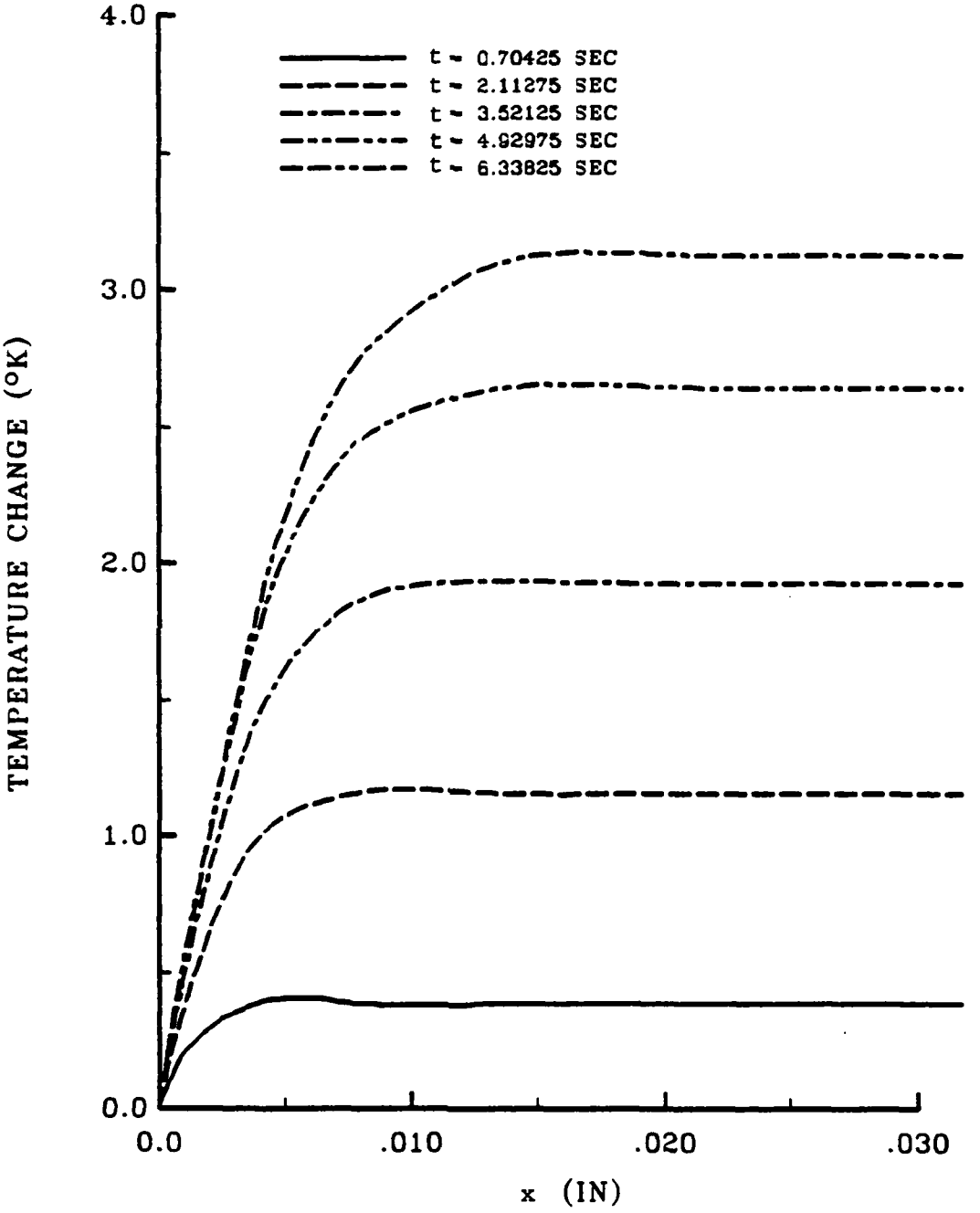

Fig. 5. Temperature vs. Spacial Location for Various Times for Constant Strain Rate $\dot{\varepsilon} = -.00142\ sec^{-1}$ (x = 0.3175 is the Midpoint of the Bar).

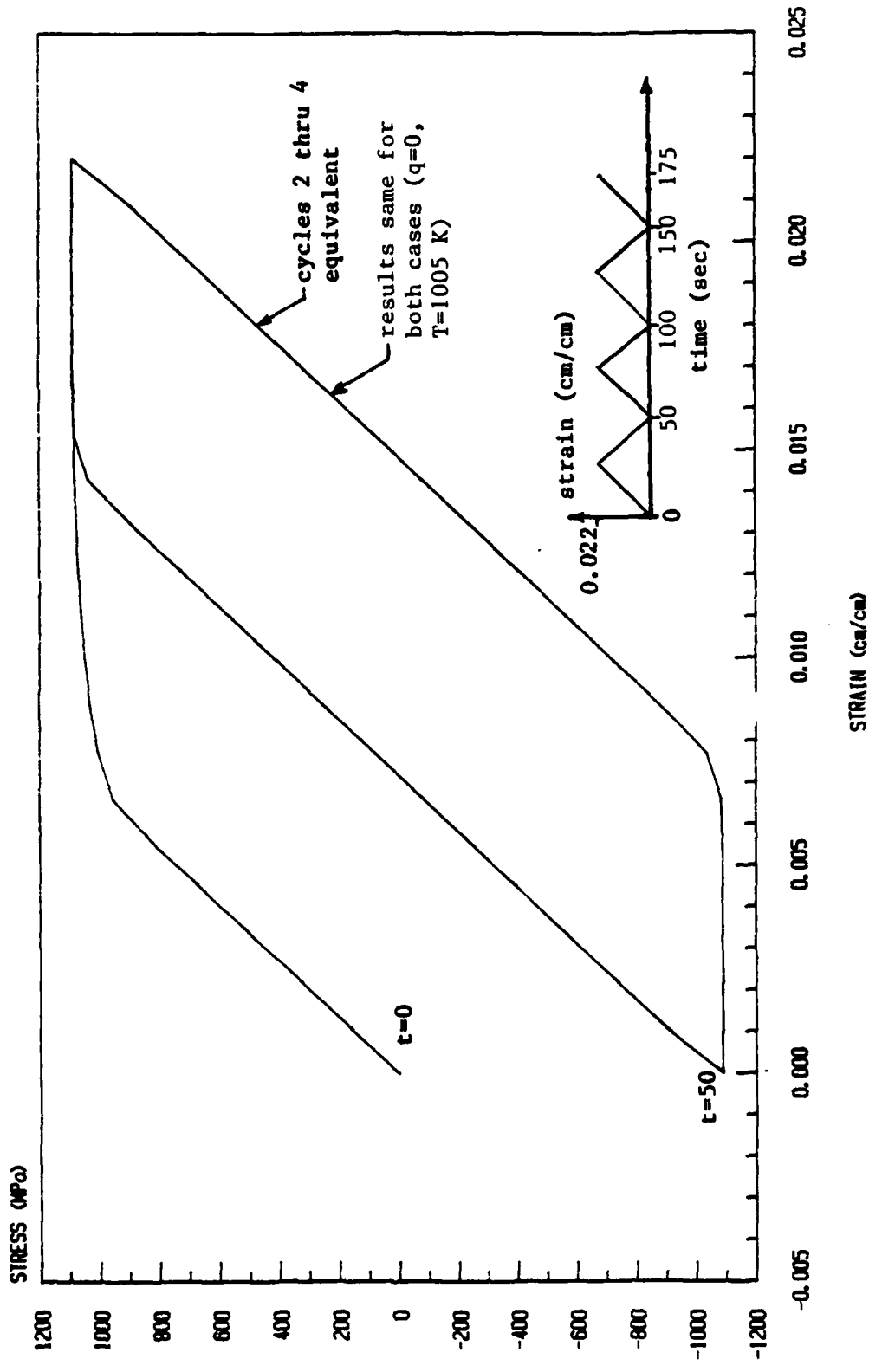

Fig. 6. Stress-Strain Curve and Strain input curve for cyclic load.

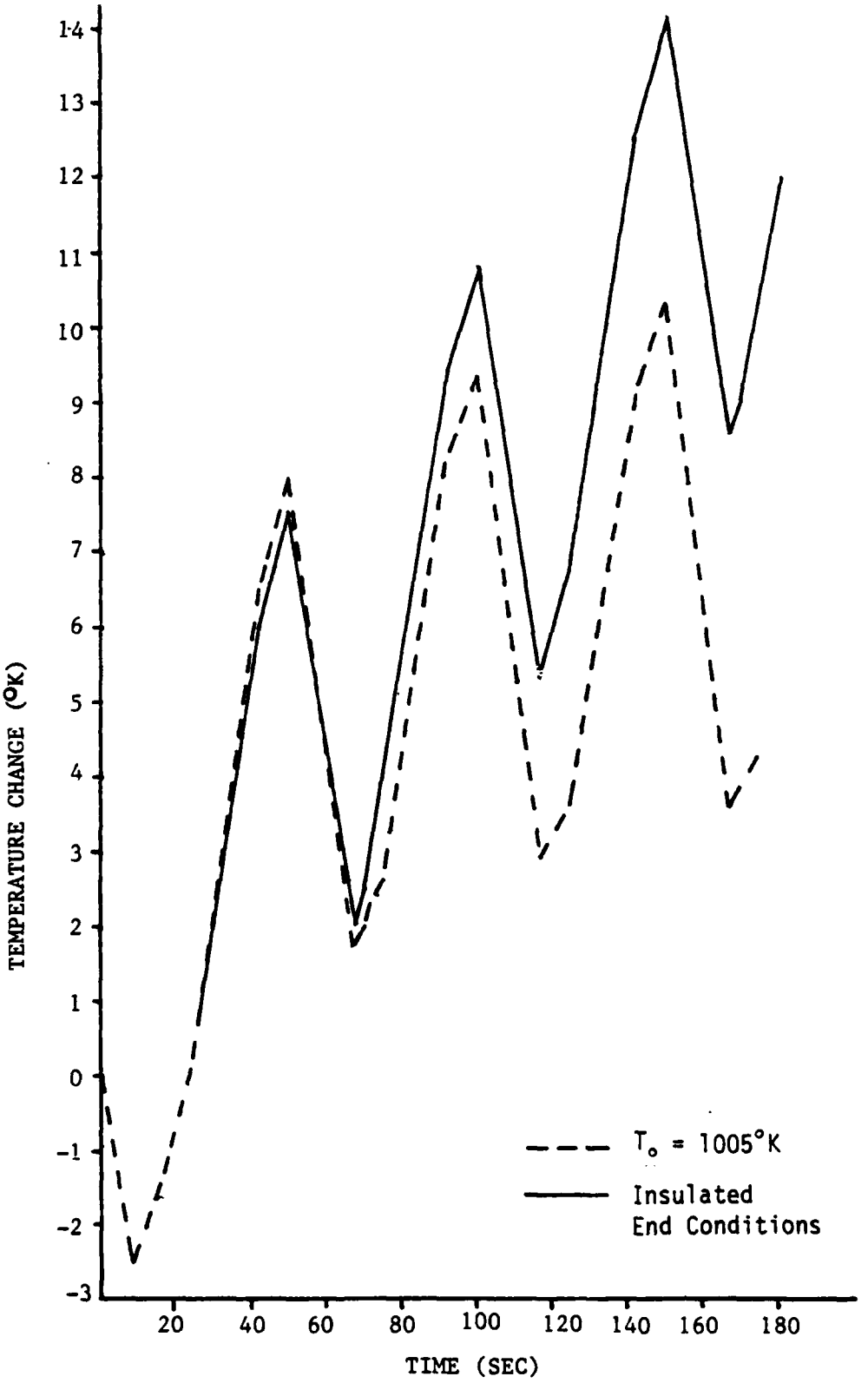

Fig. 7. Temperature Change at x=L/2 Versus Time for the Cyclically Loaded Bar Described in Fig. 6.

CONCLUSION

The current research has attemped to demonstrate the effects of mechanical loading on one-dimensional temperature gradients in a class of viscoplastic media. Due to the nonlinearity and stiffness of the field equations, it was necessary to utilize a numerical algorithm. This algorithm has been shown to be very inefficient for solving even one-dimensional examples. Therefore, it is apparent that significant refinement of the procedure will be necessary before multi-dimensional analyses can be performed by this method. Specifically, it would be significant to determine the effect of transverse temperature gradients on the stress-strain behavior of constitutive specimens. Furthermore, the effects of thermal boundary conditions on the longitudinal surface needs attention. The author is currently studying a perturbation technique for more efficient solution of these issues.

The above points notwithstanding, the current research demonstrates some important results. These are:

1) The axial temperature gradient in a viscoplastic uniaxial bar is strongly affected by the thermal boundary conditions on the ends.

2) The end temperature boundary conditions can cause temperature gradients which are substantial enough to induce spacial variations in stress and strains which invalidate the standard procedure of using average quantities, although when grips are mounted within a furnace at spacially constant temperature, it appears that the standard procedure is accurate.

3) There is a trend toward increasing average temperature in cyclically loaded bars; whether or not this effect is significant is strongly dependent on the thermal boundary conditions and the loading rate.

ACKNOWLEDGEMENT

The author gratefully acknowledges the support provided for this research by the Air Force Office of Scientific Research under contract no. F49620-83-C-0067.

REFERENCES

[1] J.M.C. Duhamel, Memoire sur le calcul des actions moleculaires developpees par les changements de temperature dan les corps solides. Memoires par divers savans, vol. 5, pp. 440-498, (1838).

[2] F. Neumann, Vorlesungen uber die theorie der elasticitat der festen Korper und des lichtathers. Leipzig, 107-120, (1885).

[3] B.A. Boley and J.H. Weiner, Theory of Thermal Stresses. Wiley, New York, (1960).

[4] O.W. Dillon, Jr., An experimental study of the heat generated during torsional oscillations. J. Mech. Phys. Solids, vol. 10, 235-244 (1962).

[5] O.W. Dillon, Jr., Temperature generated in aluminum rods undergoing torsional oscillations. J. Appl. Mech. 33, vol. 10, 3100-3105 (1962).

[6] O.W. Dillon, Jr., Coupled thermoplasticity. J. Mech. Phys. Solids, vol. 11, 21-33 (1963).

[7] G.R. Halford, Stored Energy of Cold Work Changes Induced by Cyclic Deformation. Ph.D. Thesis, University of Illinois, Urbana, Illinois (1966).

[8] O.W. Dillon, Jr., The heat generated during the torsional oscillations of copper tubes. Int. J. Solids Structures, vol. 2, 181-204 (1966).

[9] W. Olszak and P. Perzyna, Thermal Effects in Viscoplasticity. IUTAM Symp., East Kilbride, 206-212, Springer-Verlag, New York (1968).

[10] J. Kratochvil and R.J. DeAngelis, Torsion of a titanium elastic viscoplastic shaft. J. Appl. Mech. vol. 42, 1091-1097 (1971).

[11] E.P. Cernocky and E. Krempl, A theory of thermoviscoplasticity based on infinitesimal total strain. Int. J. Solids Structures, vol. 16, 723-741 (1980).

[12] D.H. Allen, A prediction of heat generation in a thermoviscoplastic uniaxial bar. Texas A&M University Mechanics and Materials Center Report no. MM 4875-83-10 (July 1983), (accepted for publication by Int. J. Solids Structures).

[13] D.H. Allen and W.E. Haisler, Introduction to Aerospace Structural Analysis. John Wiley (1985), in press.

[14] B.D. Coleman and M.E. Gurtin, Thermodynamics with internal state variables. J. Chem. Phys., vol. 47, 597-613 (1967).

[15] J. Kratochvil and O.W. Dillon, Jr., Thermodynamics of crystalline elastic-viscoplastic materials. J. Appl. Phys., vol. 41, 1470-1479 (1970).

[16] D.H. Allen, Thermodynamic constraints on the constitution of a class of thermoviscoplastic solids. Texas A&M University Mechanics and Materials Center, Report no. MM 12415-82-10, December (1982).

[17] J.N. Reddy, An Introduction to the Finite Element Method. McGraw-Hill, New York (1984).

[18] T.M. Milly and D.H. Allen, "A Comparative Study of Nonlinear Rate-Dependent Mechanical Constitutive Theories for Crystalline Solids at Elevated Temperatures, Virginia Polytechnic Institute and State University, March, 1982 (M.S. Thesis).

[19] D.H. Allen and J.M. Beek, "On the Use of Internal State Variables in Thermoviscoplastic Constitutive Equations," Proceedings 2nd Symposium on Nonlinear Constitutive Relations for High Temperature Applications, June, 1984.

[20] S.R. Bodner and Y. Partom, "Constitutive Equations for Elastic-Viscoplastic Strain-Hardening Materials," J. Appl. Mech, Vol. 42, 385-389 (1975).

APPENDIX 6.4

Mechanics and Materials Center
TEXAS A&M UNIVERSITY
College Station, Texas

PREDICTED TEMPERATURE FIELD IN A THERMOMECHANICALLY HEATED VISCOPLASTIC SPACE TRUSS STRUCTURE

D. H. ALLEN

W. E. HAISLER

MM-4875-85-1

JANUARY 1985

SECURITY CLASSIFICATION OF THIS PAGE

REPORT DOCUMENTATION PAGE

1a. REPORT SECURITY CLASSIFICATION unclassified	1b. RESTRICTIVE MARKINGS NA
2a. SECURITY CLASSIFICATION AUTHORITY NA	3. DISTRIBUTION/AVAILABILITY OF REPORT unlimited
2b. DECLASSIFICATION/DOWNGRADING SCHEDULE NA	
4. PERFORMING ORGANIZATION REPORT NUMBER(S) MM-4875-85-1	5. MONITORING ORGANIZATION REPORT NUMBER(S) NA
6a. NAME OF PERFORMING ORGANIZATION Aerospace Engr. Dept.	6b. OFFICE SYMBOL (If applicable) NA
7a. NAME OF MONITORING ORGANIZATION Air Force Office of Scientific Research	
6c. ADDRESS (City, State and ZIP Code) Texas A&M University College Station, Texas 77843	7b. ADDRESS (City, State and ZIP Code) Bolling AFB Washington, D.C. 20332
8a. NAME OF FUNDING/SPONSORING ORGANIZATION Air Force Office of Scien. Res.	8b. OFFICE SYMBOL (If applicable)
9. PROCUREMENT INSTRUMENT IDENTIFICATION NUMBER NA	
8c. ADDRESS (City, State and ZIP Code) Bolling AFB Washington, D.C. 20332	10. SOURCE OF FUNDING NOS. PROGRAM ELEMENT NO.: F49620-83-C-0067 PROJECT NO. TASK NO. WORK UNIT NO.
11. TITLE (Include Security Classification) Predicted Temp. Field in a Thermomechanically	
12. PERSONAL AUTHOR(S) D.H. Allen and W.E. Haisler	
13a. TYPE OF REPORT Interim	13b. TIME COVERED FROM _____ TO _____
14. DATE OF REPORT (Yr., Mo., Day) January 1985	15. PAGE COUNT
16. SUPPLEMENTARY NOTATION	

17. COSATI CODES			18. SUBJECT TERMS (Continue on reverse if necessary and identify by block number)
FIELD	GROUP	SUB. GR.	

19. ABSTRACT (Continue on reverse if necessary and identify by block number)

This paper focuses on the effect of thermomechanically induced heating on the response of a single member of a space truss structure which behaves viscoplastically. The governing equations are given for a typical truss member, wherein material inelasticity is reflected in constitutive equations via a set of internal state variables, each characterized by a history dependent growth law. The governing equations are coupled in the sense that temperature and displacement are dependent on each other. This difficulty, toghether with the fact that the inelastic constitutive equations are nonlinear and numerically stiff, requires that a computationally complex semidiscretized finite element spatial technique be utilized to obtain a solution. This procedure, detailed herin, is utilized to predict the response of a typical metallic space truss member under vibrational or cyclic loading. Particular interest is placed on the temperature rise in such a member due to hysteretic loss during structural vibrations and in the presence of complex thermal boundary conditions representative of space conditions. (over)

20. DISTRIBUTION/AVAILABILITY OF ABSTRACT UNCLASSIFIED/UNLIMITED ☒ SAME AS RPT. ☐ DTIC USERS ☐	21. ABSTRACT SECURITY CLASSIFICATION UNCLASSIFIED
22a. NAME OF RESPONSIBLE INDIVIDUAL DAVID H. ALLEN	22b. TELEPHONE NUMBER (Include Area Code) (409)845-1669
	22c. OFFICE SYMBOL

DD FORM 1473, 83 APR EDITION OF 1 JAN 73 IS OBSOLETE.

UNCLASSIFIED
SECURITY CLASSIFICATION OF THIS PAGE

Predicted Temperature Field in a Thermomechanically Heated Viscoplastic Space Truss Structure

by

D.H. Allen
and
W.E. Haisler

Aerospace Engineering Department
Texas A&M University
College Station, TX 77843

to be presented at the

26th SDM Conference
April 5-7, 1985
Orlando, Florida

MM 4875-85-1

January 1985

PREDICTED TEMPERATURE FIELD IN A THERMOMECHANICALLY HEATED VISCOPLASTIC SPACE TRUSS STRUCTURE

D.H. Allen*
W.E. Haisler**
Texas A&M University
College Station, Texas

Abstract

This paper focuses on the effect of thermomechanically induced heating on the response of a single member of a space truss structure which behaves viscoplastically. The governing equations are given for a typical truss member, wherein material inelasticity is reflected in constitutive equations via a set of internal state variables, each characterized by a history dependent growth law. The governing equations are coupled in the sense that temperature and displacement are dependent on each other. This difficulty, together with the fact that the inelastic constitutive equations are nonlinear and numerically stiff, requires that a computationally complex semidiscretized finite element spatial technique be utilized to obtain a solution. This procedure, detailed herein, is utilized to predict the response of a typical metallic space truss member under vibrational or cyclic loading. Particular interest is placed on the temperature rise in such a member due to hysteretic loss during structural vibrations and in the presence of complex thermal boundary conditions representative of space conditions. Example cases are constructed for a typical cylindrical bar of 6061-T6 aluminum both with and without special coatings. Results indicate that significant, possibly even catastrophic, heating can occur due to thermomechanical coupling.

Nomenclature

t - time

P - axial internal resultant force

p_x - axial externally applied force per unit length

x - axial coordinate dimension

σ - axial stress component

A - cross-sectional area

T_x - end traction in units of force per unit area

s - surface area

S_c - area of the longitudinal surface of the bar

ε - axial strain component

u - axial displacement component

α_1 - internal state variable representing axial inelastic strain

E - Young's modulus in the axial coordinate direction

α - coefficient of thermal expansion in the axial coordinate direction

T - temperature

T_R - reference temperature at which no deformation is observed at zero load

α_2 - internal state variable representing drag stress

$\vec{q}$ - heat flux vector

q - axial component of heat flux

k - coefficient of axial thermal conductivity

C_v - specific heat at constant elastic strain

ρ - mass density

r - internal heat source per unit mass

L - length of the structural element

D_o, n, m, Z_1, Z_I, Z_o, r - material constant used in Bodner and Partom's model[1]

q_c - flux on longitudinal boundary

c - absorbing portion of perimeter of an element normal to longitudinal axis

q_s - solar radiation flux

q_E - earth radiation flux

*Assistant Professor, Aerospace Engineering, Member AIAA

**Professor, Aerospace Engineering, Associate Fellow AIAA

α_s - absorptivity

F_E - earth radiation view factor

λ_s - incident angle of solar radiation on structural component

λ_E - incident angle of earth radiation on structural component

σ_s - Stefan-Boltzmann constant = 5.775×10^{-11} MPa m/sec/(°K)^4

T_D - deep space temperature

Introduction

It is well known that in viscoplastic metals a certain amount of mechanically induced hysteretic mechanic energy loss is converted to heat, thus resulting in a temperature rise in the medium. In recent research[2,3] a model has been developed for predicting this effect by utilizing thermodynamic constraints together with constitutive equations of internal state variable type[4]. Furthermore, it has been shown that in a perfectly insulated uniaxial bar[3], as well as in a uniaxial bar with insulated longitudinal surface and fixed end temperature[5], significant temperature rise can occur in the component during cyclic loading.

The purpose of the current research is to simulate the response of a typical metallic space truss structural element (see Fig. 1) in the postyielded state and to determine if significant heating occurs when this component is subjected to cyclic mechanical loading. This problem is of interest because a certain amount of material inelasticity is desirable in order to produce passive structural damping. The factors of interest in this simulation are the effects of thermal boundary conditions and loading rate on the thermal response. In particular, it is of interest to determine if radiative boundary conditions on the longitudinal surface of the truss component are significant enough to carry off all heat generated due to hysteretic loss.

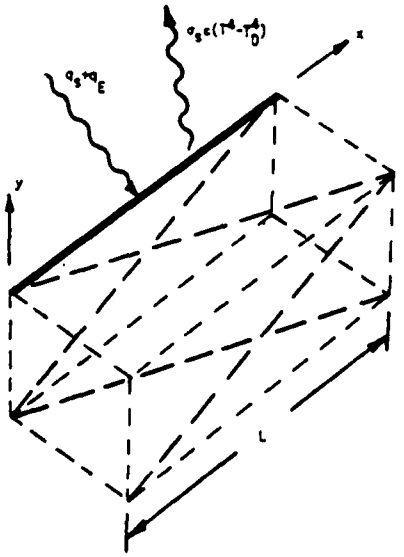

Fig. 1. Typical Space Truss Structural Element.

The paper first reviews the governing field equations, then briefly discusses the procedure whereby a numerical algorithm is constructed for modeling the problem. This is followed by a detailed discussion of the implementation of thermal boundary conditions. Finally, example results are obtained for representative space structural components.

Governing Field Equations

The governing field equations were presented in reference 5 for quasi-static conditions. For problems involving inertial effects, the governing equations are as follows:

a) equilibrium[6],

$$\frac{\partial P}{\partial x} = p_x(x) \tag{1}$$

where the axial resultant P is defined by

$$P = \int \sigma dA \tag{2}$$

$$p_x \equiv \int_{S_c} T_x \, ds \tag{3}$$

b) strain-displacement relation

$$\varepsilon = \frac{\partial u}{\partial x} \tag{4}$$

c) thermomechanical constitution,

$$\sigma = E[\varepsilon - \alpha_1 - \alpha(T-T_R)] \tag{5}$$

$$\dot{\alpha}_1 = \frac{2}{\sqrt{3}} D_o \frac{\sigma}{|\sigma|} \exp\left[-\left(\frac{n+1}{2n}\right)\left(\frac{\alpha_2}{\sigma}\right)^{2n}\right] \tag{6}$$

$$\dot{\alpha}_2 = m(Z_1-\alpha_2)\sigma\dot{\alpha}_1 - A_1 Z_1 \left(\frac{\alpha_2 - Z_I}{Z_1}\right)^r \tag{7}$$

$$q = -k \frac{\partial T}{\partial x} \tag{8}$$

where α_1 and α_2 are the internal state variables (ISV) representing inelastic strain and drag stress, respectively, in the constitutive model developed by Bodner and Partom[7]. Several other constitutive models have been developed for viscoplastic metals, and these are reviewed in references 1 and 8. Finally,

d) conservation of energy[3,5],

$$[(E\varepsilon - E\alpha_1 + E\alpha T_R)\frac{\partial \alpha_1}{\partial t} + E\alpha^2 T\frac{\partial T}{\partial t}] - E\alpha T\frac{\partial \varepsilon}{\partial t} - \rho C_v \frac{\partial T}{\partial t} - \frac{\partial q}{\partial x} + \rho r = 0 \tag{9}$$

Conservation of mass is satisfied trivially (under the assumption of small motions in a closed system), and the second law of thermodynamics has been previously shown to be satisfied by the above equations[2,4].

The governing equations are adjoined with appropriate initial and boundary conditions[5] such that a well-posed boundary value problem is constructed in terms of the following dependent

variables which are sought as functions of x and t: $\sigma,\varepsilon,u,q,T,P,\alpha_1$, and α_2. Due to ISV growth laws (6) and (7) (as well as radiative boundary conditions), the problem is nonlinear.

Solution Procedure

As described in detail in reference 5 for the quasistatic problem, the solution is obtained using the semi-discretized finite element technique, wherein finite elements are constructed spatially, and finite differencing is used in time. The result is a time marching algorithm which is reviewed here briefly.

First, equations (4) and (5) are substituted into (2) and this result is substituted into (1) to give the following equilbrium equation:

$$\frac{\partial}{\partial x}\left\{EA\left[\frac{\partial u}{\partial x}-\alpha_1-\alpha(T-T_R)\right]\right\}=-p_x(x) \tag{10}$$

Next, equation (4) is substituted into equation (9) to obtain the coupled energy balance law:

$$\left[\left(E\frac{\partial u}{\partial x}-E\alpha_1+E\alpha T_R\right)\frac{\partial \alpha_1}{\partial t}+E\alpha^2 T\frac{\partial T}{\partial t}\right]-E\alpha T\frac{\partial^2 u}{\partial t\partial x}$$
$$-\rho C_v\frac{\partial T}{\partial t}-\vec{\nabla}\cdot\vec{q}+\rho r=0 \tag{11}$$

The result is a set of two coupled partial differential equations in terms of axial displacement u=u(x,t) and temperature T=T(x,t).

Variational Principles and Finite Element Discretization

Selecting a suitably smooth test function v=v(x) over the domain of some element Ω_e: $x_e<x<x_{e+1}$, one may construct the following variational principle from equation (12):

$$-\int_{x_e}^{x_{e+1}} EA\frac{\partial v}{\partial x}\left[\frac{\partial u}{\partial x}-\alpha_1-\alpha(T-T_R)\right]dx=$$
$$-v(x_{e+1})P(x_{e+1})+v(x_e)P(x_e)-\int_{x_e}^{x_{e+1}} vp_x dx \tag{12}$$

where the boundary terms result from the standard integration by parts.

The variational principle for heat equation (11) is constructed by first integrating this equation against a test function w=w(x) on Ω_e to obtain

$$\int_{\Omega_e} w\left\{\left[(E\varepsilon-E\alpha_1+E\alpha T_R)\frac{\partial \alpha_1}{\partial t}+E\alpha^2 T\frac{\partial T}{\partial t}\right]-E\alpha T\frac{\partial^2 u}{\partial x\partial t}\right.$$
$$\left.-\rho C_v\frac{\partial T}{\partial t}+\vec{\nabla}\cdot\vec{q}+\rho r\right\}dV=0 \tag{13}$$

Integrating the flux term by parts, assuming that nonaxial components of flux are negligible, and substituting equation (8) will thus result in

$$\int_{x_e}^{x_{e+1}} w\left\{A\left[\left(E\frac{\partial u}{\partial x}-E\alpha_1+E\alpha T_R\right)\frac{\partial \alpha_1}{\partial t}+E\alpha^2 T\frac{\partial T}{\partial t}\right]\right.$$
$$\left.-AE\alpha T\frac{\partial^2 u}{\partial t\partial x}-A\rho C_v\frac{\partial T}{\partial t}-kA\frac{\partial w}{\partial x}\frac{\partial T}{\partial x}\right\}dx$$
$$=-w(x_{e+1})Aq(x_{e+1})+w(x_e)Aq(x_e)-\int_{x_e}^{x_{e+1}} c\,w\,q_c dx$$
$$+\int_{x_e}^{x_{e+1}} wA\left(\rho C_v\frac{\partial T}{\partial t}-\rho r\right)dx \tag{14}$$

Variational equations (12) and (14) are now discretized by assuming the following displacement and temperature fields in a typical element (superscripted e):

$$u(x,t)=\sum_{i=1}^{3} u_i^e(t)\psi_i^e(x) \quad x_e<x<x_{e+1} \tag{15}$$

$$T(x,t)=\sum_{i=1}^{2} T_i^e(t)\phi_i^e(x) \quad x_e<x<x_{e+1} \tag{16}$$

where u_i^e and T_i^e are nodal displacements and temperatures, respectively, and ψ_i^e and ϕ_i^e are quadratic and linear shape functions, respectively[9]. Furthermore, v and w are endowed with the properties of u and T. Note that a higher order element must be used for displacement than temperature due to the fact that temperature produces strain rather than displacement.

Timewise discretization is implemented via the following backward finite difference equations:

$$\frac{dT_m^e}{dt}(t)\cong[T_m^e(t)-T_m^e(t-\Delta t)]/\Delta t \quad m=1,2 \tag{17}$$

$$\frac{du_m^e}{dt}(t)\cong[u_m^e(t)-u_m^e(t-\Delta t)]/\Delta t \quad m=1,2,3 \tag{18}$$

The above equations require small time steps in order to guarantee numerical accuracy. However, they are unconditonally stable which is necessary because ISV growth laws (6) and (7) are numerically stiff[10].

Substitution of equations (15) through (18) into the governing field equations in variational form will result in the following algebraic equations:

$$\underbrace{\begin{bmatrix} 3x3 & 3x2 \\ K^e & S^e \\ \hline \bar{K}^e & \bar{S}^e \\ 2x3 & 2x2 \end{bmatrix}}_{5x5} \quad \underbrace{\begin{Bmatrix} U^e \\ \hline T^e \end{Bmatrix}}_{5x1} = \underbrace{\begin{Bmatrix} F^e \\ \hline \bar{F}'^e \end{Bmatrix}}_{5x1} \tag{19}$$

where $[K^e]$, $[S^e]$, $[\bar{K}^e]$, $[\bar{S}^e]$, and $\{F^e\}$ are as described in reference 5, and

$$\bar{F}'^e_i \equiv \bar{F}^e_i-\int_{x_e}^{x_{e+1}} c\phi_i^e\, q_c\, dx \tag{20}$$

where $\bar{F}_i^e$ is as defined in reference 5. The last term in the above equation accounts for thermal flux boundary conditions on the longitudinal surface of an element.

After global assembly and imposition of boundary conditions equations (19) can be solved in a time marching scheme in order to obtain the nodal displacements and temperatures as functions of time.

Global assembly of the element equations is accomplished in the standard way using the Boolean matrix[9].

Imposition of Boundary Conditions

For a typical space truss structural element, the boundary conditions are assumed to be of the following type:

$$\begin{aligned} u(0,t) &= u_t^o = \text{known} \\ u(L,t) &= u_t^L = \text{known} \\ T(0,t) &= T_t^o = \text{known} \\ T(L,t) &= T_t^L = \text{known} \end{aligned} \tag{21}$$

and [11]

$$q_c = -\alpha_s\left[q_s \cos\lambda_s + F_E(1-\alpha_E)q_s\cos\lambda_e + F_E q_E \cos\lambda_e\right] + \sigma_s\varepsilon(T^4 - T_D^4) \quad (22)$$

where the first term in the above equation is the solar radiation flux absorbed by the body, the second term is the solar radiation flux reflected by the earth and absorbed by the body, the third term is the earth radiation flux absorbed by the body, and the last term is the flux radiated by the member to space.

The above boundary conditons may be implemented to the discretized global equations in the standard way[9]. Although equation (22) technically includes the unknown temperature field, the component temperature is treated as a known quantity in this term for each time step. This approximation is acceptable due to the fact that the numerical stiffness[10] of constitutive equations (6) and (7) requires extremely small time steps in order to obtain an accurate solution.

EXAMPLE PROBLEMS

A typical structural element has been modeled with properties shown in TABLE 1. The material properties were obtained experimentally in the Mechanics and Materials Center at Texas A&M University[12] for Al 5086 at room temperature, which is similar to Al 6061-T6.

Sample cases were constructed for various cyclic loading rates for two different sets of thermal boundary conditions, as described in TABLE 2. Both cases are considered to be "worst cases" in that the component is in a maximum radiation flux condition at the maximum equilibrium temperature during one orbital cycle. The two cases differ in the emmissivity and absorptivity values for the component due to differences in surface treatment of the component. For case I, the component is anodized, and for case II, the component is painted with high emmissivity ITTRE-S13GLO white paint[13].

We now consider two elements in a large space structure (see Fig. 1). Both elements are constructed of the same material and are geometrically identical. However, element one is painted with the high emmissivity paint described above and is in full view of both earth and sun, whereas element two is anodized and is in view of earth only. For this case, as described in Table 2, the components have identical equilibrium temperatures T_E = 295°K(obtained by setting q_c=0 in equation (22)).

In both cases the structural members have been subjected to 50 cycles of loading at three different frequencies: 1 Hz, 5 Hz, and 25 Hz. These frequencies have been selected as representative of resonant frequencies in a representative space structure. For example, a typical structure analyzed in reference 14 has resonant frequencies of 4.1 Hz and 3.4 Hz in the first two modes. Because the resonant frequency of the first mode in the structural element itself is 240 Hz, inertial effects may be neglected in these examples.

Results for the cases described above are shown in Figs. 2 through 8. In Figs. 2 through 4 the cyclic stress-strain curve is shown at the

C_v = 900 J/kg/°K (0.215 Btu/lb/°F)

α = 23.8x10^{-6}in./in./°K (13.2x10^6 in./in./°F)

k = 1.27 x 10^{-4} MPa m^2/sec/°K (73.4 Btu/ft/h/°F)

E = 71.0 x 10^3 MPa (10.3 x 10^6 psi)

A = 6.45 x 10^{-4} m^2 (1.00 in^2)

T_R = 295 °K (72°F)

L = 3.66 m (12.0 FT)

D_o = 10 x 10^3 m/m

A_1 = 1.685 x 10^{-7} sec^{-1}

n = 2.355

m = 0.1770 MPa^{-1} (1.2205 Ksi^{-1})

Z_1 = 620.1 MPa (89.93 Ksi)

Z_I = 0.

r = 0.

ρ = 2.66 Mg/m^3 (0.096 lb/in.^{3})

c = 0.0508 m (0.8333 Ft.)

Z_o = 387.8 MPa (56.25 Ksi)

TABLE 1. Material and Geometric Properties for a Typical Truss Structural Element (from reference 11).

	CASE I	CASE II
α_s	0.20 (degraded)	0.3218 (degraded)
ε	0.85	0.24
λ_s	0°	0°
q_s	1.39 MPa m/sec	0
q_E	0.20 MPa m/sec	0.20MPa m/sec (4,080 km altitude)
λ_e	0°	0°
T_D	0°K	0°K
α_E	0.30	0.30
F_E	0.4	0.4
T_{EQ}	296.2°K (73.6°F)	296.2°K

CASE I - Surface painted with S13GLO white

CASE II - Chromic anodized surface

TABLE 2. Thermal Properties for Example Cases I and II (from references 12 and 13).

location x=L/2 for CASE I and at all three loading rates. It is found that in all cases the specimen reaches cyclic saturation after approximately five cycles. Thereafter, the hysteretic energy loss per cycle becomes a constant value.

In Figs. 5 through 7 the temperature rise is plotted for both cases at all three loading rates. As expected, the amount of temperature rise increases dramatically with loading rate. For example, after 50 cycles the total temperature rise at x=L/2 is 17.5°K(1 Hz), 62.5°K(5 Hz), and 119.7°K (25 Hz) for case I. Furthermore, it is apparent that while neither surface treatment can be regarded as resulting in negligible heating; at the higher loading rates the anodized surface treatment produces temperature rises which are significantly higher than those where the surface is painted with ITTRE-S13GLO paint. Finally, it is believed by these researchers that the nonlinear nature of the average temperature rise per cycle suggests that the temperature rise asymptotically approaches some upper bound, although this belief cannot be corroborated at this time due to the large computer times required in the current algorithm.

Fig. 8 shows that the spatial temperature variation at 5 Hz is approximately spatially homogeneous. Apparently, a very thin boundary layer forms near the end of the component, and this boundary layer has little effect on the temperature at x=L/2. In fact, subsequent investigations by the authors have shown that, at least for the geometry and physical conditions considered herein, identical results may be obtained more efficiently by neglecting spatial variations in displacement and temperature.

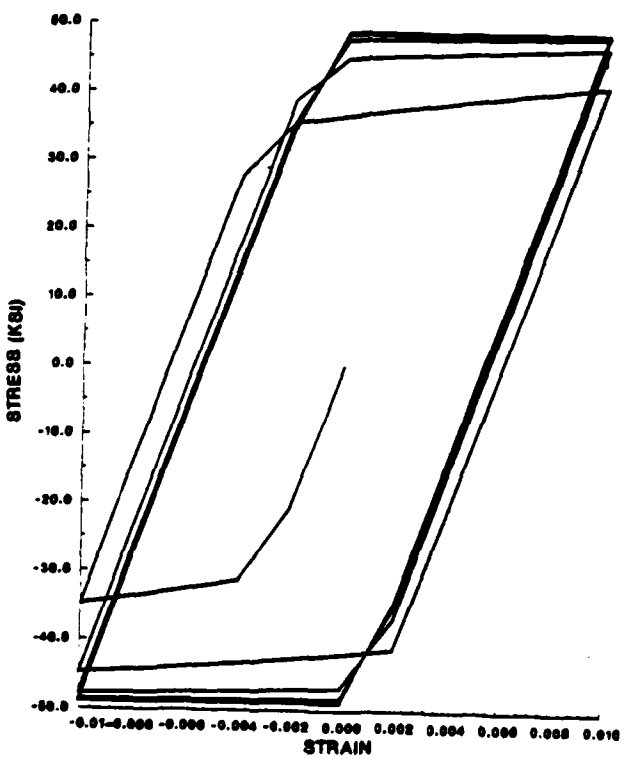

Fig. 2. Cyclic Stress-Strain Curve at x=L/2 for Case I Coating Loaded at 1 Hz.

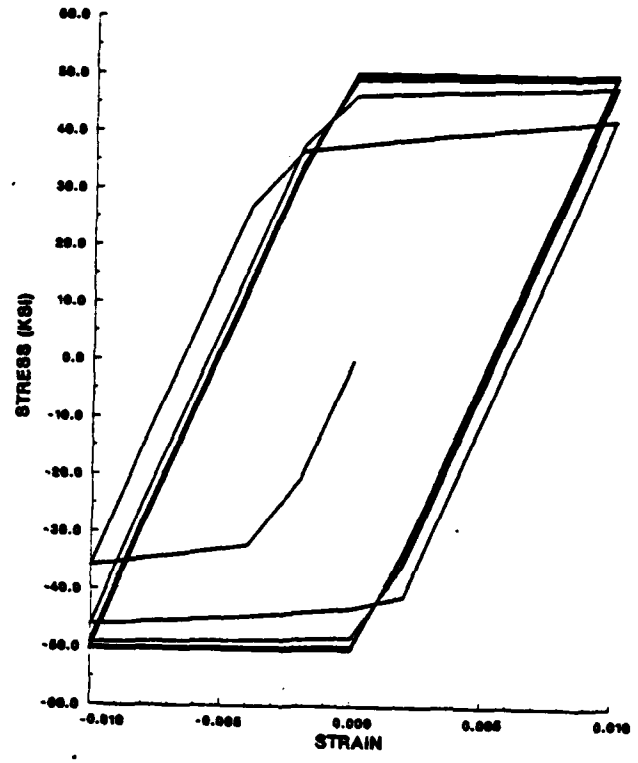

Fig. 3. Cyclic Stress-Strain Curve at x=L/2 for Case I Coating Loaded at 5 Hz.

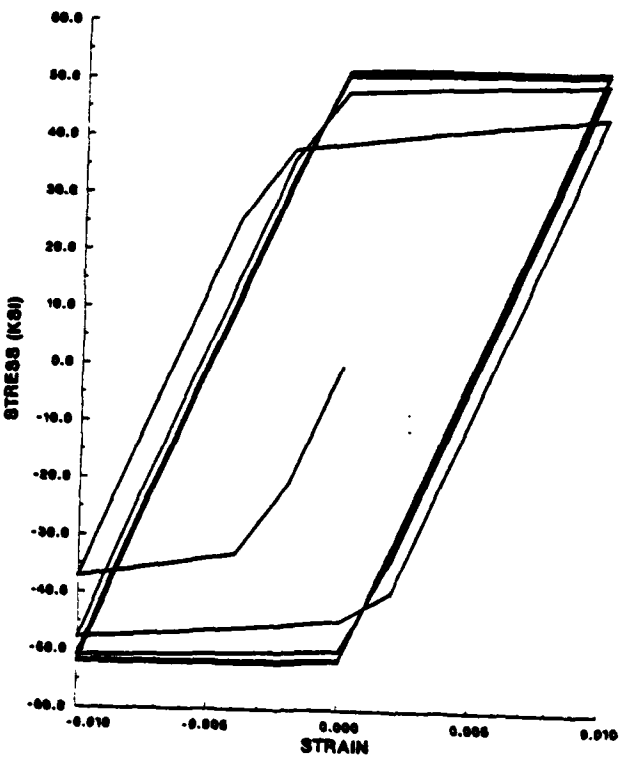

Fig. 4. Cyclic Stress-Strain Curve at x=L/2 for Case I Coating Loaded at 25 Hz.

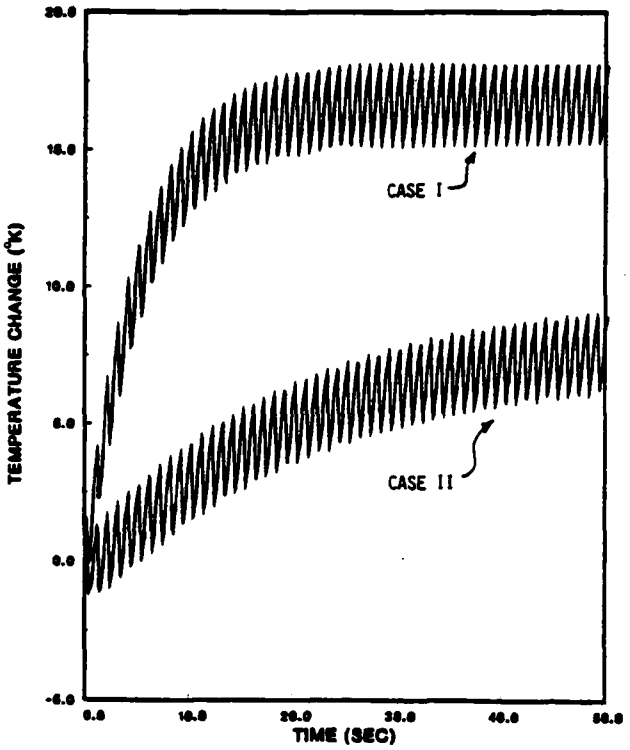

Fig. 5. Temperature vs. Time Curves at x=L/2 for Loading at 1 Hz.

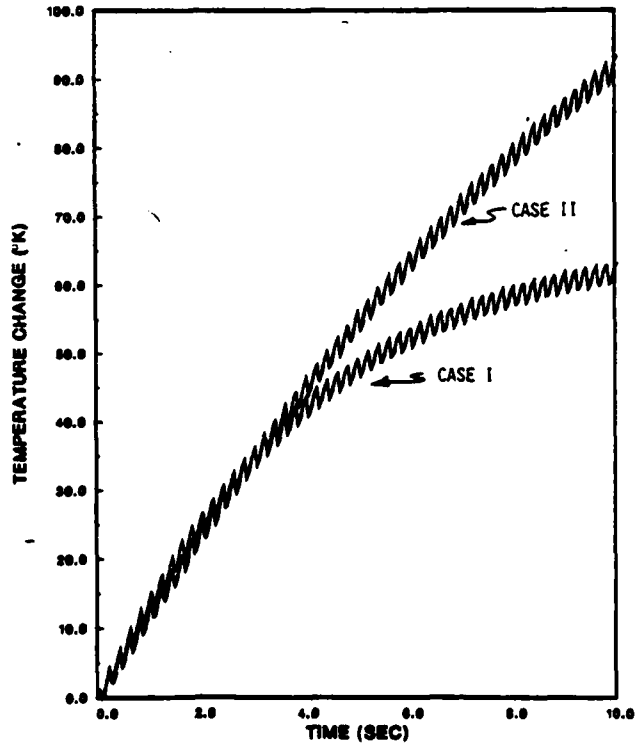

Fig. 6. Temperature vs. Time Curves at x=L/2 for Loading at 5 Hz.

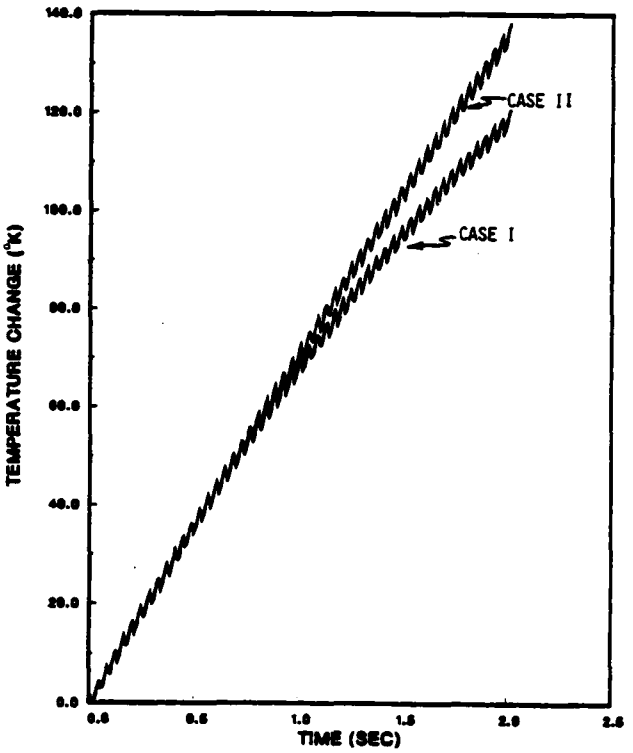

Fig. 7. Temperature vs. Time Curves at x=L/2 for Loading at 25 Hz.

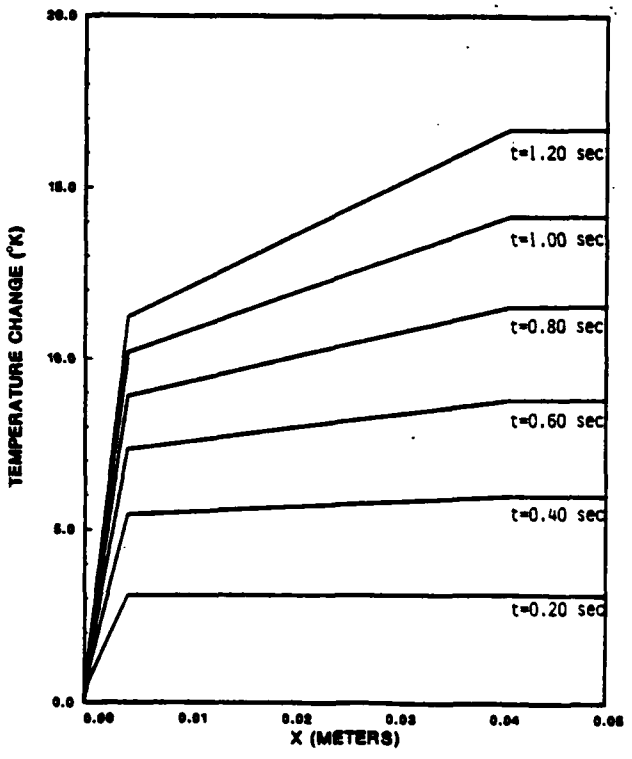

Fig. 8. Spatial Temperature Variation for Case I Coating Loaded at 5 Hz.

Conclusion

The current research has attempted to predict the response of a typical space structural element which is viscoplastic and is subjected to various cyclic loading conditions in the presence of radiation boundary conditions. Several general conclusions can be made as a result of this reasearch:

1) significant temperature rises may occur due to hysteretic loss, although the precise amount depends on loading rate and surface treatment;

2) the special paint ITTRE-S13GLO appears to produce significantly lower temperature rises than anodized surface treatment;

3) the temperature rise appears to be approaching an upper bound which is loading rate and surface treatment dependent; and

4) the thermal boundary layer which forms near the end of the member appears to have little effect on the far-field temperature rise.

These conclusions indicate that future research on this subject should perhaps concentrate on spatial variations in the radial direction rather than the axial direction. More importantly, these results indicate that an inelastic structural component may undergo temperature rises during structural vibrations which are so substantial that the material properties of the component may be further degraded, thus leading to failure of the component and perhaps even failure of the entire structure.

Acknowledgement

The authors wish to thank Dr. M.S. Pilant for his interesting discussion and helpful advice on this research. Support was provided by the Air Force Office of Scientific Research under contract no. F49620-83-C-0067.

References

1. S.R. Bodner and Y. Partom, "Constitutive Equations for Elastic-Viscoplastic Strain-Hardening Materials," J. Appl. Mech, Vol. 42, 385-389 (1975).

2. D.H. Allen, "Thermodynamic Constraints on the Constitution of a Class of Thermoviscoplastic Solids," Texas A&M University Mechanics and Materials Center, Report no. MM 12415-82-10, December (1982).

3. D.H. Allen, "A Prediction of Heat Generation in a Thermoviscoplastic Uniaxial Bar," Texas A&M University Mechanics and Materials Center Report no. MM 4875-83-10 (July 1983), (accepted for publication by Int. J. Solids Structures).

4. B.D. Coleman and M.E. Gurtin, "Thermodynamics with Internal State Variables," J. Chem. Phys., vol. 47, 597-613 (1967).

5. D.H. Allen, "Predicted Axial Temperature Gradient in a Viscoplastic Uniaxial Bar Due to Thermomechanical Coupling," Texas A&M University Mechanics and Materials Center Report no. MM 4875-84-15 (Nov. 1984).

6. D.H. Allen and W.E. Haisler, Introduction to Aerospace Structural Analysis, John Wiley, New York (1985).

7. T.M. Milly and D.H. Allen, "A Comparative Study of Nonlinear Rate-Dependent Mechanical Constitutive Theories for Crystalline Solids at Elevated Temperatures," Virginia Polytechnic Institute and State University, March, 1982.

8. D.H. Allen and J.M. Beek, "On the Use of Internal State Variables in Thermoviscoplastic Constitutive Equations," Proceedings 2nd Symposium on Nonlinear Constitutive Relations for High Temperature Applications, June, 1984.

9. J.N. Reddy, An Introduction to the Finite Element Method, McGraw-Hill, New York (1984).

10. Gear, C.W., "The Automatic Integration of Stiff Ordinary Differential Equations," Information Processing 68, North Holland, Vol. 1, p. 187 (1968).

11. E.W. Brogren, D.L. Barclay, and J.W. Straayer, "Simplified Thermal Estimation Techniques for Large Space Structures," NASA-CR-145253 (Oct. 1977).

12. J.M. Beek, "A Comparison of Current Models for Nonlinear Rate-dependent Material Behavior of Crystalline Solids," Texas A&M University Thesis (May 1985).

13. "Long Duration Exposure Facility (LDEF) Experimenter Users Handbook," NASA Langley Research Center, LDEF No. 840-2 (1978).

14. S. Kalyanasundaram, J.D. Lutz, W.E. Haisler, and D.H. Allen, "Effect of Degradation of Material Properties on the Dynamic Response of Large Structures," Texas A&M Mechanics and Materials Center, MM 4875-84-14 (June 1984).

APPENDIX 6.5

Mechanics and Materials Center
TEXAS A&M UNIVERSITY
College Station, Texas

ANALYSIS OF A THERMOVISCOPLASTIC UNIAXIAL BAR UNDER PRESCRIBED STRESS

PART I - THEORETICAL DEVELOPMENT

M.S. PILANT

MM-4875-85-2

JANUARY 1985

REPORT DOCUMENTATION PAGE

1a. REPORT SECURITY CLASSIFICATION unclassified	1b. RESTRICTIVE MARKINGS NA
2a. SECURITY CLASSIFICATION AUTHORITY NA	3. DISTRIBUTION/AVAILABILITY OF REPORT Unlimited
2b. DECLASSIFICATION/DOWNGRADING SCHEDULE NA	
4. PERFORMING ORGANIZATION REPORT NUMBER(S) MM 4875-85-2	5. MONITORING ORGANIZATION REPORT NUMBER(S) NA
6a. NAME OF PERFORMING ORGANIZATION Aerospace Engineering Dept. 6b. OFFICE SYMBOL (If applicable)	7a. NAME OF MONITORING ORGANIZATION Air Force of Scientific Research
6c. ADDRESS (City, State and ZIP Code) Texas A&M University College Station, Texas 77843	7b. ADDRESS (City, State and ZIP Code) Bolling AFB Washington, D.C. 20332
8a. NAME OF FUNDING/SPONSORING ORGANIZATION Air Force Office of Scien. Res. 8b. OFFICE SYMBOL (If applicable)	9. PROCUREMENT INSTRUMENT IDENTIFICATION NUMBER NA
8c. ADDRESS (City, State and ZIP Code) Washington, D.C. 20332	10. SOURCE OF FUNDING NOS. PROGRAM ELEMENT NO.: F49620-83-C-0067 PROJECT NO.: TASK NO.: WORK UNIT NO.:
11. TITLE (Include Security Classification) Analysis of A Thermo. Uniaxial Bar..Part I	
12. PERSONAL AUTHOR(S) M.S. Pilant	
13a. TYPE OF REPORT Interim 13b. TIME COVERED FROM _____ TO _____	14. DATE OF REPORT (Yr., Mo., Day) January 1985 15. PAGE COUNT
16. SUPPLEMENTARY NOTATION	
17. COSATI CODES FIELD / GROUP / SUB. GR.	18. SUBJECT TERMS (Continue on reverse if necessary and identify by block number)

19. ABSTRACT (Continue on reverse if necessary and identify by block number)

Under the assumption that the stress is a known function of time, the equations governing the behavior of a homogeneous, thermoviscoplastic uniaxial bar can be reduced to a single linear partial differential equation for the temperature in terms of stress. This is solved by means of Laplace transforms. Expressing the strain in terms of stress leads to an explicit compliance relationship for Bodner's model. The spatial dependence of the temperature can be recovered from the spatially homogeneous case by a convolution in time with an appropriate heat kernel.

20. DISTRIBUTION/AVAILABILITY OF ABSTRACT UNCLASSIFIED/UNLIMITED ☒ SAME AS RPT. ☐ DTIC USERS ☐	21. ABSTRACT SECURITY CLASSIFICATION Unclassified
22a. NAME OF RESPONSIBLE INDIVIDUAL M.S. Pilant	22b. TELEPHONE NUMBER (Include Area Code) (409) 845-3721 22c. OFFICE SYMBOL

ANALYSIS OF A THERMOVISCOPLASTIC UNIAXIAL BAR UNDER PRESCRIBED STRESS

PART I - THEORETICAL DEVELOPMENT

by

M.S. Pilant
Assistant Professor
Mathematics Department
Texas A&M University
College Station, TX 77843

MM-4875-85-2

January 1985

ABSTRACT

Under the assumption that the stress is a known function of time, the equations governing the behavior of a homogeneous, thermoviscoplastic uniaxial bar can be reduced to a single linear partial differential equation for the temperature in terms of stress. This is solved by means of Laplace transforms. Expressing the strain in terms of stress leads to an explicit compliance relationship for Bodner's model. The spatial dependence of the temperature can be recovered from the spatially homogeneous case by a convolution in time with an appropriate heat kernel.

Introduction

A general model for describing the time-dependent inelastic behavior of a thermo-viscoplastic material has been derived by D.H. Allen in [1].

The differential equations are highly nonlinear, and stiff with respect to the time variable. Consequently, a great deal of computational effort is needed to integrate the equations forward in time. Alternate methods for solving the equations are therefore desirable from a standpoint of numerical efficiency.

In the special case where the stress, σ, is a known function of time, it can be shown that the equations reduce to a single linear partial differential equation.

The modified temperature

$$T^*(x,t) = \exp\left(\frac{\alpha\sigma(t)}{\rho c_v}\right)(T(x,t)-T_\infty)$$

which we introduce in this report, satisfies the heat equation

$$\frac{\partial}{\partial t} T^* - \varepsilon^2 \frac{\partial^2}{\partial x^2} T^* = F[\sigma(t)]. \qquad (1.19)$$

In the spatially homogeneous case, with insulated boundaries, the modified temperature satisfies

$$\frac{d}{dt} T^* = F[\sigma(t)].$$

The solution of the partial differential equation (1.19) is related to the solution of the ordinary differential equation above by

$$\underset{\text{p.d.e.}}{T^*(x,t)} = G(x,t) * \underset{\text{o.d.e.}}{T^*} \qquad (f) \quad .$$

$G(x,t)$ is an appropriate heat kernel incorporating the boundary conditions of the problem, and the convolution is with respect to time.

The spatially dependent temperature solution can be recovered from the spatially uniform case given the kernel G(x,t), which is derived in this report.

The term ε^2 in (1.19) is typically on the order of 10^{-5} in nondimensionalized units, and causes a boundary layer to form near the ends of the bar. Away from the ends the temperature is very nearly spatially uniform. [2].

1. Stress Decoupling in Bodner's Model

As derived by D.H. Allen in [1], the coupled set of partial differential equations describing a homogeneous, thermoviscoplastic, uniaxial bar can be written in the form

$$\frac{\partial}{\partial x}\left\{EA\left[\frac{\partial u}{\partial x} - \alpha_1 - \alpha(T-T_R)\right]\right\} = -P_x \tag{1.1}$$

$$A\left\{E\left(\frac{\partial u}{\partial x} - \alpha_1 + \alpha T_R\right)\frac{\partial \alpha_1}{\partial t} + E\alpha^2 T\frac{\partial T}{\partial t}\right\} \tag{1.2}$$

$$- AE\alpha T\frac{\partial^2 u}{\partial x \partial t} - A\rho c_v\frac{\partial T}{\partial t} + A\frac{\partial}{\partial x}\left(k\frac{\partial T}{\partial x}\right) = -Ar\rho$$

with the addition of internal state variables $\alpha_1, \alpha_2, \ldots, \alpha_n$ satisfying

$$\frac{\partial \alpha_i}{\partial t} = \Omega_i(\varepsilon, T, \alpha_j) \quad j=1, \ldots, n \quad i=1, \ldots, n.$$

The strain ε is defined as $\varepsilon = \frac{\partial u}{\partial x}$. We also define the stress σ by

$$\sigma = E(\varepsilon - \alpha_1 - \alpha(T-T_R)).$$

For the Bodner model, we have two internal state variables, α_1, the axial inelastic strain, and α_2, the drag stress. By assumption these satisfy

$$\frac{\partial \alpha_1}{\partial t} = f_1(\alpha_2, \sigma) = \sqrt{\frac{2}{3}} D_o \frac{\sigma}{|\sigma|} \exp\left(-\frac{n+1}{2n}\left(\frac{\alpha_2}{\sigma}\right)^{2n}\right) \tag{1.3}$$

and

$$\frac{\partial \alpha_2}{\partial t} = f_2(\alpha_2, \sigma) = m(z_1 - \alpha_2)\,\sigma\frac{\partial \alpha_1}{\partial t} - \bar{A} z_1 \left(\frac{\alpha_2 - z_I}{z_1}\right)^r \tag{1.4}$$

where D_o, n, m, z_1, z_I, $\bar{A}$, and r are experimentally determined parameters (constants).

From the definition of stress, we may write the stress strain relation as

$$\varepsilon = E^{-1}\,\sigma + \alpha_1 + \alpha(T-T_R). \tag{1.5}$$

Another relation which easily follows is

$$E\left(\frac{\partial u}{\partial x} - \alpha + \alpha T_R\right) = \sigma + E\alpha T \tag{1.6}$$

This will be used later to simplify the Fourier heat conduction equation (1.2).

If we assume that $p_x = 0$, then we can write equation (1.1) as

$$\frac{\partial}{\partial x}\{A\sigma\} = 0 \tag{1.7}$$

which, for constant cross sectional area A, implies that

$$\sigma = \sigma(t). \tag{1.8}$$

Consequently, no matter how complicated the relationship between σ and ε, (1.8) will hold as long as there is no applied load p_x.

Instead of solving the forward problem, that is determining α_1, α_2, u and T from (1.1) - (1.4), we will regard $\sigma = \sigma(t)$ as being known. As we will see, this allows simplification of (1.2). Viewing $\sigma = \sigma(t)$ as a known function, we will derive expressions for α_1, α_2 and T in terms of σ, which yields an implicit relationship between ε and σ via (1.5).

First we derive a relation between α_2 and σ. If we substitute (1.3) into (1.4), a first order differential equation results.

$$\frac{\partial \alpha_2}{\partial t} = m(z_1 - \alpha_2)\,\sigma\left[\frac{2}{\sqrt{3}} D_o \frac{\sigma}{|\sigma|}\left(\exp\left(\frac{-n+1}{2n}\right)\left(\frac{\alpha_2}{\sigma}\right)^{2n}\right]\right. \tag{1.9}$$

$$\left. -\bar{A} z_1 \left(\frac{\alpha_2 - z_I}{z_1}\right)^r\right]$$

$$= F_2[\alpha_2, \sigma]$$

Given $\sigma = \sigma(t)$, α_2 is uniquely determined by the initial conditions

$$\alpha_2(x,o)=\alpha_2^{(0)}(x).$$

If, initially $\alpha_2^{(0)}(x)$= constant, then α_2 is a function only of the variable t. Therefore the integral relation

$$\alpha_2(t) = \alpha_2^{(0)} + \int_0^t F_2(\sigma(s),\alpha_2(s))ds \qquad (1.10)$$

defines α_2 implicity as a function of σ. We will occasionally write

$$\alpha_2 = \alpha_2(t;\sigma(t))$$

to emphasize the dependence of α_2 on σ.

Once α_2 has been determined, by numerically integrating (1.9) if necessary, we may solve for α_1. Again, assuming that the initial data for α_1 is constant,

$$\alpha_1(t) = \alpha_1^{(0)} + \int_0^t f_1(\alpha_2(s),\sigma(s))ds. \qquad (1.11)$$

Therefore, knowledge of $\sigma = \sigma(t)$ determines the internal state variables α_1 and α_2 as functions of time uniquely. Mathematically, we have effectively <u>decoupled</u> (1.3), (1.4) from (1.1) and (1.2). Since σ is a function only of t, (1.1) is automatically satisfied. In this formulation, (1.1) becomes a compatibility condition between the stress σ, and the displacement, u.

Substituting (1.5) and (1.6) into (1.2), we obtain

$$(\sigma+E\alpha T)\frac{\partial\alpha_1}{\partial t} + E\alpha^2 T\frac{\partial T}{\partial t} - E\alpha T\frac{\partial}{\partial t}\left[\frac{\sigma}{E} + \alpha_1 + \alpha(T-T_R)\right]$$

$$- \rho c_v\frac{\partial T}{\partial t} + k\frac{\partial^2 T}{\partial X^2} = 0 \qquad (1.12)$$

This may be simplified, after cancelling terms, to the linear equation

$$-\rho c_v \frac{\partial T}{\partial t} + k \frac{\partial^2 T}{\partial x^2} + \sigma(t) \frac{\partial \alpha_1}{\partial t} - \alpha\sigma'(t)T = 0$$

which we will write as

$$\frac{\partial T}{\partial t} - \varepsilon^2 \frac{\partial^2 T}{\partial x^2} + \left[\frac{\alpha\sigma'(t)}{\rho c_v}\right] T = \frac{\sigma(t)}{\rho c_v} \frac{\partial \alpha_1(t)}{\partial t} \qquad (1.13)$$

where $\varepsilon^2 = \frac{k}{\rho c_v}$ is typically of the order of 10^{-5} in nondimensionalized units. The presence of $\varepsilon^2 << 1$ causes a boundary layer to form, near the ends of the uniaxial rod. Near the center of the rod, for small time, the temperature field is nearly spatially homogeneous and is in close agreement with the solution of (1.13) obtained by setting $\varepsilon = 0$. Eventually, however, the boundary layer reaches the center and influences the temperature field. The investigation of this boundary layer phenomenon will be the subject of a future technical report.

The boundary conditions we consider are those appropriate for a symmetric temperature distribution, with T initially equal to T_R, and with convection boundary conditions holding at the ends of the rod. We normalize the domain by setting the length = 2 units.

$$\begin{aligned} &T(x,0) = T_R \\ &T_x(1,t) = 0 \\ &kT_x(0,t) - \beta(T(0,t) - T_\infty) = 0 \end{aligned} \qquad (1.14)$$

By a simple transformation, we make the boundary conditions homogeneous. Define the quantity

$$\bar{T} = T(x,t) - T_\infty.$$

$\bar{T}$ satisfies

$$\frac{\partial}{\partial t}\,\bar{T} - \varepsilon^2 \frac{\partial^2 \bar{T}}{\partial x^2} + \left[\frac{\alpha\sigma'(t)}{\rho c_v}\right]\bar{T} = \frac{\sigma(t)}{\rho c_v}\,\frac{\partial \alpha_1}{\partial t} - \frac{T_\infty\ \alpha\sigma'(t)}{\rho c_v} \tag{1.15}$$

$$\bar{T}(x,0) = T_R - T_\infty$$
$$\bar{T}_x(1,t) = 0$$
$$k\bar{T}_x(0,t) - \beta\bar{T}(0,t) = 0$$

The boundary value problem (1.15) may be further simplified by introducing the modified temperature

$$T^*(x_1 t) = \bar{T}(x_1 t)\ \exp\left(\frac{\alpha\sigma(t)}{\rho c_v}\right) \tag{1.16}$$

Multiplying (1.15) by the factor $\exp\left(\frac{\alpha\sigma(t)}{\rho c_v}\right)$

(essentially an integrating factor), we obtain

$$\frac{\partial}{\partial t}\,T^* - \varepsilon^2 \frac{\partial^2 T^*}{\partial x^2} = \left[\frac{\sigma(t)}{\rho c_v}\,\frac{\partial \alpha_1}{\partial t} - T_\infty\,\frac{\alpha\sigma'(t)}{\rho c_v}\right]\ \exp\left[\frac{\alpha\sigma(t)}{\rho c_v}\right] \tag{1.17}$$

Assuming $\sigma(0) = 0$, we obtain

$$T^*(x,0) = T_R - T_\infty$$
$$T^*_x(1,t) = 0$$
$$kT^*_x(0,t) - \beta T^*(0,t) = 0.$$

We set

$$F(t) := \left[\frac{\sigma(t)}{\rho c_v}\ \frac{\partial \alpha_1}{\partial t} - T_\infty\,\frac{\alpha\sigma'(t)}{\rho c_v}\right]\ \exp\left[\frac{\alpha\sigma(t)}{\rho c_v}\right] \tag{1.18}$$

which is a uniquely determined function of t, given $\sigma = \sigma(t)$

We have therefore derived the following linear, constant coefficient, heat equation, satisfied by T*

$$\frac{\partial}{\partial t} T^* - \varepsilon^2 \frac{\partial^2 T^*}{\partial x^2} = F(t) \tag{1.19}$$

$$T^*(x,0) = T_R - T_\infty$$

$$T_x^*(1,t) = 0$$

$$kT_x^*(0,t) - \beta T^*(0,t) = 0$$

The temperature, T, may be recovered by computing (1.20)

$$T = T(x,t) = T_\infty + \bar{T}(x,t)$$

$$= T_\infty + T^*(x,t) \exp\left(\frac{-\alpha\sigma(t)}{\rho c_v}\right).$$

The solution of (1.19), by Laplace transform methods, is the subject of the next section.

2. Solving for the Modified Temperature by means of Laplace Transforms.

First we define the quantities

$$\hat{T}(x,s) = L[T^*(x,t)] = \int_0^\infty e^{-st} T^*(x,t)dt$$

and

$$\hat{F}(s) = L[F(t)].$$

Applying the Laplace transform L to both sides of (1.19) and to the boundary conditions, we obtain a second order, linear, ordinary differential equation for $\hat{T}(x,s)$.

$$s\hat{T}(x,s) - [T_R - T_\infty] - \varepsilon^2 \frac{\partial^2 \hat{T}}{\partial x^2}(x,s) = \hat{F}(s) \tag{2.1}$$

$$\hat{T}_x(1,s) = 0$$

$$k\hat{T}_x(0,s)-\beta\hat{T}(0,s)=0.$$

A particular solution of (2.1) is

$$\hat{T} = \frac{1}{s}(\hat{F}(s)+T_R-T_\infty)$$

So the general solution of (2.1) may be written in the form

$$\hat{T}(x,s)= \frac{1}{s}\ [\hat{F}(s)+T_R-T_\infty]+A(s)\exp(\frac{-x\sqrt{s}}{\varepsilon})+B(s)\exp(\frac{+x\sqrt{s}}{\varepsilon}) \qquad (2.2)$$

for s>o, where A(s) and B(s) are uniquely determined by the boundary conditions. If $\beta\neq 0$, the expressions for A(s) and B(s) are rather complicated:

$$B(s) = \left\{\frac{k\sqrt{s}}{\varepsilon}(1-\exp\frac{2\sqrt{s}}{\varepsilon})-\beta(1+\exp\frac{2\sqrt{s}}{\varepsilon})\right\}^{-1} \beta\frac{1}{s}\ [\hat{F}(s)+T_R-T_\infty]$$

$$A(s) = B(s)\exp(\frac{2\sqrt{s}}{\varepsilon}). \qquad (2.3)$$

Substituting these expressions into (2.2) we obtain

$$\hat{T}(x,s) = \frac{1}{s}\ [\hat{F}(s)+T_R-T_\infty] + B(s)\exp[(\frac{2-x}{\varepsilon})\sqrt{s}]+B(s)\exp(\frac{+x\sqrt{s}}{\varepsilon})$$

Therefore

$$\hat{T}(x,s) = \frac{1}{s}\ [\hat{F}(s)+T_R-T_\infty] + \beta\frac{1}{s}\ [\hat{F}(s)+T_R-T\infty]\left[\frac{\exp(\frac{2-x\sqrt{s}}{\varepsilon}) + \exp(\frac{x\sqrt{s}}{\varepsilon})}{\frac{k\sqrt{s}}{\varepsilon}(1-\exp(\frac{2\sqrt{s}}{\varepsilon}) - \beta(1+\exp(\frac{2\sqrt{s}}{\varepsilon})}\right]$$

$$= \frac{1}{s}\ [\hat{F}(s) + T_R-T_\infty]\left\{1-\beta\ \frac{[\exp(\frac{1-x\sqrt{s}}{\varepsilon}) + \exp(\frac{x-1\sqrt{s}}{\varepsilon})]}{\frac{k\sqrt{s}}{\varepsilon}[\exp(\frac{-\sqrt{s}}{\varepsilon}) - \exp(\frac{\sqrt{s}}{\varepsilon})]-\beta[\exp(\frac{-\sqrt{s}}{\varepsilon})+\exp(\frac{+\sqrt{s}}{\varepsilon})]}\right\}$$

$$= \frac{1}{s}\left[\hat{F}(s) + T_R - T_\infty\right] \left\{1 - \beta \cdot \frac{\cosh\left[\frac{(1-x)\sqrt{s}}{\varepsilon}\right]}{\frac{k\sqrt{s}}{\varepsilon}\sinh\left(\frac{\sqrt{s}}{\varepsilon}\right) + \cosh\frac{\sqrt{s}}{\varepsilon}}\right\} \qquad (2.4)$$

We will find it convenient to define the kernel function $G(x,t)$ by

$$\hat{G}(x,s) = 1 - \beta \cdot \cosh\left[(1-x)\frac{\sqrt{s}}{\varepsilon}\right]\left[\frac{k\sqrt{s}}{\varepsilon}\sinh\frac{\sqrt{s}}{\varepsilon} + \beta\cosh\frac{\sqrt{s}}{\varepsilon}\right]^{-1} \qquad (2.5)$$

The expression (2.4) reduces to

$$\hat{T}(x,s) = \frac{1}{s}\left[\hat{F}(s) + T_R - T_\infty\right]\hat{G}(x,s) \qquad (2.6)$$

which implies

$$T^*(x,t) = L^{-1}[\hat{T}(x,s)] = L^{-1}\left\{\frac{1}{s}\left[\hat{F}(s) + T_R - T_\infty\right]\right\} * G(x,t) \qquad (2.7)$$

$$= G(x,t) * \left[\int_0^t F(\tau)d\tau + T_R - T_\infty\right]$$

Therefore, from (1.20), (2.7), and (1.18)

$$T = T_\infty + T^*(x,t)\exp\left(\frac{-\alpha\sigma(t)}{\rho c_v}\right)$$

$$= T_\infty + \exp\left(\frac{-\alpha\sigma(t)}{\rho c_v}\right) G(x,t) * \left[\int_0^t F(\tau)d\tau + T_R - T_\infty\right]$$

$$= T_\infty + \exp\left(\frac{-\alpha\sigma(t)}{\rho c_v}\right) G(x,t) * \left\{T_R - T_\infty + \int_0^t \left[\frac{\sigma(t)}{\rho c_v}\frac{\partial\alpha_1}{\partial t} - T_\infty\frac{\alpha\sigma'(t)}{\rho c_v}\right]\exp\left(\frac{\alpha\sigma(\tau)}{\rho c_v}\right)d\tau\right\}$$

$$= T_\infty + \exp\left(\frac{-\alpha\sigma(t)}{\rho c_v}\right) G(x,t) * \left\{T_R - T_\infty + \int_0^t \frac{\sigma(t)}{\rho c_v}\frac{\partial\alpha_1}{\partial t}\exp\left(\frac{\alpha\sigma(t)}{\rho c_v}\right)d\tau - \left[T_\infty\exp\left(\frac{\alpha\sigma(t)}{\rho c_v}\right) - T_\infty\right]\right\}$$

Substituting (1.3) for $\frac{\partial\alpha_1}{\partial t}$ and cancelling T_∞, we finally obtain the result

$$T(x,t) = T_\infty + \exp\left(-\frac{\alpha\sigma(t)}{\rho c_v}\right) G(x,t)* \left\{T_R + \right.$$

$$\int_0^t \frac{|\sigma(\tau)|}{\rho c_v} \frac{2}{\sqrt{3}} D_0 \exp\left(-\frac{n+1}{2n}\left(\frac{\alpha_2(\tau)}{\sigma(\tau)}\right)^{2n}\right) \exp\left(\frac{\alpha\sigma(\tau)}{\rho c_v}\right) d\tau$$

$$\left. - T_\infty \exp\left(\frac{\alpha\sigma(t)}{\rho c_v}\right)\right\} \qquad (2.8)$$

$$= T[\alpha_2, \sigma]$$

where α_2 is given by solving (1.4), $G(x,t)$ is given by (2.5), and $\sigma(t)$ is a prescribed function of time.

We note, that in the case, $\beta = 0$, the expression for $\hat{G}$ simplifies to

$$\hat{G}(x,s)=1$$

consequently, for $\beta = 0$.

$$\hat{T}(x,s)= \frac{1}{s}\left[\hat{F}(s)+ T_R - T_\infty\right]$$

and $T^*(x,t)= \int_0^t F(\tau)d\tau + T_R - T_\infty$. This implies that

$$T=T_\infty + \exp\left(-\frac{\alpha\sigma(t)}{\rho c_v}\right)\left[T_R - T_\infty\right.$$

$$\left. + \int_0^t \frac{\sigma(\tau)}{\rho c_v} \frac{\partial\alpha_1}{\partial t} \exp\left(\frac{\alpha\sigma(\tau)}{\rho c_v}\right) d\tau - T_\infty \exp\left(\frac{\alpha\sigma(t)}{\rho c_v}\right) + T_\infty \right]$$

$$= \exp\left(-\frac{\alpha\sigma(t)}{\rho c_v}\right) T_R +$$

$$+ \exp\left(-\frac{\alpha\sigma(t)}{\rho c_v}\right) \int_0^t \frac{\sigma(\tau)}{\rho c_v} \frac{\partial\alpha_1}{\partial t} \exp\left(\frac{\alpha\sigma(\tau)}{\rho c_v}\right) d\tau$$

$$= \exp\left(-\frac{\alpha\sigma(t)}{\rho c_v}\right) \left\{T_R + \int_0^t \frac{|\sigma(\tau)|}{\rho c_v} \frac{2}{\sqrt{3}} D_0 \exp\left(-\frac{n+1}{2n}\left(\frac{\alpha_2}{\sigma}\right)^{2n}\right).\exp\left(\frac{\alpha\sigma(\tau)}{\rho c_v}\right)d\tau \exp\right\}$$

This reduces finally to

$$T = \exp\left(-\frac{\alpha\sigma(t)}{\rho c_v}\right) \left\{T_R + \int_0^t \frac{|\sigma(\tau)|}{\rho c_v} \frac{2D_0}{\sqrt{3}} \exp\left[-\left(\frac{n+1}{2n}\right)\left(\frac{\alpha_2(\tau)}{\sigma(\tau)}\right)^{2n} + \frac{\alpha\sigma(\tau)}{\rho c_v}\right] d\tau\right\} \quad (2.9)$$

We note that this is a function only of time, and also that the integrand is strictly positive. This implies that the bracketed quantity is monotonically increasing function of time. This implies that even in the periodic stress case, after one cycle, a relative temperature difference of

$$0 < \int_0^{tp} \frac{|\sigma(\tau)|}{\rho c_v} \frac{2D_0}{\sqrt{3}} \exp\left[-\frac{(n+1)}{2n}\left(\frac{\alpha_2(\tau)}{\sigma(\tau)}\right)^{2n} + \frac{\alpha\sigma(\tau)}{\rho c_v}\right] d\tau \quad (2.10)$$

has developed; where t_p denotes the period of $\sigma(t)$.

A numerical investigation of (2.9) and (2.10) with $\sigma = \sigma(t) = \sigma_0 \sin wt$, will be done in a subsequent report.

3. Nonlinear Compliance in terms of Convolutions:

In order to express the strain as a function of stress, we utilize (1.5), (1.11), and (2.8) to obtain:

$$\varepsilon = E^{-1}\sigma(t) + \alpha_1[\sigma(t)] + \alpha[T[\alpha_2,\sigma] - T_R]$$

$$= E^{-1}\sigma + \int_0^t f_1(\alpha_2,\sigma(t)dt + \alpha_1^{(0)} \quad (3.1)$$

$$+ \alpha\left\{T_\infty - T_R + \exp\left(-\frac{\alpha\sigma(t)}{\rho c_v}\right) G(x,t)*\right.$$

$$\left.\left[T_R + \int \frac{|\sigma(t)|}{\rho c_v}\frac{2}{\sqrt{3}} D_0 \exp\left(-\frac{n+1}{2n}\left(\frac{\alpha_2(\tau)}{\sigma(\tau)}\right)^{2n} + \frac{\alpha\sigma(\tau)}{\rho c_v}\right) d\tau - T_\infty \exp\left(\frac{\alpha\sigma(\tau)}{\rho c_v}\right)\right]\right\}$$

We will write this in the form:

$$\varepsilon = E^{-1}\sigma(t)+C+\int_0^t H_1[\sigma]d\tau \quad +\alpha \exp\left(-\frac{\alpha\sigma(t)}{\rho c_v}\right) \quad G*H_2[\sigma] \tag{3.2}$$

where $C = \alpha_1^{(0)} + \alpha[T_\infty - T_R]$,

$$H_1[\sigma] = f_1(\alpha_2;\sigma(t)] = \frac{2}{\sqrt{3}} \; D_o \; \frac{\sigma}{|\sigma|} \exp\left(-\frac{n+1}{2n}\left(\frac{\alpha_2(\sigma)}{\sigma}\right)^{2n}\right)$$

and

$$H_2[\sigma]=T_R + \int_0^t \frac{|\sigma(\tau)|}{\rho c_v} \frac{2}{\sqrt{3}} D_o \exp\left[\frac{-n+1}{2n}\left[\frac{\alpha_2(t,\sigma(t))}{\sigma(\tau)}\right]^{2n} + \frac{\alpha\sigma(t)}{\rho c_v}\right]$$

$$- T_\infty \exp\left[\frac{\alpha\sigma(t)}{\rho c_v}\right]$$

$\alpha_2[t,\sigma(t)]$ is given by the solution of

$$\frac{d\alpha_2}{dt} = f_2(\alpha_2,\sigma) = m\,(z_1-\alpha_2)\,\sigma\,\frac{\partial\alpha_1}{\partial t} \quad - \bar{A}\, z_1\left(\frac{\alpha_2 - z_I}{z_1}\right)^r \tag{1.4}$$

and

$$G=G(x,t)=L^{-1}\left\{1-\beta\;\frac{\cosh\,(1-x)\,\sqrt{\frac{s}{\varepsilon}}}{\frac{k\sqrt{s}}{\varepsilon}\sinh\left(\frac{\sqrt{s}}{\varepsilon}\right)+\beta\cosh\frac{\sqrt{s}}{\varepsilon}}\right\}$$

from (2.5).

Equation (3.2) gives a closed form expression for the compliance of the Bodner model with two internal state variables. We note that the contribution of α_1 is the integral

$$\alpha_1^{(0)} + \int_0^t H_1[\sigma]dt = \alpha_1^{(0)} + \int_0^t H_1[\sigma(\tau),\ \alpha_2(\tau,\sigma(\tau))]\ d\tau$$

while the effect of the temperature and spatial variation is to introduce a convolution in time, multiplied by the factor $\exp(-\frac{\alpha\sigma(t)}{\rho c_v})$.

If $\sigma'(t)$ = constant, then we have a pure convolution with H_2. A non constant stress rate introduces the operator

$$\exp(-\frac{\alpha\sigma(t)}{\rho c_v}).G(x,t)*$$

rather than

$$G(x,t)*$$

A detailed examination of the asymptotic behavior of (2.8) and (3.2), as $t\to\infty$, for the cyclic case

$$\sigma(t)=\sigma_o \sin \omega t$$

will appear in a future report.

The function G contains the diffusion phenomena and thermomechanical coupling within it. A detailed analysis of G=G(x,t) and asymptotic representations of the solution to (1.1)-(1.4) will appear in a future report.

4. Conclusions.

In the spatially uniform case, that is when insulated boundary conditions hold at the ends of the rods, instead of (1.19) we have

$$\frac{d}{dt} T^* = F[\sigma(t)] \tag{4.1}$$

$$T^*(o) = T_R - T_\infty$$

which has the solution

$$T^*(t) = \int_o^t F[\sigma(\tau)]d\tau + T_R - T_\infty \tag{4.2}$$

which we denote by $T^*_{o.d.e}(t)$. We therefore arrive at the important conclusion that

$$T^*_{p.d.e.}(x,t) = G(x,t) * T^*_{o.d.e}(t). \tag{4.3}$$

Therefore, given the solution of the problem in the case of insulated boundary conditions and known stress history $\sigma(t)$, the solution of the problem for general boundary conditions is recovered by a convolution in time with an appropriate heat kernel $G(x,t)$.

The effect of the term ε^2 in (1.13) is to force a boundary layer to form at the ends of the rod. Away from the ends, and for small time, the solution is very nearly spatially independent. [2].

Acknowledgement

The author wishes to acknowledge the helpful discussions and comments provided by D.H. Allen. This research was supported by the Air Force Office of Scientific Research under contract no. F49620-83-C-0067.

REFERENCES

[1] Allen, D.H., "A Prediction of Heat Generation in a Thermoviscoplastic Uniaxial Bar," Texas A&M Mechanics and Materials Center, MM 4875-83-10, July, 1983 (to be published in International Journal of Solids and Structures).

[2] Allen, D.H., "Predicted Axial Temperature Gradient in a Viscoplastic Uniaxial Bar Due to Thermomechanical Coupling," Texas A&M Mechanics and Materials Center, MM 4875-84-15, November, 1984.

APPENDIX 6.6

Mechanics and Materials Center
TEXAS A&M UNIVERSITY
College Station, Texas

ANALYSIS OF A THERMOVISCOPLASTIC UNIAXIAL BAR UNDER PRESCRIBED STRESS

PART II - BOUNDARY LAYER AND ASYMPTOTIC ANALYSIS

M. S. PILANT

MM-4875-85-6

MAY 1985

SECURITY CLASSIFICATION OF THIS PAGE

REPORT DOCUMENTATION PAGE

1a. REPORT SECURITY CLASSIFICATION unclassified	1b. RESTRICTIVE MARKINGS NA
2a. SECURITY CLASSIFICATION AUTHORITY NA	3. DISTRIBUTION/AVAILABILITY OF REPORT unlimited
2b. DECLASSIFICATION/DOWNGRADING SCHEDULE NA	
4. PERFORMING ORGANIZATION REPORT NUMBER(S) MM 4875-85-6	5. MONITORING ORGANIZATION REPORT NUMBER(S) NA
6a. NAME OF PERFORMING ORGANIZATION Aerospace Engineering Dept. 6b. OFFICE SYMBOL (If applicable)	7a. NAME OF MONITORING ORGANIZATION Air Force of Scientific Research
6c. ADDRESS (City, State and ZIP Code) Texas A&M University College Station, Texas 77843	7b. ADDRESS (City, State and ZIP Code) Bolling AFB Washington, D. C. 20332
8a. NAME OF FUNDING/SPONSORING ORGANIZATION Air Force Office of Scien. Res. 8b. OFFICE SYMBOL (If applicable)	9. PROCUREMENT INSTRUMENT IDENTIFICATION NUMBER NA
8c. ADDRESS (City, State and ZIP Code) Washington, D. C. 20332	10. SOURCE OF FUNDING NOS. PROGRAM ELEMENT NO.: F49620-83-C-0067 PROJECT NO.: TASK NO.: WORK UNIT NO.:
11. TITLE (Include Security Classification) Analysis of a Thermo. Uniaxial Bar...Part II	
12. PERSONAL AUTHOR(S) M. S. Pilant	
13a. TYPE OF REPORT Interim 13b. TIME COVERED FROM _____ TO _____	14. DATE OF REPORT (Yr., Mo., Day) May 1985 15. PAGE COUNT 17
16. SUPPLEMENTARY NOTATION	
17. COSATI CODES FIELD / GROUP / SUB. GR.	18. SUBJECT TERMS (Continue on reverse if necessary and identify by block number)

19. ABSTRACT (Continue on reverse if necessary and identify by block number)

Under the assumption that the stress is a known function of time, the equations governing the behavior of a homogeneous, thermoviscoplastic uniaxial bar (Bodner Model) can be reduced to a single linear partial equation for the temperature in terms of the stress. This can be solved by transform methods.

In this report, an explicit series representation of the temperature in terms of the stress is obtained by separation of variables techniques. With the assumption of periodic stress, bounds on the time averaged maximum temperature increase obtained.

In order to describe the thermal boundary layers near the ends of the rod, an asymptotic model is developed which used a spatially homogeneous solution as a starting point.

Finally, various mathematical details regarding the Green's function and series are investigated.

20. DISTRIBUTION/AVAILABILITY OF ABSTRACT UNCLASSIFIED/UNLIMITED ☒ SAME AS RPT. ☐ DTIC USERS ☐	21. ABSTRACT SECURITY CLASSIFICATION Unclassified
22a. NAME OF RESPONSIBLE INDIVIDUAL M. S. Pilant	22b. TELEPHONE NUMBER (Include Area Code) (409) 845-3721 22c. OFFICE SYMBOL

DD FORM 1473, 83 APR EDITION OF 1 JAN 73 IS OBSOLETE.

unclassified

SECURITY CLASSIFICATION OF THIS PAGE

ANALYSIS OF A THERMOVISCOPLASTIC UNIAXIAL BAR UNDER PRESCRIBED STRESS PART II - BOUNDARY LAYER AND ASYMPTOTIC ANALYSIS

by

M. S. Pilant
Assistant Professor
Mathematics Department
Texas A & M University
College Station, TX 77843

ABSTRACT

Under the assumption that the stress is a known function of time, the equations governing the behavior of a homogeneous, thermoviscoplastic uniaxial bar (Bodner Model) can be reduced to a single linear partial differential equation for the temperature in terms of the stress. This can be solved by transform methods.

In this report, an explicit series representation of the temperature in terms of the stress is obtained by seperation of variables techniques. With the assumption of periodic stress, bounds on the time averaged maximum temperature increase are obtained.

In order to describe the thermal boundary layers near the ends of the rod, an asymptotic model is developed which uses a spatially homogeneous solution as a starting point. Finally, various mathematical details regarding the Green's function and series solution are investigated.

Introduction.

In [1], we showed that the equations describing the behavior of a thermovisco-plastic uniaxial bar (as derived in [2])

$$\frac{\partial}{\partial x}\left\{EA\left[\frac{\partial u}{\partial x}-\alpha_1-\alpha(T-T_R)\right]\right\}=-p_x \tag{0.1}$$

$$A\left\{E\left(\frac{\partial u}{\partial x}-\alpha_1+\alpha T_R\right)\frac{\partial \alpha_1}{\partial t}+E\,\alpha^2 T\frac{\partial T}{\partial t}\right\} \tag{0.2}$$

$$-AE\,\alpha T\frac{\partial^2 u}{\partial x\,\partial t}-A\,\rho c_v\frac{\partial T}{\partial t}+A\frac{\partial}{\partial x}\left(k\frac{\partial T}{\partial x}\right)=-Ar\,\rho,$$

$$\frac{\partial \alpha_1}{\partial t}=\frac{2}{\sqrt{3}}D_0\frac{\sigma}{|\sigma|}\exp\left[-\frac{n+1}{2n}\left|\frac{\alpha_2}{\sigma}\right|^{2n}\right] \tag{0.3}$$

and

$$\frac{\partial \alpha_2}{\partial t}=m(z_1-\alpha_2)\sigma\frac{\partial \alpha_1}{\partial t}-A_1 z_1\left|\frac{\alpha_2-z_I}{z_1}\right|^r \tag{0.4}$$

with prescribed stress , $\sigma=\sigma(t)$, could be reduced to a single linear, constant coefficient, partial differential equation

$$\frac{\partial}{\partial t}\theta-\epsilon^2\frac{\partial^2\theta}{\partial x^2}=F[\sigma(t)]:=F(t) \tag{0.5}$$

$$\theta(x,0)=T_R-T_\infty$$

$$\theta_x(1,t)=0$$

$$k\,\theta_x(0,t)-\beta\theta(0,t)=0$$

for the modified temperature

$$\theta=\theta(x,t)=(T-T_\infty)\exp\left(\frac{\alpha\sigma(t)}{\rho c_v}\right) \tag{0.6}$$

where

$$F[\sigma(t)]=\left|\frac{\sigma(t)}{\rho c_v}\frac{\partial \alpha_1}{\partial t}-\frac{\alpha T_\infty\sigma'(t)}{\rho c_v}\right|\exp\left|\frac{\alpha\sigma(t)}{\rho c_v}\right| \tag{0.7}$$

and

$$\epsilon^2=\frac{k}{\rho c_v}. \tag{0.8}$$

In this report, we solve (0.5) by means of separation of variables and write down an explicit power series solution of (0.5). This will enable us to examine the relative importance of each term in the series expansion, evaluate various asymptotic expressions involving the solution, follow the formation of boundary layers in the bar, and to examine the effect of modifying the choice of $\sigma(t)$. Finally, in the appendices, we examine the integral representation of $\theta(x,t)$ by means of the Green's function which was introduced in [1].

Section 1. Series expansion of the modified temperature.

We write the solution of the problem (0.5) in series form

$$\theta(x,t)=\sum_{n=1}^{\infty}\theta_n(t)\psi_n(x).$$

Substituting this into (0.5), we have :

$$\sum_{n=1}^{\infty}\left[\theta_n'(t)\psi_n(x)-\epsilon^2\theta_n(t)\psi_n''(x)\right]=F(t) \tag{1.1}$$

$$\sum_{n=1}^{\infty}\theta_n(0)\psi_n(x)=T_R-T_\infty \tag{1.2}$$

$$\sum_{n=1}^{\infty}\theta_n(t)\psi_n'(1)=0 \tag{1.3}$$

$$\sum_{n=1}^{\infty}\theta_n(t)\left[k\,\psi_n'(0)-\beta\psi_n(0)\right]=0. \tag{1.4}$$

We solve (1.1) by assuming that

$$\theta_n'(t)+\epsilon^2\omega_n^2\theta_n(t)=d_n F(t) \tag{1.5}$$

$$\psi_n''(x)+\omega_n^2\psi_n(x)=0 \tag{1.6}$$

Therefore,

$$\sum_{n=1}^{\infty}\theta_n'(t)\psi_n(x)-\epsilon^2\theta_n(t)\psi_n''(x)=$$

$$\sum_{n=1}^{\infty}\theta_n'(t)\psi_n(x)+\epsilon^2\omega_n^2\theta_n(t)\psi_n(x)$$

$$=\sum_{n=1}^{\infty}\psi_n(x)\left[\theta_n'(t)+\epsilon^2\omega_n^2\theta_n(t)\right]$$

$$=\sum_{n=1}^{\infty}\psi_n(x)d_n F(t)$$

$$=\left[\sum_{n=1}^{\infty}d_n\psi_n(x)\right]F(t)$$

This will satisfy (1.1) if and only if

$$\sum_{n=1}^{\infty}d_n\psi_n(x)=1 \tag{1.7}$$

on the interval $0<x<1$. Equations (1.3) , (1.4) , and (1.6) determine ω_n uniquely. Writing

$$\psi_n(x)=a_n\sin(1-x)\omega_n+b_n\cos(1-x)\omega_n$$

we have

$$0=\psi_n'(1)=-a_n\omega_n .$$

This implies that $a_n=0$. The second condition implies

$$0=k\psi_n'(0)-\beta\psi_n(0)=-b_n\left[k\omega_n\sin\omega_n+\beta\cos\omega_n\right]$$

which implies that

$$\frac{k}{\beta}\omega_n=-\cot\omega_n \tag{1.8}$$

Asymptotically ,

$$\omega_n \to n\pi.$$

We note that ω_n is nonzero, so that $\psi(x)=1$ is not an eigenfunction. Therefore, (1.7) determines the coefficients d_n by

$$\sum_{n=1}^{\infty} d_n \cos(1-x)\omega_n = 1 \tag{1.9}$$

The eigenfunctions $\psi_n(x)=cos(1-x)\omega_n$ can be shown to be a complete orthogonal basis, consequently

$$d_n = \frac{\int_0^1 \cos(1-x)\omega_n \, dx}{\int_0^1 \cos^2(1-x)\omega_n \, dx} = \frac{4\sin\omega_n}{2\omega_n - \sin 2\omega_n}. \tag{1.10}$$

Asymptotically ,

$$d_n \to \frac{2\sin\omega_n}{\omega_n} \to \frac{2\beta}{kn^2\pi^2}$$

It remains to satisfy (1.2).

$$T_R - T_\infty = \sum_{n=1}^{\infty} \theta_n(0)\psi_n(x) = \sum_{n=1}^{\infty} \theta_n(0)\cos(1-x)\omega_n$$

Comparing this expression to (1.9) we see that it suffices to choose

$$\theta_n(0) = d_n(T_R - T_\infty). \tag{1.11}$$

The remaining differential equation

$$\theta_n'(t) + \epsilon^2\omega_n^2 = d_n F(t)$$

$$\theta_n(0) = d_n(T_R - T_\infty)$$

has the solution :

$$\theta_n(t) = d_n(T_R - T_\infty)\exp(-\omega^2\epsilon^2 t) + \int_0^t d_n \exp(-\epsilon^2\omega_n^2(t-s))F(s)ds$$

Therefore the solution of (0.5) can be written down concisely as

$$\theta(x,t)=\sum_{n=1}^{\infty}\left\{d_n(T_R-T_\infty)\exp(-\omega_n^2\epsilon^2 t)+d_n\int_0^t\exp(-\epsilon^2\omega_n^2(t-s))F(s)ds\right\}\cos(1-x)\omega_n \quad (1.12)$$

$$=(T_R-T_\infty)\sum_{n=1}^{\infty}d_n\exp(-\omega_n^2\epsilon^2 t)\cos(1-x)\omega_n+\sum_{n=1}^{\infty}d_n\exp(-\epsilon^2\omega_n^2 t)*F(t)\cos(1-x)\omega_n$$

(" * " signifying convolution in time), ω_n satisfies

$$\frac{k}{\beta}\omega_n=-\cot\omega_n, \quad (1.8)$$

and d_n satisfies (1.10).

Section 2. Contribution of Series Terms.

We will examine two cases , $F(t)=t$ and $F(t)=1$, in order to examine the decay of the terms $\theta_n(t)$.

Case 1 , $F(t)=t$. We have, after some computations which we omit,

$$\theta_n(t)=\frac{d_n}{\epsilon^2\omega_n^2}\left[t-\frac{1}{\epsilon^2\omega_n^2}\right]+d_n\left[T_R-T_\infty+\frac{1}{\epsilon^4\omega_n^4}\right]\exp(-\omega_n^2\epsilon^2 t) \quad (2.1)$$

This implies that each mode contributes a term asymptotically of order

$$\frac{d_n}{\epsilon^2\omega_n^2}t$$

and therefore each term is of the same order in t .

In the second case, $F(t)=1$, we have (again after some easy computations)

$$\theta_n(t)=\frac{d_n}{\epsilon^2\omega_n^2}\left[1-exp(-\epsilon^2\omega_n^2 t)\right]+d_n(T_R-T_\infty)\exp(-\epsilon^2\omega_n^2 t) \quad (2.2)$$

and therefore, as $t\to\infty$, each term contributes

$$\frac{d_n}{\epsilon^2\omega_n^2}.$$

As $t\to\infty$ we have the following result

$$\theta(x,t)\to\sum_{n=1}^{\infty}\frac{d_n}{\omega_n^2\epsilon^2}\cos(1-x)\omega_n . \tag{2.3}$$

At the right endpoint then, the temperature is given asymptotically by

$$\theta_\infty(1)=\sum_{n=1}^{\infty}\frac{d_n}{\epsilon^2\omega_n^2} \tag{2.4}$$

which is bounded.

Section 3. Upper bounds on the temperature increase.

Equation (0.5) can be considered as an ordinary heat equation describing the evolution of a symmetrical temperature distribution in a rod, with convection boundary conditions at $x=0$ and $x=2$, starting from a constant temperature, with a source strength $F(t)$ which is spatially homogeneous. From this analogy, or using maximum principles of parabolic equations, one can see that the maximum temperature is achieved at the center of the rod (for $F(t)\geqslant 0$) and that if $F(t)\leqslant F_{\max}$ then the temperature distribution $\theta_{\max}(x,t)$ satisfying (0.5) with $F(t)$ replaced by $F_{\max}$

$$\frac{\partial}{\partial t}\theta-\epsilon^2\frac{\partial^2\theta}{\partial x^2}=F_{\max}=constant \tag{3.1}$$

$$\theta(x,0)=T_R-T_\infty$$

$$\theta_x(1,t)=0$$

$$k\,\theta_x(0,t)-\beta\theta(0,t)=0$$

satisfies the relation

$$\theta(x,t)\leqslant\theta_{\max}(x,t). \tag{3.2}$$

The steady state solution of (3.1) is very easy to compute. It is

$$\theta_{\max}(x)=\epsilon^{-2}(-\frac{1}{2}x^2+x+\frac{k}{\beta})F_{\max} \tag{3.3}$$

At the center point, where the maximum temperature occurs, we have

$$\theta_{\max}(1)=\epsilon^{-2}(\frac{1}{2}+\frac{k}{\beta})F_{\max} \tag{3.4}$$

This then bounds the solution of (0.5) at the point $x=1$, and therefore everywhere.

Section 4. Computing F_{max} given $\sigma(t)$.

If $|\sigma(t)|<C_1$ and $|\sigma'(t)|<C_2$ then we can estimate F_{max} as follows. In the appendix it is shown that if $z_1<\alpha_2(0)<z_1$ then $z_1<\alpha_2(t)<z_1$ for all t. This then yields the inequality

$$|\frac{\partial\alpha_1}{\partial t}|<\frac{2}{\sqrt{3}}D_0\exp\left|-\frac{n+1}{2n}\left|\frac{z_1}{C_1}\right|\right|:=C_3 \tag{4.1}$$

and therefore

$$F(t)\leqslant F_{max}=\left|\frac{C_1}{\rho c_v}C_3+\frac{\alpha T_\infty C_2}{\rho c_v}\right|\exp\left|\frac{\alpha C_1}{\rho c_v}\right| \tag{4.2}$$

This leads to a tremendous overestimate in general. Since the series solution (1.12) is analytically correct (i.e. not an approximation) one can obtain the temperature at the midpoint by substituting $x=1$ into (1.12) to obtain

$$\theta(1,t)=\sum_{n=1}^{\infty}d_n\exp(-\omega_n^2\epsilon^2t)\left|T_R-T_\infty+\int_0^t\exp(\epsilon^2\omega_n^2s)F(s)ds\right| \tag{4.3}$$

$$\rightarrow\sum_{n=1}^{\infty}d_n\int_0^t\exp(-\epsilon^2\omega_n^2(t-s))F(s)ds \tag{4.4}$$

If $F(s)$ does not decay as $s\rightarrow\infty$ then many terms will have to be included in (4.4). Examples of various choices of $\sigma=\sigma(t)$ will be investigated in a subsequent report.

Section 5. Computing the time-averaged mean (modified) temperature.

Since the right hand side of (0.5) depends only on t, through $\sigma(t)$, we can derive a better asymptotic bound on the behavior of $\theta(x,t)$ with respect to time in the following way. First, integrate (0.5) with respect to time, and then divide by t. If we define

$$\phi(x,t)=t^{-1}\int_0^t\theta(x,\tau)d\tau \tag{5.1}$$

and

$$<F(t)>=t^{-1}\int_0^t F(\sigma(\tau))d\tau$$

we have the following equation

$$t^{-1}(\theta(x,t)-\theta(x,0))-\epsilon^2\phi(x,t)=<F(t)>$$

$$\phi_x(1,t)=0$$

$$k\phi_x(0,t)-\beta\phi(0,t)=0$$

Since $\theta(x,t)$ is bounded, $t^{-1}(\theta(x,t)-\theta(x,0))\to 0$ regardless of initial conditions. Therefore the quantity

$$\Phi(x)=\lim_{t\to\infty} t^{-1}\int_0^t \theta(x,\tau)d\tau \tag{5.2}$$

satisfies the ordinary differential equation

$$-\epsilon^2\Phi''(x)=<F> \tag{5.3}$$

$$\Phi(1)=0$$

$$k\Phi'(0)-\beta\Phi(0)=0$$

where $<F>=\lim_{T\to\infty}<F(t)>$, This can be solved to yield

$$\Phi(x)=\epsilon^{-2}(-\frac{1}{2}x^2+x+\frac{k}{\beta}) \tag{5.4}$$

$\Phi(x)$ is the asymptotic state of the (time averaged) mean (modified) temperature. In particular at the center point, $x=1$,

$$\Phi(1)=\epsilon^{-2}(\frac{1}{2}+\frac{k}{\beta})<F> \tag{5.5}$$

If the exponential term in (0.6) is approximately unity, then $\Phi(x)$ is the asymptotic mean temperature change. Therefore,

$$<T(x)>\sim T_\infty+\Phi(x)$$

In order to compute $<F>$, we note that if $F(t)$ is periodic then

$$<F>=\lim_{T\to\infty}\frac{1}{T}\int_0^T F(t)dt=\frac{1}{P}\int_0^P F(t)dt$$

where P is the period of F. If, in addition, $\int_0^P F(t)dt=0$, then $<F>=0$ and

consequently, there is no net mean contribution to the temperature. Consider the second term of (0.7). It is a total derivative of the quantity

$$T_\infty \exp\left|\frac{\alpha\sigma(t)}{\rho c_v}\right|.$$

Therefore ,

$$\int_t^P \frac{\alpha T_\infty}{\rho c_v}\sigma'(t)\exp\left(\frac{\alpha\sigma(t)}{\rho c_v}\right)dt$$

$$= T_\infty \exp\left|\frac{\alpha\sigma(t)}{\rho c_v}\right|_{t=0}^{t=P} = 0.$$

If α_2 approaches a constant then,

$$<F> = \lim_{T\to\infty}\frac{1}{T}\int_0^T \frac{\sigma(t)}{\rho c_v}\frac{\partial\alpha_1}{\partial t}dt \tag{5.8}$$

$$= \frac{1}{P}\int_0^P \frac{2}{\sqrt{3}}\frac{D_0}{\rho c_v}|\sigma(t)|\exp\left|-\frac{n+1}{2n}|\frac{\alpha_2}{\sigma(t)}|^{2n}\right|dt$$

Given $\sigma(t)$ periodic, one can compute (5.8) and then substitute into (5.5) to compute the asymptotic mean (modified) temperature change at $x=1$. If $\alpha_2(t)$ does not approach a constant, then one cannot use equation (5.8). In many applications however, the value of α_2 approaches a constant. This is an effect of the phenomenon of "saturation". The parameter n is seen to be crucial in predicting the temperature rise in the purely one-dimensional model.

In general, the temperature rise predicted by substituting (5.8) into (3.4) is much larger than physically realized. This is a result of the simplification of the problem into one-dimension. In reality, we cannot ignore radial effects, and the radiation boundary conditions along the longitudinal surface of the bar. (Neglecting these is equivalent to assuming that the rod is insulated along its length , which accounts for the much larger predicted temperature increase.)

The one-dimensional analysis is still important for a study of the various models for thermoviscoplastic materials, and the effects of various parameters on the maximum temperature changes. For short times an alternate representation of the solution can be obtained by singular perturbation techniques. This is analyzed in the next section.

Section 6. Boundary Layer Model.

In order to examine the behavior of the boundary layer, we expand the function $\theta(x,t)$ in terms of the small parameter ϵ. We define the stretched coordinate $\xi=\epsilon^{-1}x$. This implies that $\partial_x=\epsilon^{-1}\partial_\xi$, and that therefore

$$\theta_t-\theta_{\xi\xi}=F(t) \tag{6.1}$$

$$\theta(\epsilon\xi,0)=T_R-T_\infty$$

$$\epsilon^{-1}\theta_\xi(\epsilon^{-1},t)=0$$

$$k\,\epsilon^{-1}\theta_\xi(0,t)-\beta\theta(0,t)=0$$

In the usual way, we write

$$\theta(\xi,t)=\sum_{n=0}^{\infty}\epsilon^n\,\theta_n(\xi,t)$$

For n=0 this reduces to

$$\theta_{0,t}-\theta_{0,\xi\xi}=F(t) \tag{6.2}$$

$$\theta_0(.,0)=T_R-T_\infty$$

$$\theta_{0,\xi}(\infty,t)=0$$

$$\theta_{0,\xi}(0,t)=0$$

which implies that $\theta_0=\theta_0(t)$, and that

$$\theta_0=\theta_0(t)=\int_0^t F(\tau)d\,\tau+T_R-T_\infty \tag{6.3}$$

Equation (6.3) describes the evolution of the modified temperature $\theta(x,t)$ under insulated boundary conditions. For $n>1$, we obtain a coupled set of linear differential equations

$$\theta_{n,t} - \theta_{n,\xi\xi} = 0 \tag{6.4}$$

$$\theta_n(\cdot, 0) = 0$$

$$\theta_{n,\xi}(\infty, t) = 0$$

$$\theta_{n,\xi}(0, t) - \beta\theta_{n-1}(0, t) = 0$$

This can be solved using Laplace transforms , which yields

$$\theta_n(\xi, t) = -\frac{\beta}{k}\frac{1}{\sqrt{\pi t}}\exp(-\frac{\xi^2}{4t}) * \theta_{n-1}(0, t) \tag{6.5}$$

Note that if $\theta_0(t) > 0$ then each term alternates in sign.

The first order approximation is therefore

$$\theta(x, t) \sim \theta_0(t) + \epsilon\theta_1(\xi, t) \tag{6.6}$$

$$= \theta_0(t) - \frac{\epsilon\beta}{k}\int_0^t \frac{1}{\sqrt{\pi\tau}}\exp(-\frac{x^2}{4\epsilon^2\tau})\theta_0(t-\tau)d\tau$$

The integrand is negligible except when $\frac{x^2}{\epsilon^2 t}$ is of order one. This leads to a boundary layer which is described by

$$x \sim \epsilon\sqrt{t}.$$

We also obtain the following important result, when x=0, that

$$\theta(0, t) \sim \theta_0(t) - \epsilon\frac{\beta}{k}\int_0^t \frac{1}{\sqrt{\pi t}}\theta_0(t-\tau)d\tau \tag{6.7}$$

which to leading order computes the temperature as a function of time of the left end-point of the bar. The first order correction is in fact monotonic in x (if $\theta_0(t) > 0$) , as expected. Equation (6.7) shows that the first order term *overcorrects* and that the next term (of opposite sign) attempts to compensate for this.

Appendix I . Estimating α_2.

By examining (0.3) and (0.4) with D_0 , m , z_1 , z_I , A_1 , and r positive constants, and noting that the product of σ and $\frac{\partial \alpha_1}{\partial t}$ is intrinsically positive, we have the following conclusions : If initially

$$z_I < \alpha_2(0) < z_1$$

then as one approaches z_1 from below, $\frac{\partial \alpha_2}{\partial t}$ approaches

$$-A_1 z_1 \left| \frac{z_1 - z_I}{z_1} \right|^r < 0$$

and if one aproaches z_I from above, then $\frac{\partial \alpha_2}{\partial t}$ approaches

$$m(z_1 - z_I)\sigma \frac{\partial \alpha_1}{\partial t} > 0$$

Consequently, $\alpha_2(t)$ can never cross these two limit lines.

Appendix II . Integral representation of $\theta(x,t)$ by means of a Green's function.

In [1], we derived the following expression for the Laplace transform of θ

$$\hat{\theta}(x,s) = \frac{1}{s}\left[\hat{F}(s) + T_R - T_\infty\right]\left[1 - \beta \hat{G}(x,s)\right].$$

where

$$\hat{G}(x,s) = \frac{\cosh\left[(1-x)\frac{\sqrt{s}}{\epsilon}\right]}{k\frac{\sqrt{s}}{\epsilon}\sinh\frac{\sqrt{s}}{\epsilon} - \beta\cosh\frac{\sqrt{s}}{\epsilon}}.$$

We can derive a series expression for the inverse transform by means of a contour integral

$$G(x,t) = \frac{1}{2\pi i}\int_{c-i\infty}^{c+i\infty} \frac{e^{st}\cosh\left[(1-x)\frac{\sqrt{s}}{\epsilon}\right]}{k\frac{\sqrt{s}}{\epsilon}\sinh\frac{\sqrt{s}}{\epsilon} - \beta\cosh\frac{\sqrt{s}}{\epsilon}} ds.$$

The poles of the integrand are the roots of the expression

$$k\frac{\sqrt{s}}{\epsilon}\sinh\frac{\sqrt{s}}{\epsilon}-\beta\cosh\frac{\sqrt{s}}{\epsilon}$$

Setting $\frac{\sqrt{s}}{\epsilon}=i\omega$, we have

$$0=ki\,\omega\sinh(i\,\omega)-\beta\cosh(i\,\omega)$$

$$=-2k\,\omega\sin\omega-2\beta\cos\omega$$

Therefore

$$\frac{k}{\beta}\omega=-\frac{\cos\omega}{\sin\omega}=-\cot\omega_n \qquad \text{(A2.1)}$$

which is the same equation as (1.8). Therefore $s=-\epsilon^2\omega^2$ where ω satisfies (A2.1).

Because the integrand is even, there is no contribution of the branch line to the contour integral. Similarly, there is no contribution of the branch point at $s=0$. The contour at infinity goes to zero as $s\to\infty$ if $\mathrm{Re}\,s<0$. Consequently, by the residue theorem,

$$G(x,t)=\sum residues=\sum_{n=0}^{\infty}d_n\,e^{-s_n t}\cosh(1-x)\frac{\sqrt{s_n}}{\epsilon}$$

$$=\sum_{n=1}^{\infty}\exp(-\epsilon^2\omega_n^2 t)\cos(1-x)\omega_n$$

and

$$\theta(x,t)=\left|\int_0^t F(\tau)d\,\tau+T_R-T_\infty\right|-\beta G(x,t)*\left|+T_R-T_\infty+\int_0^t F(\tau)d\,\tau\right|$$

$$=\theta_0(t)-\beta G(x,t)*\theta_0(t)$$

$$=\theta_0-\beta\sum_{n=1}^{\infty}\cos(1-x)\omega_n\exp(-\epsilon^2\omega_n^2 t)*\theta_0(t).$$

This identity motivates the series expression for the function $\theta(x,t)$ given in section 1.

ACKNOWLEDGEMENT

The author wishes to acknowledge the helpful discussions and comments of D. H. Allen. This research was supported by the Air Force Office of Scientific Research under contract no. F49620-83-C-0067.

REFERENCES

[1] Pilant, M. S., "Analysis of a Thermoviscoplastic Uniaxial Bar Under Prescribed Stress. Part I - Theoretical Development," Texas A & M Mechanics and Materials Center, MM 4875-85-2, January 1985.

[2] Allen, D. H., "Predicted Axial Temperature Gradient in a Viscoplastic Uniaxial Bar due to Thermomechanical Coupling," Texas A & M Mechanics and Materials Center, MM 4875-84-15, November, 1984.

APPENDIX 6.7

Mechanics and Materials Center
TEXAS A&M UNIVERSITY
College Station, Texas

ANALYSIS OF A THERMOVISCOPLASTIC UNIAXIAL BAR UNDER PRESCRIBED STRESS

PART III - NUMERICAL RESULTS FOR A BAR WITH RADIATIVE BOUNDARY CONDITIONS.

M. S. PILANT

MM-4875-85-10

JUNE 1985

REPORT DOCUMENTATION PAGE

1a. REPORT SECURITY CLASSIFICATION unclassified	1b. RESTRICTIVE MARKINGS NA
2a. SECURITY CLASSIFICATION AUTHORITY NA	3. DISTRIBUTION/AVAILABILITY OF REPORT unlimited
2b. DECLASSIFICATION/DOWNGRADING SCHEDULE NA	
4. PERFORMING ORGANIZATION REPORT NUMBER(S) MM 4875-85-10	5. MONITORING ORGANIZATION REPORT NUMBER(S) NA
6a. NAME OF PERFORMING ORGANIZATION Aerospace Engineering Dept. 6b. OFFICE SYMBOL (If applicable)	7a. NAME OF MONITORING ORGANIZATION Air Force Office of Scientific Research
6c. ADDRESS (City, State and ZIP Code) Texas A&M University College Station, Texas 77843	7b. ADDRESS (City, State and ZIP Code) Bolling AFB Washington, D.C. 20332
8a. NAME OF FUNDING/SPONSORING ORGANIZATION Air Force Office of Scientific Research 8b. OFFICE SYMBOL (If applicable)	9. PROCUREMENT INSTRUMENT IDENTIFICATION NUMBER NA
8c. ADDRESS (City, State and ZIP Code) Bolling AFB Washington, D.C. 20332	10. SOURCE OF FUNDING NOS. PROGRAM ELEMENT NO.: F49620-83-C-0067 PROJECT NO. TASK NO. WORK UNIT NO.
11. TITLE (Include Security Classification) Analysis of Thermoviscoplastic Uniaxial Bar - Part III	
12. PERSONAL AUTHOR(S) M. S. Pilant	
13a. TYPE OF REPORT Interim 13b. TIME COVERED FROM _____ TO _____	14. DATE OF REPORT (Yr., Mo., Day) 15. PAGE COUNT
16. SUPPLEMENTARY NOTATION	
17. COSATI CODES FIELD / GROUP / SUB. GR. 18. SUBJECT TERMS (Continue on reverse if necessary and identify by block number)	

19. ABSTRACT (Continue on reverse if necessary and identify by block number)

Under the assumption that the stress is a known function of time, the equations governing the response of a homogeneous, thermoviscoplastic uniaxial bar can be reduced to a single linear partial differential equation for the temperature in terms of the stress In this, the last of a three part study of this problem, upper and lower bounds are determined for the case of a bar subjects to a radiation boundary conditions on its longitudinal surface and in the presence of a cyclic stress history. The temperature rise, which is caused by inelastic conversion of strain energy to heat, is found to be significant for some example applications to realistic materials.

20. DISTRIBUTION/AVAILABILITY OF ABSTRACT UNCLASSIFIED/UNLIMITED ☒ SAME AS RPT. ☐ DTIC USERS ☐	21. ABSTRACT SECURITY CLASSIFICATION Unclassified
22a. NAME OF RESPONSIBLE INDIVIDUAL A. Amos	22b. TELEPHONE NUMBER (Include Area Code) (202)-769-4937 22c. OFFICE SYMBOL AFOSR/NA

ANALYSIS OF A THERMOVISCOPLASTIC UNIAXIAL BAR UNDER PRESCRIBED STRESS

PART III - NUMERICAL RESULTS FOR A BAR WITH RADIATIVE BOUNDARY CONDITIONS.

by
Michael S. Pilant

Assistant Professor
Department of Mathematics
Texas A&M University
College Station Texas 77843

ABSTRACT

Under the assumption that the stress is a known function of time, the equations governing the response of a homogeneous, thermoviscoplastic uniaxial bar can be reduced to a single linear partial differential equation for the temperature in terms of the stress. In this, the last of a three part study of this problem, upper and lower bounds are determined for the case of a bar subjected to radiation boundary conditions on its longitudinal surface and in the presence of a cyclic stress history. The temperature rise, which is caused by inelastic conversion of strain energy to heat, is found to be significant for some example applications to realistic materials.

INTRODUCTION

Large space structures will require significant passive damping in order to sustain structural vibrations in a microgravity field. One passive damping mechanism which has been proposed is material inelasticity. However, during this process, a substantial proportion of the strain energy in the structure is converted into heat via hysteretic loss. The purpose of the current three part research effort is to determine if this energy conversion process can produce temperature rises which are large enough to adversely affect the structural integrity of the system.

In Part I it was shown that assuming the stress to be a known function of time decoupled the equations governing the internal state variables from the heat conduction equation. This reduces the nonlinear system of partial differential equations governing the motion of the rod to a single parabolic equation for the temperature with coefficients given in terms of the stress $\sigma(t)$. We then obtained an expression for the strain ϵ in terms of a convolution of the stress σ and a suitable kernel which was derived from the heat conduction equation. This yielded the compliance relation for this material.

In Part II it was noted that the system could also be solved by series methods, and that a boundary layer formed near the ends of the rod. Series and integral expressions for the temperature were derived from a simple, spatially homogeneous solution. The boundary conditions examined did not allow for the radiation of thermal energy away from the longitudinal surface of the rod , so the temperature bounds derived in part II were not optimal.

In Part III we develop much sharper upper and lower bounds for the asymptotic temperature rise as a function of applied loading, material properties, and geometry for a typical space structural member. Graphical results are given for several example cases.

Section 1. Derivation of the equations of Equilibrium. Constitutive Laws.

The equations we use to describe the quasi-static response of a thermoviscoplastic uniaxial bar have been formulated and discussed in [1]. For brevity, we summarize the main points in this section. The principal equations are conservation of momentum

$$\sigma_{ji,j}=0 \tag{1.1}$$

and the conservation of energy , as expressed in the modified Fourier heat conduction

law

$$D_{ijkl}(\epsilon_{kl}-\alpha_{1kl}+\bar{\alpha}_{kl}T_R)\dot{\alpha}_{1ij}+D_{ijkl}(\bar{\alpha}_{ij}\bar{\alpha}_{kl}T\dot{T})-D_{ijkl}(\bar{\alpha}_{ij}T\dot{\epsilon}_{kl})-\rho c_v\dot{T}-q_{j,j}=0. \quad (1.2)$$

(Dots indicating differentiation with respect to time.)

In addition, we have the stress-strain relationship

$$\sigma_{ij}=D_{ijkl}(\epsilon_{kl}-\epsilon^I_{kl}-\epsilon^T_{kl}) \quad (1.3)$$

The internal state variables α^q_{ij} and ϵ^I obey the following evolution equations :

$$\dot{\epsilon}^I_{ij}=g(\epsilon_{kl},T,\alpha^p_{kl}) \quad (1.4)$$

$$\dot{\alpha}^q_{ij}=f^q_{ij}(\epsilon_{kl},T,\alpha^p_{kl}) \quad (1.5)$$

In the case of a homogeneous, thermoviscoplastic, uniaxial rod we further postulate that

$$\sigma_{ij}=\sigma_{11}=\sigma \quad (1.6)$$

$$\epsilon_{ij}=\epsilon_{11}=\epsilon$$

$$D_{ijkl}=D_{1111}=E$$

$$\epsilon^I_{ij}=\alpha_{1ij}=\alpha_1$$

$$\bar{\alpha}_{ij}=\bar{\alpha}_{11}=\alpha$$

$$\epsilon^T_{ij}=\epsilon^T_{11}=\epsilon^T=\alpha(T-T_R)$$

and finally

$$q_j=-kT_{,j} \quad (1.7)$$

E is a constant (Young's modulus), and T_R is a reference temperature for which there is no thermal strain under zero applied load. We also assume for simplicity that α, k, ρ are constant.

Substituting the relations (1.6) and (1.7) into (1.2) we have the following system of equations

$$\frac{\partial}{\partial x}\sigma=0 \quad (1.8)$$

$$E(\epsilon-\alpha_1+\alpha T_R)\dot{\alpha}_1+E\alpha^2 T\dot{T}-E\alpha T\dot{\epsilon}-\rho c_v\dot{T}+k\Delta T=0 \tag{1.9}$$

$$\dot{\alpha}_q=f_q(\alpha_p, T, \epsilon) \tag{1.10}$$

$$\sigma=E[\epsilon-\alpha_1-\alpha(T-T_R)] \tag{1.11}$$

and

$$\epsilon=\frac{\partial}{\partial x}u \tag{1.12}$$

For simplicity we have assumed infinitesimal deformations, (1.12). Since u and σ are now functions of the axial coordinate, x, alone, we drop the tensor subscript notation and use subscripts to label the different internal state variables (1.10).

Given initial conditions for α_q, T, and u, as well as boundary conditions for T and u, this is a well-posed mathematical problem. It has been shown in [2] to be thermodynamically consistent as well.

We make the following observations at this time. First, (1.8) implies that σ is a function of time alone. Secondly, in the special case where the f_q do not explicitly depend on T or ϵ but only on $\{\alpha_q, \sigma\}$, then given $\sigma(t)$, (1.10) is a closed system of equations, and we have $\alpha_q=\alpha_q(t;\sigma(t))$. Equation (1.8) is automatically satisfied for $\sigma=\sigma(t)$ so (1.9) essentially becomes a single, non-linear parabolic differential equation for the temperature T in terms of σ. This analysis has been carried out in [3 , 4]. Generalizing this approach, we will obtain the asymptotic behavior of T directly from the system (1.8)-(1.12).

Section 2. Radiative and convective boundary conditions.

In order to include the thermal radiation boundary conditions along the lateral surface of the rod, we integrate (1.9) over the (constant) cross-sectional area of the rod. Let (x, r, θ) denote cylindrical coordinates with x measuring the distance along the axis of the rod. In this model, all variables (except for T) are independent of r and θ. We have

$$AE(\epsilon-\alpha_1+\alpha T_R)\dot{\alpha}_1+AE\,\alpha^2 T\dot{T}-AE\,\alpha T\,\dot{\epsilon}-A\rho c_v\dot{T}+kAT_{xx}= \tag{2.1}$$

$$-k\int\int\left|(\frac{1}{r}\frac{\partial}{\partial r}(r\frac{\partial T}{\partial r}))+\frac{1}{r^2}\frac{\partial^2 T}{\partial\theta^2}\right|rdrd\,\theta$$

$$=-k\int(r\frac{\partial T}{\partial r})dr=-kC\frac{\partial T}{\partial n}=+Cq_n$$

where q_n is the integrated effect of the normal component of the thermal flux along the lateral surface of the rod, and C is the circumference of the rod. T is now interpreted as an integral average of the temperature over the cross-section of the rod.

It is clear that the term $+Cq_n$ acts as a "sink" for thermal energy. In deep space, we model the thermal flux due to radiation as

$$q_n=\sigma_s\delta(T^4-T_D^4)-Q=\sigma_s\delta T^4-Q \tag{2.2}$$

where $T_D=0^\circ K$ is the deep space ambient temperature, and $\sigma_s=5.775x\,10^{-11}$ is Boltzmann's constant. δ is an order one constant, called the emissivity, which measures the effect of the surface coating on black body radiation, and Q measures the solar, earth, and deep space thermal flux incident on the rod.

We approximate (2.2) by the first two terms of its Taylor series expansion in order to obtain the linearized convective boundary condition

$$q_n=\sigma_s\delta T_R^4+\beta(T-T_R)-Q \tag{2.3}$$

with

$$\beta\sim 4\sigma_s\delta T_R^3.$$

In order to estimate the actual temperature rise (with non-linear boundary conditions) we choose β so that

$$\sigma_s\delta T_R^4+\beta(T-T_R)>\sigma_s\delta T^4>\sigma_s\delta T_R^4+4\sigma_s\delta T_R^3(T-T_R) \tag{2.4}$$

over the region of interest. This implies that any temperature change associated with (2.3) will bound from below the actual temperature change associated with (2.2). Choosing $\beta=4\sigma_s\delta T_R^3$ will bound the temperature increase from above, via inequality (2.4).

Section 3. Further reduction of the equations.

AD-A162 139 A MODEL FOR PREDICTING THERMOMECHANICAL RESPONSE OF LARGE SPACE STRUCTURE..(U) TEXAS A AND M UNIV COLLEGE STATION MECHANICS AND MATERIALS RE.. D H ALLEN ET AL. 3/3

UNCLASSIFIED JUN 85 MM-4875-85-11 AFOSR-TR-85-1016 F/G 22/2 NL

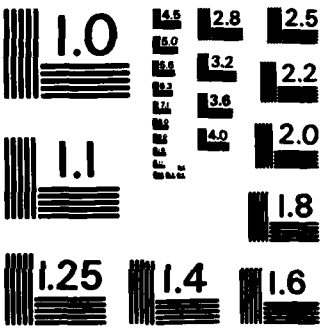

We can further simplify (1.9) by noting that the left hand side of (2.1) can be written as

$$A\left\{(\sigma+E\alpha T)\dot{\alpha}_1+E\alpha^2 T\dot{T}-\alpha T(\dot{\sigma}+E\dot{\alpha}_1+E\alpha\dot{T})-\rho c_v\dot{T}+kT_{xx}\right\} \tag{3.1}$$

$$=A\left\{-\rho c_v\dot{T}+kT_{xx}-\alpha\dot{\sigma}T+\sigma\dot{\alpha}_1\right\}$$

Consequently,

$$-\rho c_v\dot{T}+kT_{xx}-\alpha\dot{\sigma}T+\sigma\dot{\alpha}_1=+\frac{C}{A}q_n \tag{3.2}$$

$$=+\frac{C}{A}\left\{\sigma_s\delta T_R^4+\beta(T-T_R)-Q\right\}$$

We write this as

$$\rho c_v\dot{T}-kT_{xx}+\alpha\dot{\sigma}T+\frac{C\beta}{A}(T-T_R)=\sigma\dot{\alpha}_1-\frac{C}{A}\left\{\sigma_s\delta T_R^4-Q\right\} \tag{3.3}$$

Letting $\theta(x,t)=\exp(\frac{\alpha\sigma(t)}{\rho c_v})(T-T_R)$, we have

$$\frac{\partial\theta}{\partial t}-\frac{k}{\rho c_v}\frac{\partial^2\theta}{\partial x^2}+\frac{C\beta}{\rho c_v A}\theta=F(t) \tag{3.4}$$

where

$$F(t)=:\left\{\exp(\frac{\alpha\sigma(t)}{\rho c_v}\right\}\left\{\frac{\sigma(t)\dot{\alpha}_1(t)}{\rho c_v}-\frac{C\sigma_s}{A\rho c_v}\delta T_R^4+\frac{CQ}{A\rho c_v}-\frac{\alpha\dot{\sigma}}{\rho c_v}T_R\right\}$$

The *modified temperature* θ has been introduced previously in [4]. If we integrate both sides of (3.4) with respect to t, and divide by t, we obtain

$$t^{-1}(\theta(x,t)-\theta(x,0))-\frac{k}{\rho c_v}t^{-1}[\int_0^t\theta(x,\tau)d\tau]_{xx}+\frac{C\beta}{\rho c_v A}t^{-1}\int_0^t\theta(x,\tau)d\tau=t^{-1}\int_0^t F(\tau)d\tau$$

As $\tau\to\infty$, with θ bounded, this reduces to

$$\frac{C\beta}{A\rho c_v}<\theta>-\frac{k}{\rho c_v}<\theta>_{xx}=<F>$$

where

$$<\theta>(x)=\lim_{t\to\infty} t^{-1}\int_0^t \theta(x,\tau)d\tau \tag{3.5}$$

and

$$<F>=\lim_{t\to\infty} t^{-1}\int_0^t \exp(\frac{\alpha\sigma(\tau)}{\rho c_v})\left|\frac{\sigma(\tau)\dot{\alpha}_1(\tau)}{\rho c_v}+\frac{CQ}{A\rho c_v}-\frac{C\sigma_s}{A\rho c_v}\delta T_R^4-\frac{\alpha\dot{\sigma}}{\rho c_v}T_R\right|d\tau \tag{3.6}$$

$$=\lim_{t\to\infty} t^{-1}\int_0^t \exp(\frac{\alpha\sigma(\tau)}{\rho c_v})\left|\frac{\sigma(\tau)\dot{\alpha}_1(\tau)}{\rho c_v}+\frac{CQ}{A\rho c_v}-\frac{C\sigma_s}{A\rho c_v}\delta T_R^4\right|d\tau$$

are the asymptotic mean values of θ and F respectively.

In the materials under consideration, $\sigma\dot{\alpha}_1>0$. Since the integrands are bounded, the above limits exist. For simplicity, consider the following boundary conditions for the temperature T : $T(0,t)=T_R$ and $T_x(L,t)=0$. The second boundary condition results from symmetry, for a bar of length $2L$ units. Therefore θ satisfies the boundary conditions :

$$<\theta>(0)=0. \tag{3.7}$$

and

$$<\theta>(L)=0 \tag{3.8}$$

The solution of (3.4), subject to the boundary conditions (3.7,3.8) is

$$<\theta>(x)=\frac{\rho c_v A}{C\beta}<F>\left|1-\frac{\cosh\lambda(L-x)}{\cosh\lambda}\right| \tag{3.9}$$

where

$$\lambda=(\frac{C\beta}{Ak})^{1/2}$$

Note that if we ignore the spatial variation of the temperature, we have

$$<\theta>(x)=\frac{\rho c_v A}{C\beta}<F>$$

which is a good approximation to (3.9) if λ is large. This accounts for the close approximation observed between the spatially homogeneous solution and the spatially varying

solution with boundary layer in [5].

Since $\rho, c_v, \beta, C, A, L$, and k are all known, the spatial dependence of $<\theta>(x)$ is determined. Only the magnitude is a function of the loading history, through $<F>$. The crucial term to estimate therefore is $<F>$. If $\sigma(t)$ is periodic, and if $\dot{\alpha}_1$ is a periodic, then (3.6) reduces to

$$<F>=P^{-1}\int_0^P \exp\left(\frac{\alpha\sigma}{\rho c_v}\right)\left|\frac{\sigma\dot{\alpha}_1}{\rho c_v}-\frac{C}{A\rho c_v}\sigma_s\delta T_R^4+\frac{CQ}{A\rho c_v}\right|d\tau \tag{3.10}$$

where P is the period of σ and $\dot{\alpha}_1$.

A case of particular interest is the **Bodner model** [7], for which

$$\dot{\alpha}_1=\frac{2}{\sqrt{3}}D_0\frac{\sigma}{|\sigma|}\exp\left[-\frac{n+1}{2n}\left|\frac{\alpha_2}{\sigma}\right|^{2n}\right]$$

At saturation, the drag stress $\alpha_2=\bar{\alpha}_2$ is constant, and $<F>$ becomes a function only of σ.

$$<F>=P^{-1}\int_0^P \exp\left[\frac{\alpha\sigma(\tau)}{\rho c_v}\right]\left\{\frac{2}{\sqrt{3}\rho c_v}D_0|\sigma(\tau)|\exp\left[-\frac{n+1}{2n}\left|\frac{\bar{\alpha}_2}{\sigma(\tau)}\right|^{2n}\right]\right. \tag{3.11}$$

$$\left.-\frac{C}{A\rho c_v}\sigma_s\delta T_R^4+\frac{C}{A\rho c_v}Q\right|d\tau$$

Since

$$<\theta>(x)=\lim_{t\to\infty}t^{-1}\int_0^t\theta(x,\tau)d\tau=\lim_{t\to\infty}t^{-1}\int_0^t\exp\left(\frac{\alpha\sigma(\tau)}{\rho c_v}\right)(T-T_R)d\tau$$

we can recover a mean temperature $\bar{T}$ by

$$\bar{T}=<\theta>(x)\left|\lim_{t\to\infty}t^{-1}\int_0^t\exp\frac{\alpha\sigma(\tau)}{\rho c_v}d\tau\right|^{-1}+T_R \tag{3.12}$$

For stress amplitudes of interest, the factor $\exp\left[\frac{\alpha\sigma(t)}{\rho c_v}\right]$ is very close to unity. Fixing the material parameters $\{\alpha, \rho, c_v, D_0, n, \beta, k, \bar{\alpha}_2\}$, one can compute the dependence of $<\theta>$ and $\bar{T}$ on $\sigma(t)$. With σ periodic, (3.12) simplifies as before to an integral

over the period. We compare the analytical results with experimental and numerical data in the next section.

Section 4. Numerical Results.

In order to verify the accuracy of the asymptotic results (3.9) and (3.12), we computed the average temperature for the parameters given in [5] with the results shown below in fig.1 . The values for the emissivity (with thermal equilibrium at 295 deg. Kelvin) are 0.24 , 0.5 , and 0.85 respectively. The cyclically saturated stress-strain curve used to compute $< F >$ for the case σ_{max}=336.5 is given in fig. 2. The values for σ_{max} and $\bar{\alpha}_2$ were taken from numerical data supplied from reference [5].

The parameters in [5] describe a hollow cylindrical bar, of uniform cross-section, orbiting at an altitude of 4,080 km., painted with a high-emissivity coating (IITRE-S13GLO) white paint, with full exposure to the sun. Under zero applied stress, equilibrium of thermal flux occurs at 72 degrees fahrenheit (295 deg. Kelvin) for which the thermodynamic parameters of the metal 6061-T6 aluminum were experimentally computed [6].

We also can compute the behavior of the thermal boundary layers near the ends of the rod. From equation (3.3) or (3.4) we compute that the diffusion constant is equal to $(\frac{k}{\rho c_v})^{1/2}$. This is typically of the order 10^{-3} to 10^{-5} in dimensionless units. This leads to very sharp boundary layers, and exponential decay to the asymptotic temperature state.

We also mention that other constitutive laws than (3.11) have been derived which describe the behavior of metal-matrix materials. Since the parameters are described by a parameter fitting procedure, essentially the same results are obtained for the asymptotic temperature rise.

Section 5. Conclusions.

The results given in reference [5] indicate that the cyclic stress amplitudes for load sequences of 1 Hz. , 5 Hz. , and 25 Hz. are 336.5 MPa (48.8 KSI) , 346.8 MPa (50.3 KSI), and 358.9 MPa (52.05 KSI) respectively.

From Fig. 1 it is found , for example, that a stress amplitude of 346.8 MPa leads to a minimum asymptotic temperature rise of $61.9^{o} K$. This temperature represents an extremely hostile environment for AL 6061-T6 which could lead to such serious losses

in material properties as to compromise the structural integrity of the system. It is therefore concluded that the use of material inelasticiy to enforce passive structural damping should be utilized with caution due to the possibility of catastrophic structural heating in space in the presence of solar flux.

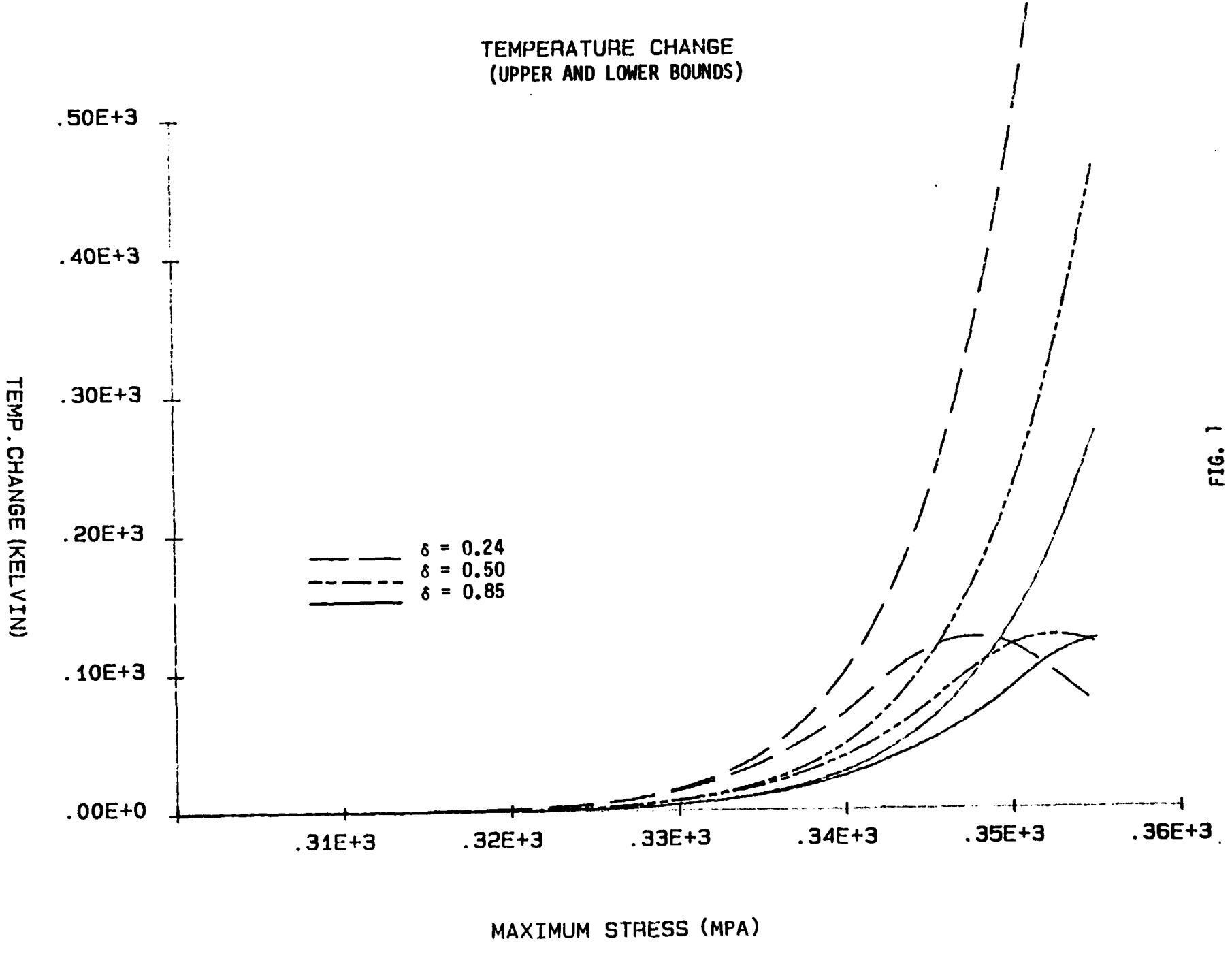
TEMPERATURE CHANGE
(UPPER AND LOWER BOUNDS)
.50E+3
.40E+3
.30E+3
.20E+3
.10E+3
.00E+0
TEMP. CHANGE (KELVIN)
δ = 0.24
δ = 0.50
δ = 0.85
.31E+3
.32E+3
.33E+3
.34E+3
.35E+3
.36E+3
MAXIMUM STRESS (MPA)

FIG. 1

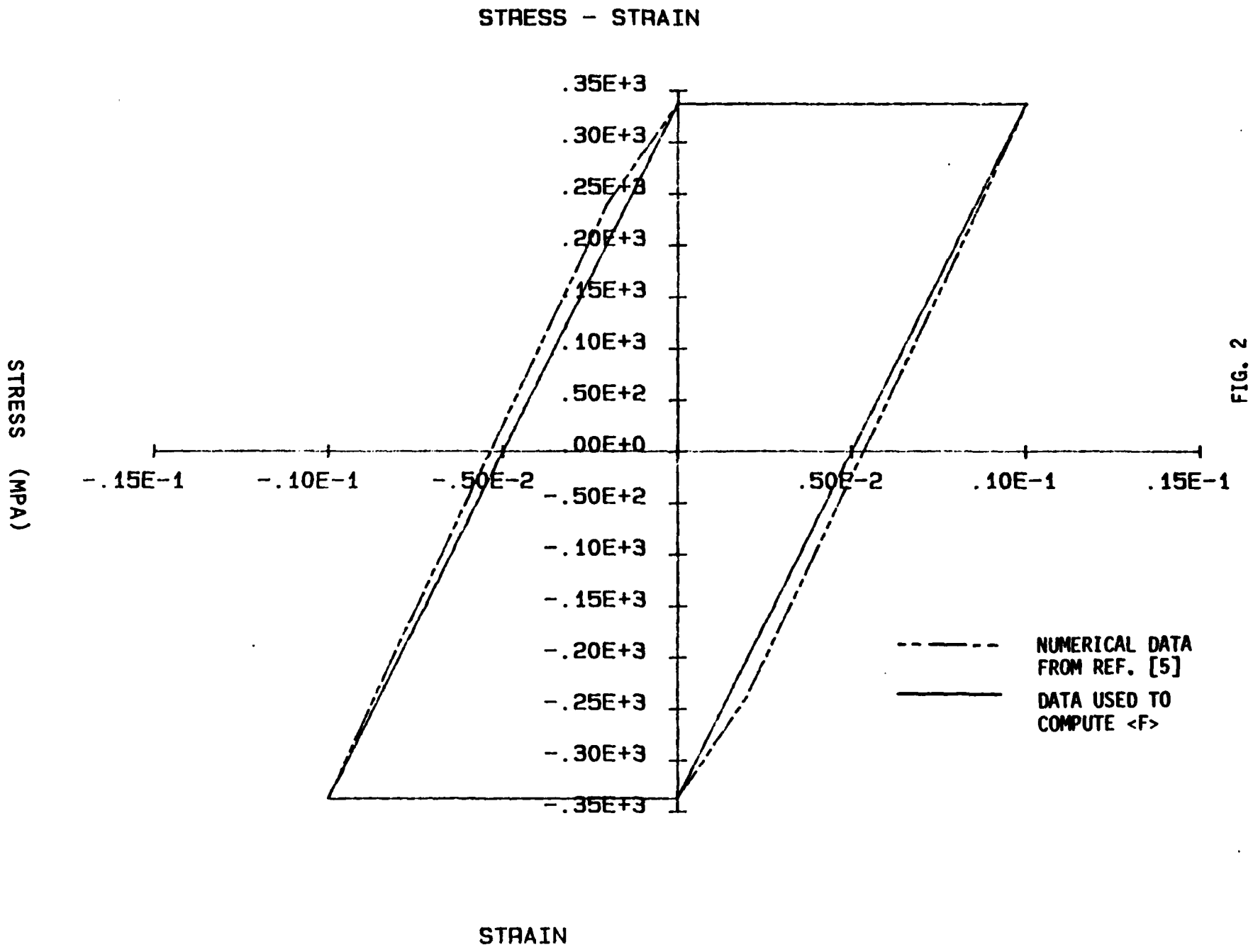
STRESS - STRAIN
.35E+3
.30E+3
.25E+3
.20E+3
.15E+3
.10E+3
.50E+2
00E+0
-.50E+2
-.10E+3
-.15E+3
-.20E+3
-.25E+3
-.30E+3
-.35E+3
-.15E-1
-.10E-1
-.50E-2
.50E-2
.10E-1
.15E-1
STRESS (MPA)
STRAIN
NUMERICAL DATA FROM REF. [5]
DATA USED TO COMPUTE <F>

FIG. 2

ACKNOWLEDGEMENT

The author wishes to acknowledge the many helpful discussions and comments of Dr. D. H. Allen. This research was supported by the Air Force Office of Scientific Research under contract no. F49620-83-C-0067.

REFERENCES

[1] Allen, D. H., and Haisler, W., "A Model for Predicting Thermomechanical Response of a Large Space Structure," Texas A & M Mechanics and Materials Center, MM 4875-84-16, June 1984.

[2] Allen, D. H., "Thermodynamic Constraints on the Constitution of a Class of Thermo-viscoplastic Solids," Texas A & M Mechanics and Materials Center, MM 12415-82-10, December 1982.

[3] Pilant, M. S., "Analysis of a Thermoviscoplastic Uniaxial Bar under Prescribed Stress. Part I - Theoretical Treatment," Texas A & M Mechanics and Materials Center, MM-4875-85-2, January 1982.

[4] Pilant, M. S., "Analysis of a Thermoviscoplastic Uniaxial Bar Under Prescribed Stress. Part II - Boundary Layer and Asymptotic Analysis," Texas A & M Mechanics and Materials Center, MM-4875-85-6, May 1985.

[5] Allen, D. H., and Haisler, W. E., "Predicted Temperature Field in a Thermomechanically Heated Viscoplastic Space Truss Structure," Texas A & M Mechanics and Materials Center, MM-4875-85-1, January 1985.

[6] Beek, J. M., "A Comparison of Current Models for Nonlinear Rate-dependent Material Behavior of Crystalline Solids," Texas A & M University Thesis (May 1985).

[7] Bodner, S. R., and Partom, Y., "Constitutive Equations for Elastic-Viscoplastic Strain-Hardening Materials," J. Appl. Mech., v. 42, 385-389 (1975).

END

FILMED

1-86

DTIC